Fall 2011

Tetraphenylethylene: a versatile supramolecular framework

Pradeep Paresh Kapadia
University of Iowa

TETRAPHENYLETHYLENE: A VERSATILE SUPRAMOLECULAR FRAMEWORK

by

Pradeep Paresh Kapadia

An Abstract

Of a thesis submitted in partial fulfillment
of the requirements for the Doctor of
Philosophy degree in Chemistry
in the Graduate College of
The University of Iowa

December 2011

Thesis Supervisor: Associate Professor F. Christopher Pigge

ABSTRACT

Supramolecular chemistry is a branch of chemistry that focuses on chemical systems that are made up of a discrete number of assembled molecular components held together by various non-covalent interactions. Supramolecular systems are rarely designed from first principles. Rather, chemists have a range of well-studied structural and functional building blocks that they are able to use to build up larger functional architectures. We have chosen tetraphenylethylene (TPE) as the supramolecular building block in designing various functional materials because of interesting optical and electronic properties of TPE derivatives. We have utilized several intermolecular interactions like hydrogen bonding, coordinate bonding and halogen bonding to obtain materials with remarkable optical and electronic properties in the solid state as well as solution phase that can have potential applications in fields like crystal engineering, material science and organic electronics.

TPE functionalized with four carboxylic acid groups was synthesized and crystallized with various bis(pyridines) to yield organic semiconducting materials. These crystals have been characterized by single crystal X-ray diffraction and conducting properties have been studied using conducting probe-atomic force microscopy. Semiconducting properties of these materials can be tuned based on bis(pyridine) component.

Two different tetrapyridyl substituted TPEs have been synthesized and their photoluminescent properties have been studied in solution. Fluorescence emission was found to be switchable as a function of solvent mixture as well as pH. Both compounds have been structurally characterized in their free base form as well as in their protonated form as tetraperchlorate salts via X-ray diffraction.

These three compounds have been utilized as supramolecular building blocks in metal organic frameworks (MOFs) as well as organic co-crystals mediated by hydrogen

bonding as well as halogen bonding. A fluorescent complex of the tetraacid with zinc has been obtained which crystallized in a non-centrosymmetric space group due to solvent and water ligands on the zinc center. A coordination polymer has been obtained via solvothermal synthesis using tetrapyridyl TPE and zinc chloride. Lewis basicity of tetrapyridyl TPE's has also been utilized in organic co-crystalline assemblies mediated by halogen bonding interactions with iodoperfluoroarenes. Finally, Halobenzoyl esters of TPE based compounds have been synthesized and halogen bonding properties of these compounds have been exploited to achieve solid state porous networks.

Abstract Approved: _____
Thesis Supervisor

_____
Title and Department

_____
Date

TETRAPHENYLETHYLENE: A VERSATILE SUPRAMOLECULAR FRAMEWORK

by

Pradeep Paresh Kapadia

A thesis submitted in partial fulfillment
of the requirements for the Doctor of
Philosophy degree in Chemistry
in the Graduate College of
The University of Iowa

December 2011

Thesis Supervisor: Associate Professor F. Christopher Pigge

Graduate College
The University of Iowa
Iowa City, Iowa

CERTIFICATE OF APPROVAL

_____

PH.D. THESIS

_____

This is to certify that the Ph.D. thesis of

Pradeep Paresh Kapadia

has been approved by the Examining Committee
for the thesis requirement for the Doctor of Philosophy
degree in Chemistry at the December 2011 graduation.

Thesis Committee: _____
F. Christopher Pigge, Thesis Supervisor

_____
Leonard R. MacGillivray

_____
James B. Gloer

_____
Gary W. Small

_____
C. Allan Guymon

To My Parents Parul and Paresh Kapadia

Dictionary is the only place that success comes before work. Hard work is the price we must pay for success. I think you can accomplish anything if you’re willing to pay

Vince Lombardi

ACKNOWLEDGMENTS

Foremost, I would like to express my sincere gratitude to my advisor Prof. Chris Pigge for the continuous support of my Ph.D. study and research, for his patience, motivation, enthusiasm, and immense knowledge. His guidance helped me in all the time of research and writing of this thesis. He has not only inspired me as advisor, he has been an excellent instructor for my teaching assignment. He has guided me to perform my best by example.

I would like to thank all my committee members Dr. Len MacGillivray, Dr. James Gloer, Dr. Gary Small and Dr. Allan Guymon for their time and insightful questions and comments. I would also like to thank instructors for teaching assignment for making teaching experience enjoyable rather than time consuming process. I would like to thank advanced laboratory manager Brian Morrison for his help during teaching assignment.

I would like to thank Dr. Dale C. Swenson for his valuable contribution through obtaining crystal structure data as well as helping me solve structure. Without his help, this research would not have been possible. I would like to extend my gratitude towards our collaborator Dr. Alexei Tivanski and Lindsay Ditzler for AFM experiments and Dr. Jonas Baltrusaitis for theoretical calculations.

All the members of Pigge Research Group have helped my immensely during my graduate school. I would like to thank Rashmi, Mayuri, Sharavathi, Dhanya, Venu, Tim, Lokesh, Matt, Ashabha and Mary. I would like to extend special gratitude to Mayuri, and Venu for helping me with understanding of experimental synthetic chemistry and crystal engineering. My special thanks to Sharavathi for being lab mate and a constant source of entertainment for last 5 years and for her constant encouragement and guidance. I would like to thank undergraduate researchers in Pigge Research Group, John Widen and Mackenzie Magnus for their important contribution to this work via synthesis of starting materials and preparing crystalline networks.

My time at the University of Iowa was more enjoyable due to many friends. I would like to thank my closest friends Leena, Abhinaba and Suman for being a part of family away from home. I would also like to thank Bhakti, Varsha and Nisarga for numerous memorable road trips to various parts of the country. I would like to thank Adil, Samrat and Mary for hosting parties that were fun. I also extend my gratitude to Nirmal, Ashay and Oishik. My time at Iowa was also enriched by experience of being a part of University of Iowa Cricket Club and Iowa Hawkeyes Cricket Team with special mention of Sachin, Urvil, Nikhil, Ankush and Anup. I would like to thank all my other friends who made my stay at Iowa a memorable experience.

Last but not the lease I would like to thank my parents Parul and Paresh along with my sister Kinnari for their encouragement and support throughout my life and letting me pursue my dream of going to graduate school.

ABSTRACT

Supramolecular chemistry is a branch of chemistry that focuses on chemical systems that are made up of a discrete number of assembled molecular components held together by various non-covalent interactions. Supramolecular systems are rarely designed from first principles. Rather, chemists have a range of well-studied structural and functional building blocks that they are able to use to build up larger functional architectures. We have chosen tetraphenylethylene (TPE) as the supramolecular building block in designing various functional materials because of interesting optical and electronic properties of TPE derivatives. We have utilized several intermolecular interactions like hydrogen bonding, coordinate bonding and halogen bonding to obtain materials with remarkable optical and electronic properties in the solid state as well as solution phase that can have potential applications in fields like crystal engineering, material science and organic electronics.

TPE functionalized with four carboxylic acid groups was synthesized and crystallized with various bis(pyridines) to yield organic semiconducting materials. These crystals have been characterized by single crystal X-ray diffraction and conducting properties have been studied using conducting probe-atomic force microscopy. Semiconducting properties of these materials can be tuned based on bis(pyridine) component.

Two different tetrapyridyl substituted TPEs have been synthesized and their photoluminescent properties have been studied in solution. Fluorescence emission was found to be switchable as a function of solvent mixture as well as pH. Both compounds have been structurally characterized in their free base form as well as in their protonated form as tetraperchlorate salts via X-ray diffraction.

These three compounds have been utilized as supramolecular building blocks in metal organic frameworks (MOFs) as well as organic co-crystals mediated by hydrogen

bonding as well as halogen bonding. A fluorescent complex of the tetraacid with zinc has been obtained which crystallized in a non-centrosymmetric space group due to solvent and water ligands on the zinc center. A coordination polymer has been obtained via solvothermal synthesis using tetrapyridyl TPE and zinc chloride. Lewis basicity of tetrapyridyl TPE's has also been utilized in organic co-crystalline assemblies mediated by halogen bonding interactions with iodoperfluoroarenes. Finally, Halobenzoyl esters of TPE based compounds have been synthesized and halogen bonding properties of these compounds have been exploited to achieve solid state porous networks.

TABLE OF CONTENTS

LIST OF TABLES

LIST OF FIGURES

LIST OF SCHEMES

CHAPTER I

INTRODUCTION TO SUPRAMOLECULAR CHEMISTRY OF TETRAPHENYLETHYLENE AND ITS DERIVATIVES

1.1 Supramolecular Chemistry

Supramolecular chemistry refers to 'chemistry beyond the molecule', and involves investigating new molecular systems in which the most important feature is that the compounds are held together reversibly by non-covalent intermolecular forces.[1] Significantly, proper positioning of individual covalently bonded molecular building blocks via various intermolecular forces can create functional architectures with desirable bulk properties.

The existence of intermolecular forces between molecules was first postulated by van der Waals in 1873. In 1920, Latimer and Rodebush first proposed hydrogen bonding.[2] Since then, the importance of hydrogen bonding has been established in many biological systems like enzyme-substrate complexes and the DNA double helix.[3] A breakthrough in gaining control over non-covalent attractions came in 1960 when crown ethers for binding alkali metal ions were synthesized by Pederson.[4] Cram[5] and Lehn[6] were also pioneers in synthesizing shape and ion specific receptors. The importance of supramolecular chemistry was recognized in the 1980's when Cram, Lehn and Pederson were awarded the Nobel Prize in Chemistry in 1987 for their contributions toward host-guest chemistry.[7]

Non-covalent interactions that are at the disposal of the supramolecular chemist are not limited to hydrogen bonding. They also include electrostatic interactions, π-π interactions, halogen bonding, dispersion forces, and coordination bonding. All these interactions are much weaker as compared to a typical covalent bond.[8]

The principles of supramolecular chemistry are utilized in self-assembly, molecular recognition and template directed synthesis events. They also provide a basis

for design of molecular machines and biomimetic systems. They have been applied in materials science (e.g., organizing motifs in electronic and magnetic materials), catalysis, green chemistry, and molecular sensing. Supramolecular systems are rarely designed from first principles. Rather, chemists have a range of well-studied structural and functional building blocks that they are able to use to build up larger functional architectures. Many of these exist as whole families of similar units, from which the analog with the exact desired properties can be chosen. We have chosen tetraphenylethylene (TPE) as a primary building block in designing various functional materials. It is envisioned that TPE derivatives can be used for various applications in materials chemistry according to functionality appended to the core framework.

1.2 Tetraphenylethylene

Tetraphenylethylene (TPE or **1.1**) represents the parent compound of a family of polyaromatic compounds where an olefin is flanked by four arene rings. In the solid state, TPE and its derivative adopt propeller like conformations with the four benzene rings roughly perpendicular to the central olefin. In tetraanisylethylene, planar (dihedral) angles between alkene and benzene rings are ~52° resulting in the characteristic propeller shape of the molecule which is a characteristic feature of TPE derivatives.[9]

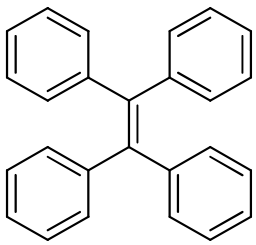

1.1

Figure 1.1 Tetraphenylethylene (TPE)

1.3 Synthesis of tetraphenylethylene and its derivatives

There are various routes available for the synthesis of TPE and its derivatives. The most common synthetic disconnection is the central alkene, although occasionally alkyl-aryl C-C bonds are also constructed during the synthesis of TPE derivatives. The first report of TPE can be traced back to 1888 by de Boissieu who prepared the compound by dry distillation of diphenylmethane in the presence of bromine.[10] Scheme 1 provides various synthetic routes described in the literature for preparation of TPE. Several of these routes are also suitable for construction of functionalized TPE's.

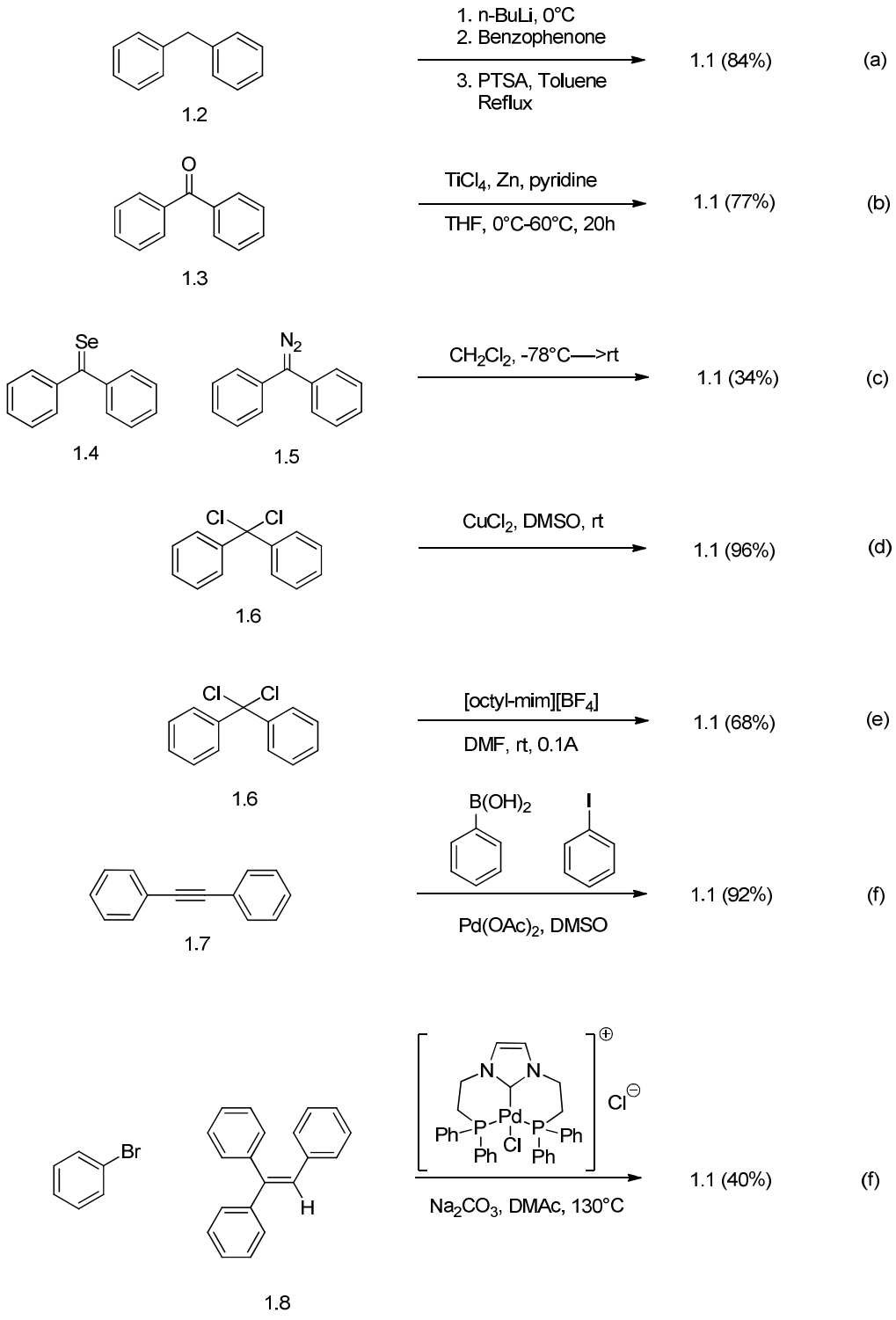

Scheme 1.1 Various routes for synthesis of tetraphenylethylene

Wang *et al.* used a Knoevenagel like condensation reaction to synthesize TPE (Scheme 1.1a). Diphenylmethane (**1.2**) was deprotonated using n-BuLi in THF at 0°C to which benzophenone was added. The resulting tertiary alcohol was dehydrated using catalytic PTSA via azeotropic removal of water from toluene.[11] This synthesis has limitations in terms of substituents on diphenylmethane as well as benzophenone components. It cannot be utilized with electron donating substituents on diphenylmethane due to formation of unstable anion and electrophilic substituents on benzophenone due to competition with ketone group.

Another common reaction to synthesize TPE and derivatives is the McMurry coupling. Ti(III) and Ti(IV) salts that are reduced to low valent titanium using Zn are capable of mediating the reductive coupling of benzophenone (**1.3**) to yield TPE.[12] Symmetrically substituted TPE's can also be prepared as this reaction is tolerant to alkyl, halogen, ether, amine, alcohol, and phenol substituents. This reaction has also been extended to cross-coupling of two benzophenones with different substituents to yield unsymmetrically substituted TPE.[12]

The reaction of selenobenzophenones (**1.4**) with diphenyldiazomethane (**1.5**) in dichloromethane at -40°C resulted in formation of TPE as described in Scheme 1.1c. This reaction is believed to proceed via a 1,3,4-selenadiazoline intermediate followed by deselenization and evolution of nitrogen gas. This strategy was also extended to afford unsymmetrical TPE derivatives.[13]

Diphenyldichloromethane (**1.6**) was found to undergo an exothermic reaction with stoichiometric copper metal in DMSO to yield TPE (Scheme 1.1d).[14] This reaction is believed to proceed via a copper carbenoid intermediate. Barhadi *et al.* developed similar electrochemical coupling reactions of diphenyldichloromethane using nickel catalyst in room temperature ionic liquids (Scheme 1.1e).[15]

Another common disconnection for the synthesis of TPE's is an alkene-arene bond. Sajna *et al.* developed a palladium catalyzed double arylation of diphenylacetylene

(**1.7**) in aqueous medium resulting in TPE.[16] Similarly Nadri *et al.* utilized Heck reaction of di- and triarylethylenes (**1.8**) to synthesize TPE and its derivatives. For this reaction, phosphapalladacycle bearing a biphenyl moiety was used as the catalyst.[17]

Like any other electron rich aromatic ring, TPE also undergoes electrophilic aromatic substitutions. The para position of each phenyl ring is the most electron rich location on the molecule. As expected, upon electrophilic substitution, TPE yields 4-substituted TPE derivatives. As shown in Scheme 1.2, TPE underwent Friedel-Crafts acylation,[11] bromination,[18] iodination[19] and nitration[12] under electrophilic aromatic substitution conditions. Halogenated TPE derivatives have been utilized as starting materials for Pd catalyzed C-C bond formation reactions.

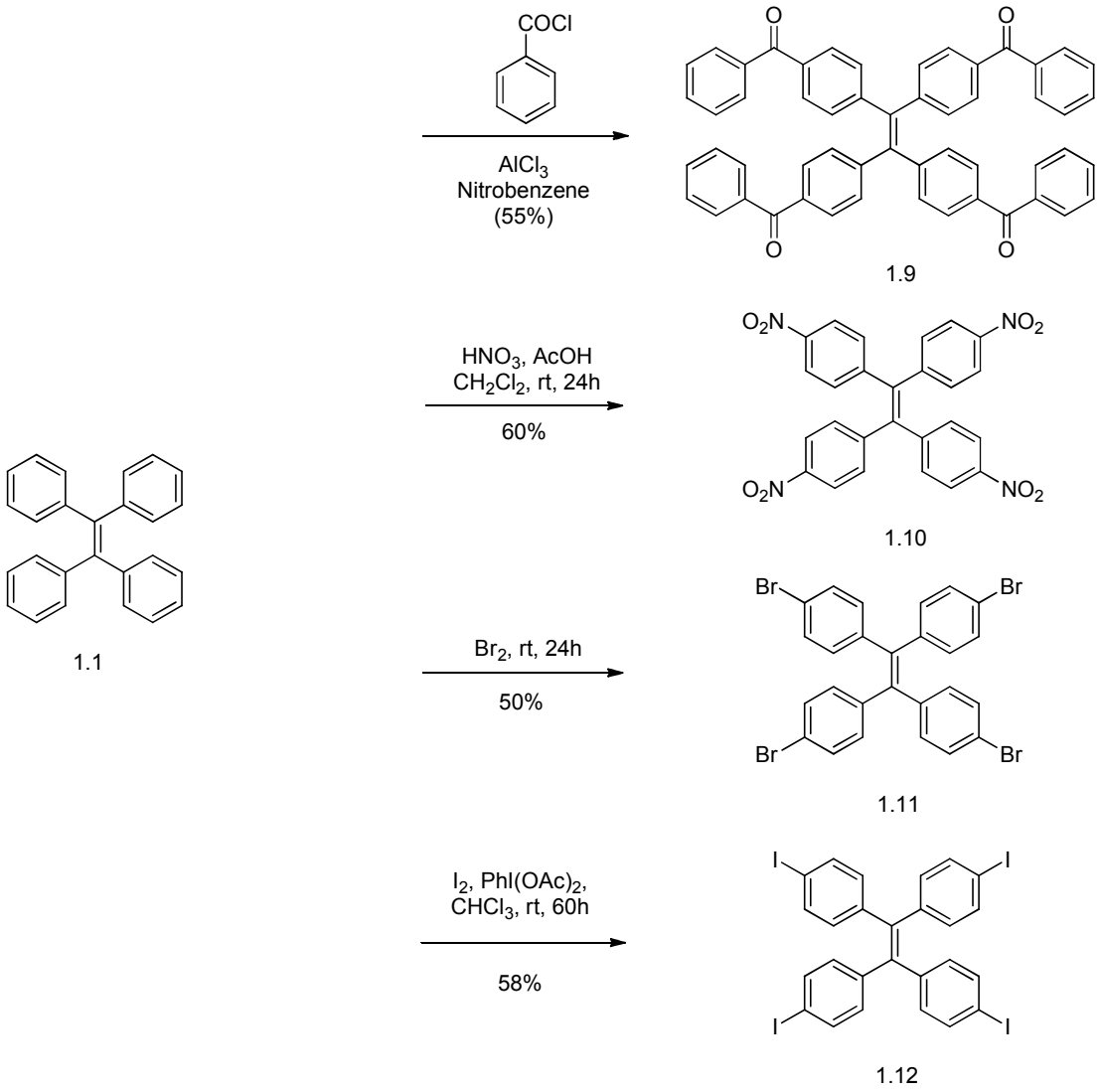

Scheme 1.2 Electrophilic aromatic substitution of TPE

Thus, the availability of several synthetic routes for construction of TPE and TPE's substituted with different peripheral functional groups facilitates the modular synthesis of functional materials that have TPE as the core structure. In the following sections, representative examples of supramolecular constructs based on tetraphenylethylene building blocks are described.

1.4 Oxidation and reduction of tetraarylethylenes

Reduction of the central olefin in TPE does not take place via hydrogenation due to the presence of four bulky phenyl rings around it in propeller shape. Stryker *et al.* have shown that at 600 psi, hydrogenation of peripheral allyl groups attached to the TPE core in the presence of Pd/C can be performed without affecting the central alkene.[20] Conversely, Fry *et al.* have used hypophosphorous acid in the presence of catalytic iodine to reduce TPE to the corresponding tetraphenylethane in quantitative yield.[21]

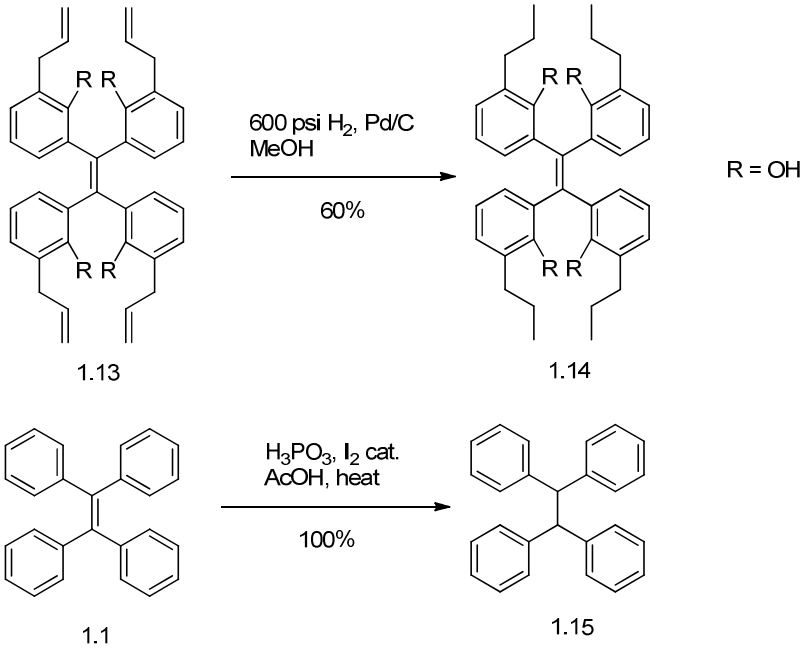

Scheme 1.3 (a) Catalytic hydrogenation of tetraarylethylene (b) Reduction of TPE

On the other hand, tetraphenylethylene and its electron-rich ring-substituted analogues are bifunctional electron donors by virtue of the fact that both aromatic and olefinic centers are susceptible to one-electron oxidation. Chemical oxidation with antimony (V) oxidants forms paramagnetic tetraarylethylene radical cations that can be further oxidized to diamagnetic dications (Scheme 1.4a). The tetraanisylethylene radical

cation and dication prepared in this way were isolated by Rathore *et al.* and structurally characterized via X-ray diffraction.[9] Among the structural differences observed between these three structures, two features were prominent. The length of the C=C in the central olefin elongated from 1.359 Å in **1.16** to 1.417 Å in **1.17** to 1.503 Å in **1.18**. Similarly, the dihedral ethylenic angles of central olefin increased linearly from 3.8° in **1.16** to 30.5° in **1.17** to 61.6° in **1.18**.[9]

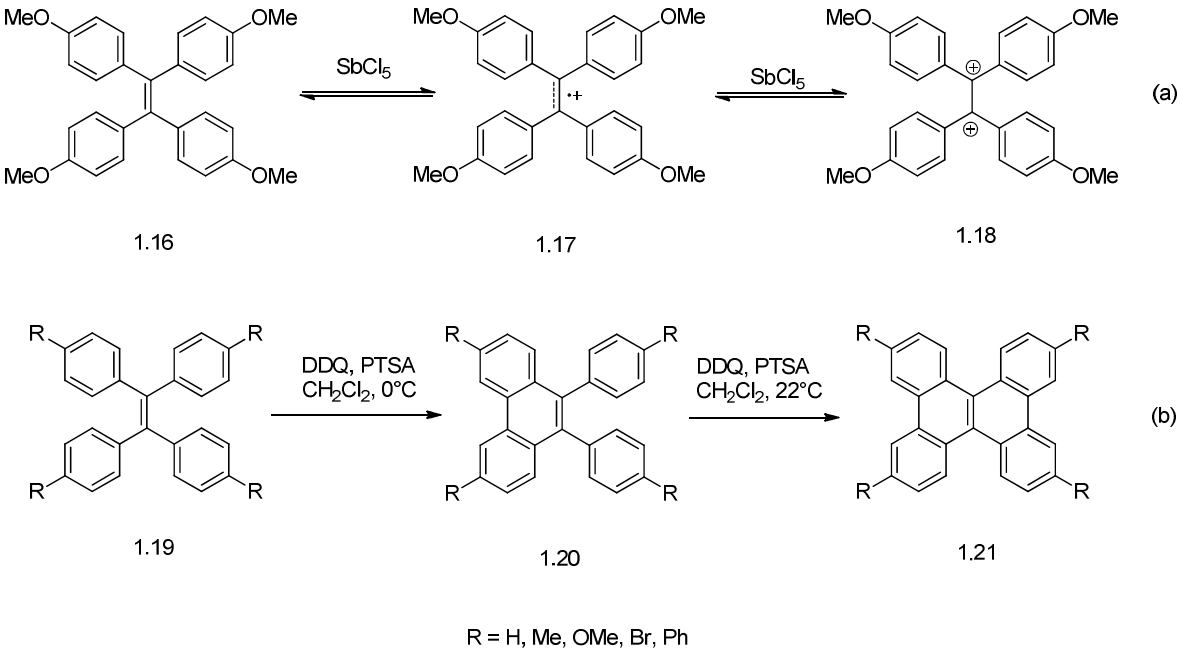

Scheme 1.4 (a) Oxidation sequence of tetraanisylethylene (b) Oxidative transformation of tetraarylethylene

The redox properties of substituted TPE's may offer opportunities to use these materials in electron transfer catalysis. In addition, Rathore *et al.* have exploited the redox reactivity of TPE's in synthetic transformations leading to 9,10-diarylphenanthrenes (**1.20**) and dibenzo[g,p]chrysenes (**1.21**) using 1 and 2 equiv of

DDQ, respectively, in CH_2Cl_2 containing methanesulfonic acid, and products were obtained in excellent yields, as shown in Scheme 1.4b.[22]

1.5 Fluorescence properties of tetraarylethylenes

Extended π-conjugation imparts interesting optical properties to TPE and its derivatives. It is well known that tetraarylethylenes are generally non-emissive in solution due to the rotations of the phenyl rings along the =C–Ph axes and twisting of the C=C bond in the excited state, both of which serve as non-radiative relaxation channels for the decay of the excited state. On the other hand, in solid state or on addition of an anti-solvent, photoluminescence of TPE derivatives is turned on.[23] It is believed that restriction of molecular motions (C_{alkene}-C_{arene} bond rotations) in solid or aggregated states is responsible for this photo-luminescent activity (i.e., aggregation-induced emission or AIE).[23] To illustrate, the fluorescence spectrum of TPE in ACN and ACN – water mixture is shown in Figure 1.2. The addition of water (a poor solvent for TPE) results in a much increased fluorescence at ~470 nm.[24]

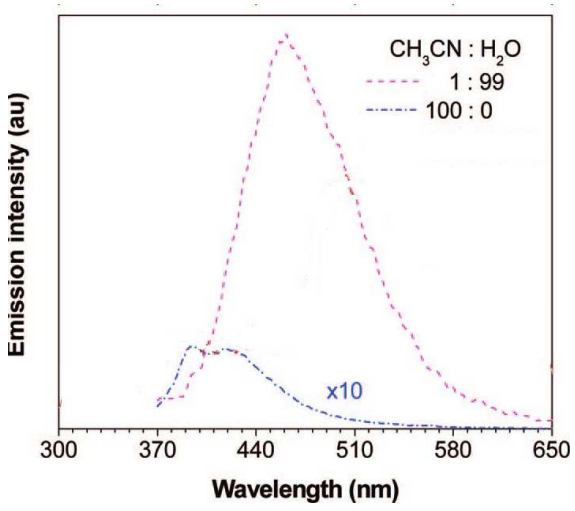

Figure 1.2 Fluorescence spectrum of TPE in ACN and ACN –water mixture

This same phenomenon is observed for other substituted TPE derivatives. Depending on the electronic nature the substituents and number of substituents attached to the TPE core, emission maxima can be modified. Cheng *et al.* have shown that combining small molecules with highly processable PMMA can result in high-quality polymer nanowires and meanwhile maintain or even enhance the original functionality of the small molecules. Thus, combination of the TPE with PMMA afforded fluorescent polymer.[24]

1.6 Applications of derivatives of tetraphenylethylene

The propeller shape of the TPE core, along with a propensity for TPE derivatives to self-assemble in the solid state to form stacked supramolecular constructs has been widely utilized in designing functional materials based on TPE frameworks. The aggregation-induced emission properties of substituted TPE's have been widely exploited in design of chemo- and biosensors for selected analytes. Fluorescent sensors for metals as well as biomolecules have been reported. The rationale behind the design is that TPE derivatives show weak fluorescence in solution, but they become strong emitters after aggregation. By attaching binding groups onto the periphery of TPE, analyte binding can be used to trigger aggregation leading to a fluorescence signal.

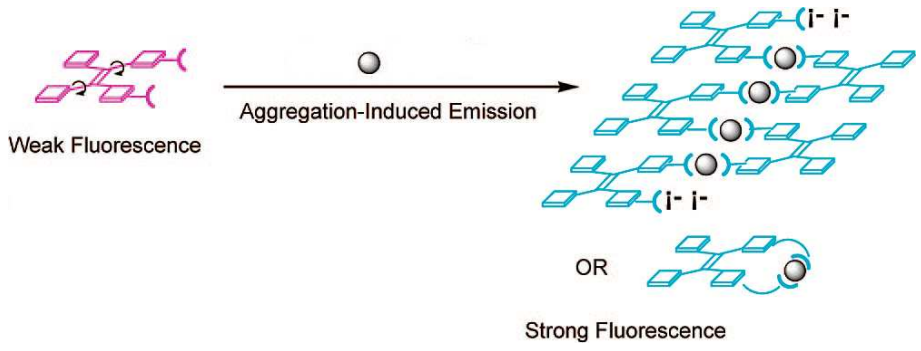

Figure 1.3 Design principle of TPE based sensors

1.6.1 TPE derivatives as metal ion sensors

Adenine-substituted TPE derivative **1.22** was synthesized and found to exhibit weak fluorescence in 5:1 THF:water mixtures. However, after addition of $AgClO_4$, an emission band at 470 nm emerged and its intensity increased gradually as displayed in Figure 1.4b. The fluorescence difference for the solution of **1.22** before and after addition of Ag^+ can be distinguished by the naked eye. The fluorescence intensity of **1.22** increases linearly with the concentration of Ag^+. This fluorescence enhancement can be attributed to coordination of adenine moieties on **1.22** with Ag^+ ions leading to formation of coordinate complexes that further aggregate due to decreased solubility. As a result, fluorescence intensity of TPE core in **1.22** increases. This enhancement in fluorescence was independent of counterion for Ag^+. [25]

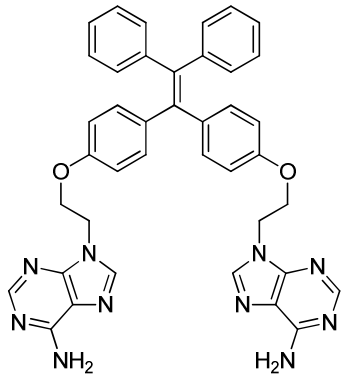
O
O
N
N
N
N
N
N
N
N
NH2
H2N

(a) 1.22

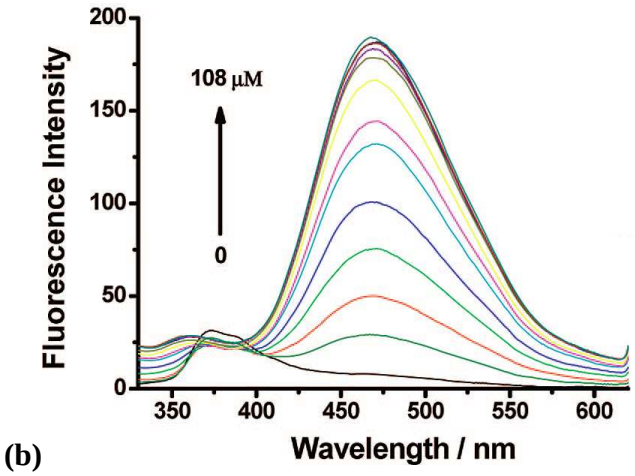
Fluorescence Intensity
200
150
100
50
0
108 μM
0
350
400
450
500
550
600
Wavelength / nm

(b)

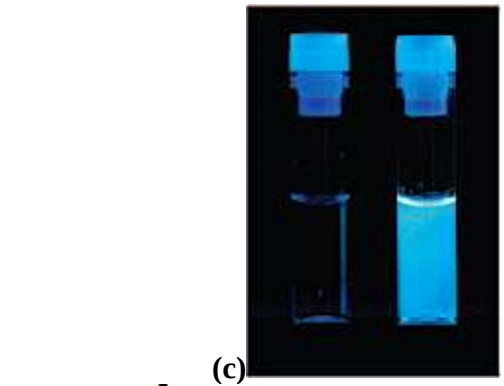

(c)

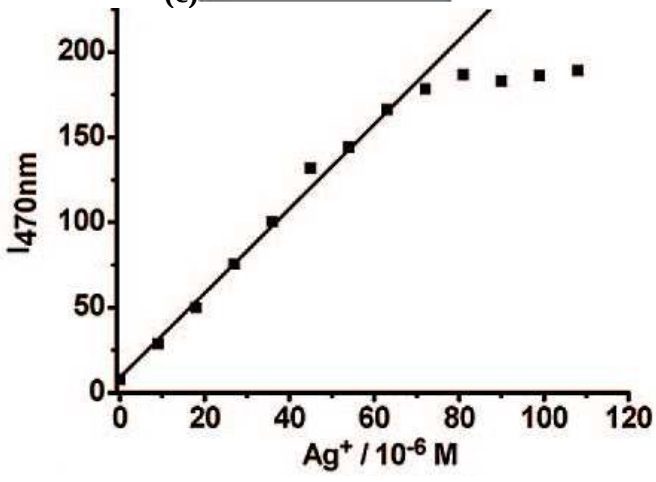

(d)

Figure 1.4 (a) Compound **1.22** used as fluorescent sensor for Ag^+ ions (b) Fluorescence spectra of **1.22** with increasing amounts of $AgClO_4$ in THF:H_2O 1:5 (c) Solution of **1.22** (left) before addition of Ag^+ and (right) after addition of Ag^+ under UV light illumination at 365 nm (d) Plot of fluoresecnce intensity vs concentration of Ag^+.[25]

Similarly, a thymine-substituted TPE derivative **1.23** was prepared and used as a detector for Hg^{2+} ions in aqueous acetonitrile:water solvent system. Similar to **1.22**, this sensor was selective to Hg^{2+} ions, even in presence of competing metal ions, due to the preference for thymine toward Hg^{2+} ions.[25]

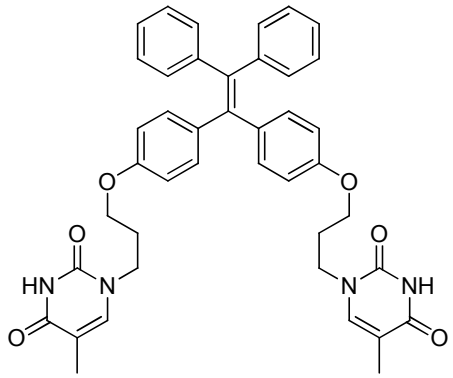
O
O
HN
N
O
N
NH
O

1.23

(a)

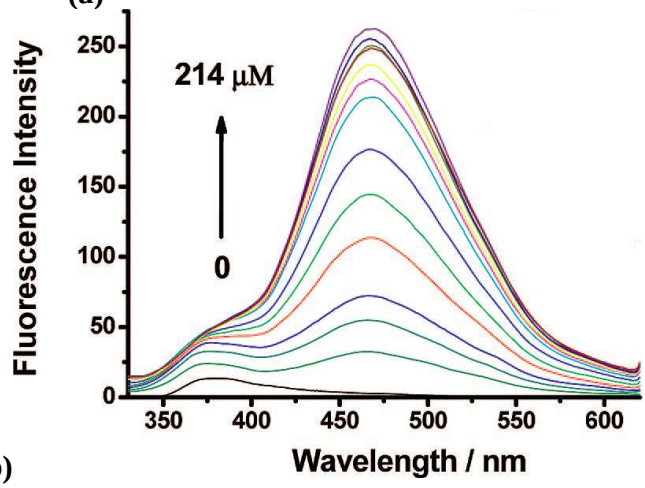
Fluorescence Intensity
214 μM
0
250
200
150
100
50
0
350
400
450
500
550
600
Wavelength / nm

(b)

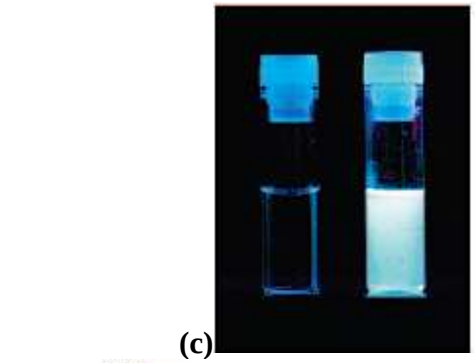

(c)

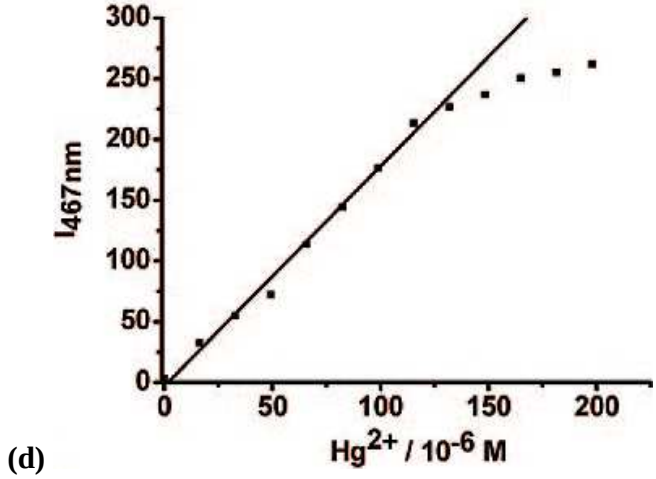

(d)

Figure 1.5 (a) Compound **1.23** used as fluorescent sensor for Hg^{2+} ions (b) Fluorescence spectra of **1.23** with increasing amounts of $Hg(ClO_4)_2$ in ACN:H_2O 1:2 (c) Solution of **1.23** (left) before addition of Hg^{2+} and (right) after addition of Hg^{2+} under UV light illumination at 365 nm (d) Plot of fluoresecnce intensity vs concentration of Hg^{2+}.[25]

Along the same lines, imidazole-substituted TPE derivative **1.24** was synthesized by Bian *et al.* This material was non-luminescent in pure THF, but upon addition of water, fluorescence was observed centered at ~471 nm. The intensity of fluorescence increased with increasing amount of water in THF with a maximum at 99:1 water:THF mixture. As compared to a blank sample, the fluorescence intensity does not change much upon addition of metal ions, except when Fe^{3+} was added, which caused fluorescence quenching, presumably due to formation of a soluble complex. This

phenomenon was observed visually as well under a UV-lamp. In this case, fluorescence quenching was selective for Fe^{3+} even in the presence of other metal ions.[26]

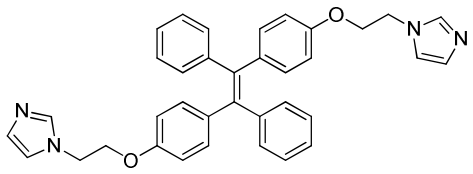

(a) 1.24

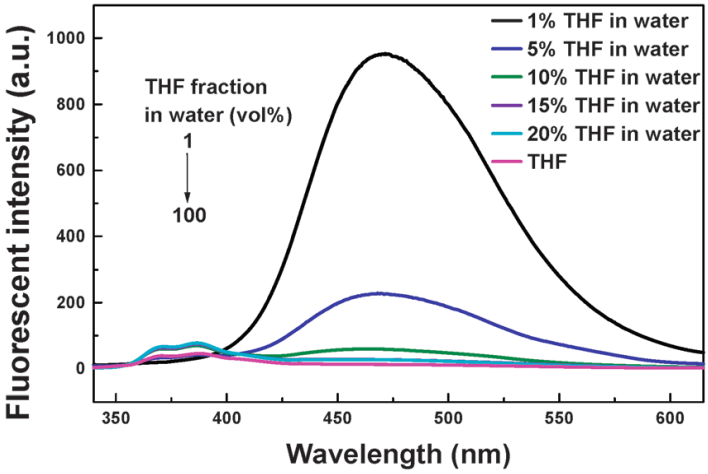

(b)

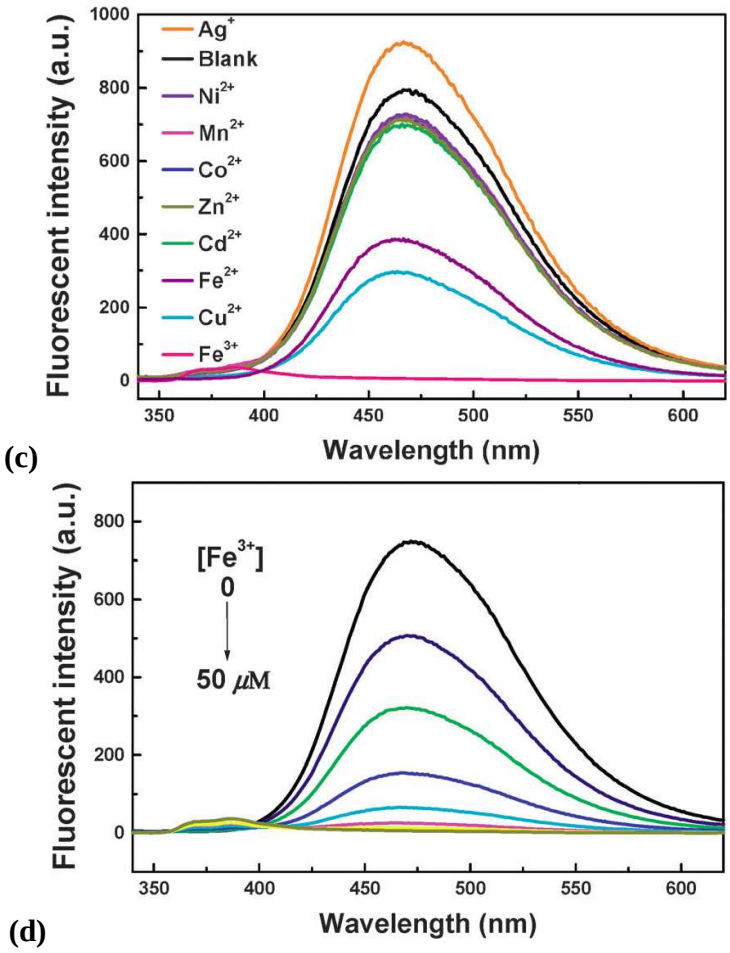

Figure 1.6 (a) Compound **1.24** used as fluorescent sensor for Fe^{3+} ions (b) Fluorescence spectra of **1.24** in THF:H_2O mixtures (c) Fluorescence of **1.24** in presence of different metal ions (d) Fluorescence spectra of **1.24** with increasing amounts of Fe^{3+} in THF:H_2O 1:99.[26]

1.6.2 TPE derivative for detection of explosives

An inorganic-organic hybrid polymer **1.25** was synthesized from dihydroxy TPE and cyclotriphosphazene through one-step polycondensation.[27] **1.25** was found to be fluorescent in the solid state as well as in 9:1 water:THF mixtures. As shown in Figures 1.7b and 1.7c, significant fluorescence quenching was observed upon addition of 2,4,6-trinitrotoluene (TNT) and 2,4,6-trinitrophenol (picric acid or PA). The main mechanism of fluorescence quenching was presumed to be electron transfer from electron-rich

polymer system **1.25** to electron-deficient nitroaromatic compounds. Thus, **1.25** has a potential to be a chemosensor for explosives containing nitroaromatic units.[27]

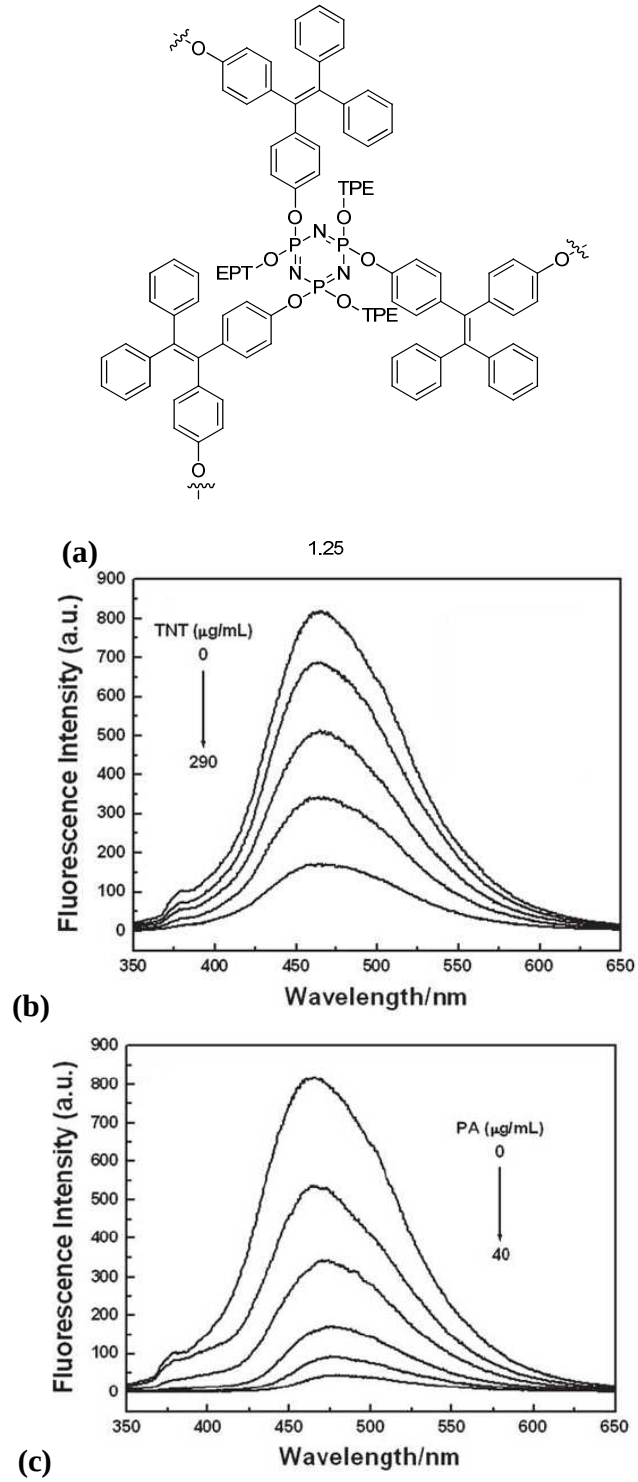

Figure 1.7 (a) Organic-inorganic hybrid polymer **1.25** used as explosive sensor Fluorescence spectra of **1.25** in prsence of (b) trinitrotoluene and (c) picric acid in aqueous solutions.

1.6.3 TPE derivatives as biosensors

TPE derivatives have not only been used as chemosensors, but also as sensors for biomolecules. For example, Kato *et al.* prepared a TPE derivative bearing lactose moieties via click chemistry (**1.26**).[28] This compound was non-fluorescent in buffered solutions, but upon addition of influenza virus A/WSN/33, enhancement in fluorescence was observed centered at 450 nm. It is postulated that the lactose groups interact with the surface of the virus leading to TPE aggregation. Hence, compound **1.26** has potential to be used as a probe for influenza virus.[28]

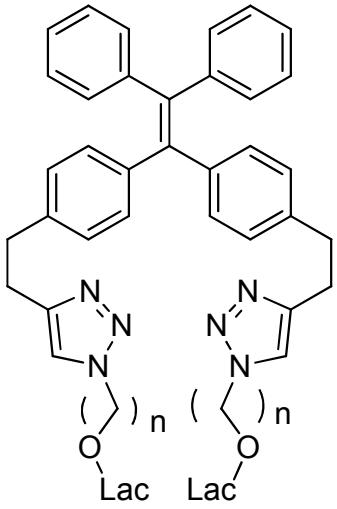

1.26

(a)

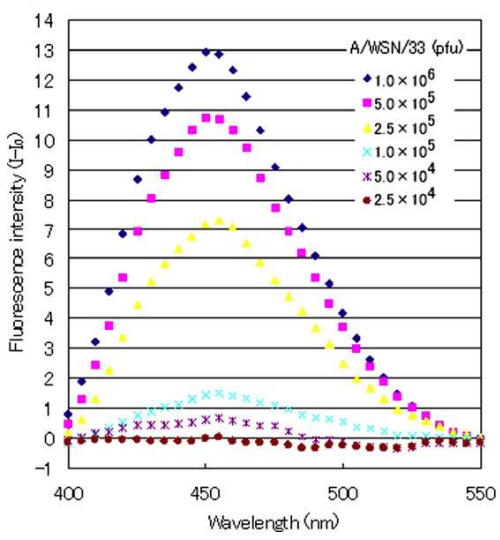

(b)

Figure 1.8 (a) Fluorescence biosensor **1.26** with lactose unit as detecting functionality for influenza virus (b) Fluorescence spectra of **1.26** in presence of increasing amounts of influenza virus A/WSN/33 in 10mM Tris-HCl (pH 7.6).[28]

1.6.4 Liquid crystalline materials from TPE derivatives

Schultz *et al.* prepared tetrakis[4-(trisalkyloxybenzoyloxy)phenyl]ethene **1.27** from the corresponding tetrahydroxy TPE derivative via esterification. In this compound,

C5-C10 and C12 alkyl chains were attached to the benzoic acid derivative. Despite the twisting of the central tetraphenylethene moiety, these compounds displayed hexagonal columnar mesophases according to polarizing microscopy as shown in Figure 1.9b. It was proposed that the molecules stack on top of each other with very disordered alkyl chains forming the hydrophobic periphery of the columns. Due to the propeller-shape of the tetraphenylethene, two neighboring molecules within a column are presumably rotated by 90° with respect to each other in order to achieve optimal space filling of the central core as shown in Figure 1.9c.[29]

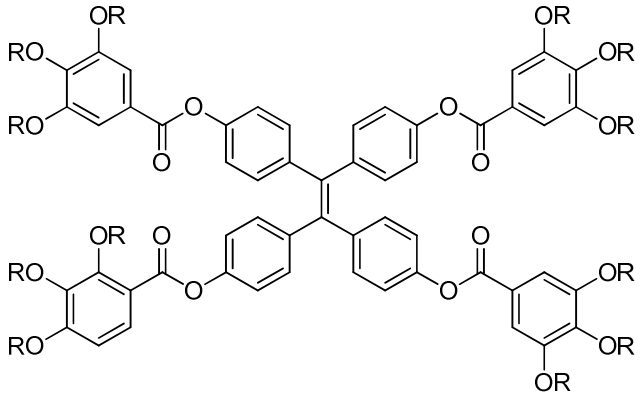

(a) 1.27 **(b)**

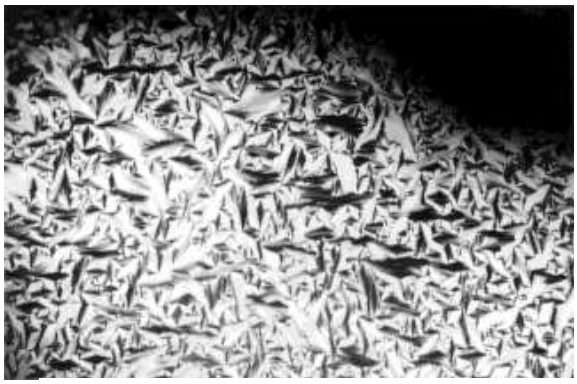

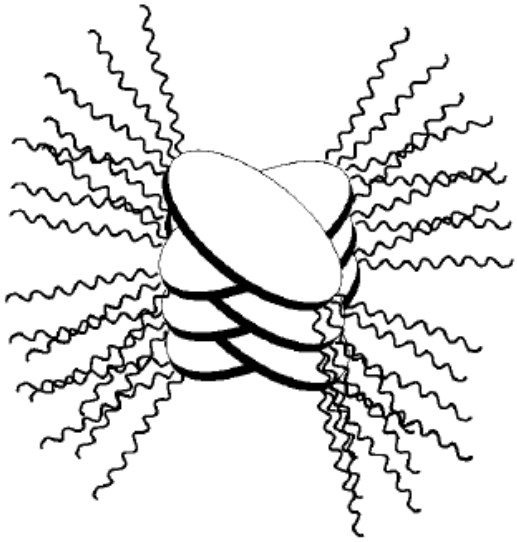

(c)

Figure 1.9 (a) TPE esters used in the study (b) Polarizing microscopy image of **1.27** showing fan shaped texture (c) Possible arrangement of **1.27** in the hexagonal columnar mesophase.[29]

1.6.5 TPE derivative in metal organic frameworks and complexes

Geometrical features inherent to the TPE core can be exploited for crystal engineering applications to design organic as well as metal organic assemblies. Stang *et al.* designed a tetragonal prism via multicomponent coordination-driven self-assembly as illustrated in Figure 1.10. Tetra(4-pyridylphenyl)ethylene incorporating four pyridine groups along the TPE periphery was designed to act as the faces of a tetragonal prism during the self-assembly event, while the linear donors 4,4′-bipyridine or *trans*-1,2-di(4-pyridyl)ethylene and platinum triflate were selected as pillars and corners of the tetragonal prism, respectively. When the three building blocks are reacted in a stoichiometric ratio of 1:2:4, the formation of tetragonal prism was expected as shown in Figure 1.10.[30]

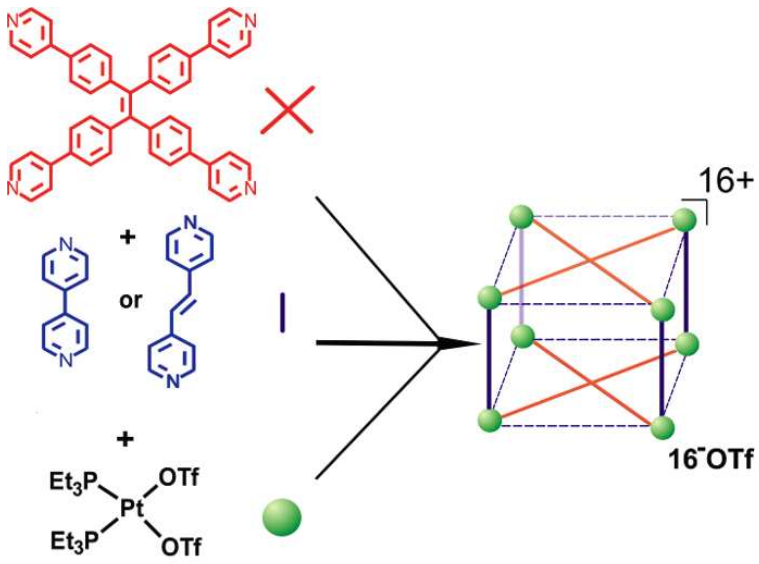

Figure 1.10 Multicomponent coordination driven self-assembly of tetragonal prisms.[30]

^{31}P and ^{1}H NMR multinuclear analysis of the reaction mixture indicated the formation of single and discrete assemblies with high symmetry. ESI-mass spectra of assemblies provided further evidence of formation of the desired tetragonal prisms by the appearance of molecular ion peak for tetracation for both assemblies along with the expected isotopic distribution.

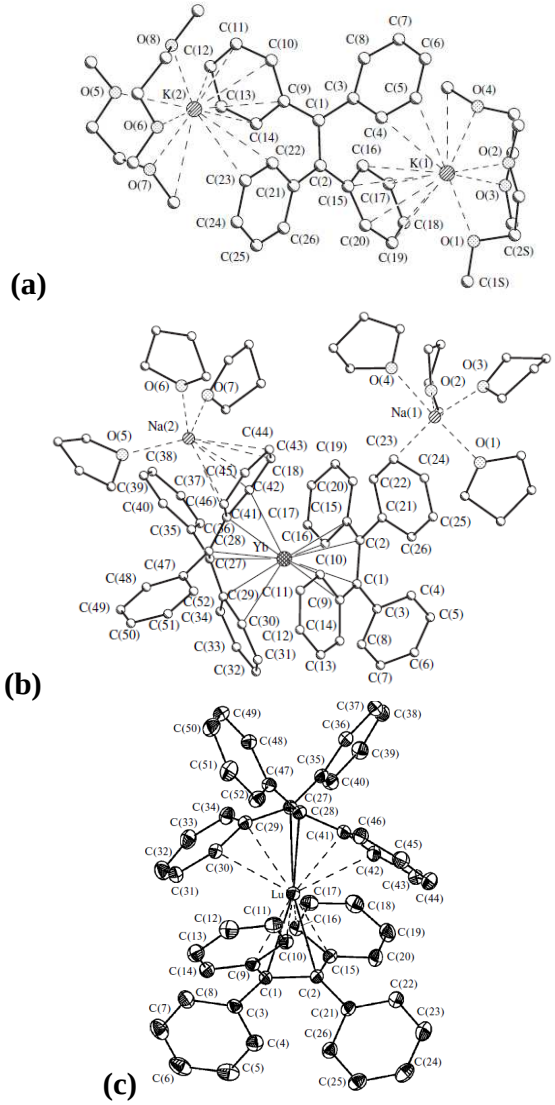

Figure 1.11 (a) Na salt of TPE dianion (b) Yb complex of TPE dianion (c) Lu complex of of TPE dianion.

Finally, the TPE skeleton is also subject to reduction, and TPE dianion can be generated via electron transfer from sodium metal.[31] The X-ray structure of the THF solvated sodium salt of TPE dianion is shown in Figure 1.11a. These salts can undergo transmetallation with lanthanides resulting in formation of inner transition metal salt. Two such complexes have been prepared, one with ytterbium[31] and one with lutetium[32] by Minyaev *et al.* These structures are shown in Figures 1.11b and c.

1.7 Summary

Supramolecular functional materials have been designed and synthesized using various core structures surrounded by known functional groups with required chemical and/or physical characteristics. One such interesting framework that has been utilized in this context is tetraphenylethylene. Functionalized derivatives of TPE are readily available via various straightforward synthetic transformations, rendering TPE derivatives attractive building blocks in supramolecular chemistry. Incorporation of functional groups along the periphery of TPE frameworks provides means to direct self-assembly events mediated by non-covalent interactions in order to construct functional materials with desirable redox and/or coordination properties

TPE's possess exciting optical and electronic properties that are unique. TPE and its derivatives are usually non-emissive in organic solutions, but when aggregated in solution or in the solid state, fluorescence is turned on which can be explained by restriction in molecular motion. This property has been exploited in design of fluorescent sensors with TPE cores for metal ions and biomolecules.

Additionally, electron rich TPE derivatives have low oxidation potentials and can be chemically oxidized in two sequential steps, yielding radical cation and dication products. This property may prove useful in design of TPE based electroactive materials. The relative rigidity and characteristic propeller like shape of TPE derivatives provide

well-defined geometric parameters that further increase the utility of these compounds in supramolecular chemistry.

The syntheses of several new TPE derivatives are described in the following chapters. These functionalized TPE's were targeted for study due to their likely ability to participate in selected non-covalent interactions important in supramolecular synthesis. Initial efforts aimed at constructing functional materials around these TPE core structures are also described.

CHAPTER II

SEMICONDUCTING ORGANIC ASSEMBLIES FROM TETRAPHENYLELTHYLENE TETRACARBOXYLIC ACID AND BIS(PYRIDINE)S

2.1 Introduction

An organic semiconductor is an organic material with electrical conductivity due to electron[33] flow intermediate in magnitude between that of a conductor and an insulator. Unlike conventional inorganic semiconducting materials, which are composed of covalent bonds between neighboring atoms, organic semiconductors are formed by weaker non-covalent interactions between molecules. These weak intermolecular attractions imbue organic semiconducting materials with greater flexibility and allow their use in novel electronic devices which cannot be fabricated using conventional brittle inorganic semiconductors. Organic semiconductors exhibit distinct advantages over their inorganic counterparts in terms of performance, cost, miniaturization and mechanical flexibility. There are two major overlapping classes of organic semiconducting compounds, cofacially stacked polyacenes-polyarenes and charge transfer organic complexes.

The first class of compounds includes polycyclic aromatic systems like pentacene (**2.1a**)[34] or various conjugated oligomeric and polymeric systems like polyacetylene[35] (**2.1b**) and its derivatives such as poly(p-phenylene vinylene) (**2.1c**).[36] Compounds like polythiophenes (**2.1d**)[37] can become conducting when electrons are added or removed from the conjugated π-orbitals via doping, a process in which impurities are intentionally added to pure material.

Organic semiconductors involving charge transfer complexes are dominated by derivatives of tetrathiafulvalene (**2.1**e or TTF). Wudl *et al.* demonstrated that the salt $[TTF^{+}]Cl^{-}$ is a semiconductor.[38] Subsequently, various charge transfer salts of TTF,

especially with quinone-based anions like TCNQ (**2.1f**) have been prepared and characterized.[39] Solid state studies of [TTF^+][$TCNQ^-$] have revealed stacks of partially oxidized TTF molecules with anionic stacks of TCNQ. This segregated stacking motif is responsible for the electrical properties. Various analogues of TTF like tetramethyltetrathiafulvalene,[40] tetramethylselenafulvalenes,[41] and bis(ethylenedithio)tetrathiafulvalene[41] have also been utilized for organic semiconducting applications.

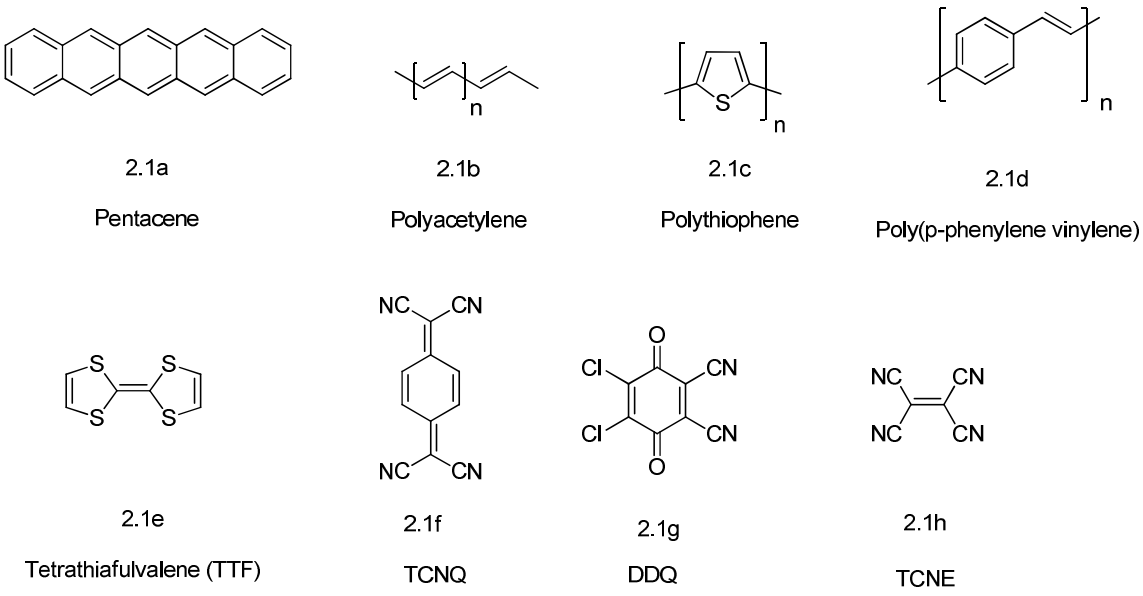

Figure 2.1 Some commonly used organic semiconducting materials

Analogous to conventional inorganic semiconductors like silicon and germanium, the performance of organic semiconductors is directly related to their molecular packing, crystallinity, growth, mode and purity. Typical current carriers in organic semiconductors are holes and electrons in π bonds. Almost all organic solids are insulators but when their constituent molecules have conjugated systems, electrons can move via π cloud overlap, especially by hopping, tunneling, and related mechanisms. In order to achieve the best

possible performance, it is important to understand electron or hole transport. Apart from TTF derivatives and various polyarenes (including ethylene diimides), semiconducting properties of other organic compounds have not been extensively examined.

2.2 Objective

In connection with efforts aimed at utilizing tetraphenylethylenes (TPEs) as organic scaffolds for various crystal engineering applications, we became interested in exploring the solid state redox activity of electron-rich derivatives. Specifically, we envisioned constructing ordered solid state charge transfer complexes via the combination of TPE donors and suitable electron acceptors, each incorporating elements of molecular recognition (e.g., H-bond donor and acceptors). While this original plan failed to yield tractable results, a series of charge transfer complexes was successfully prepared when a carboxylic acid functionalized TPE derivative was crystallized with several bis(pyridine)s. Significantly, computational and microscopy studies revealed these composites to possess semiconducting properties.

2.3 Results and Discussion

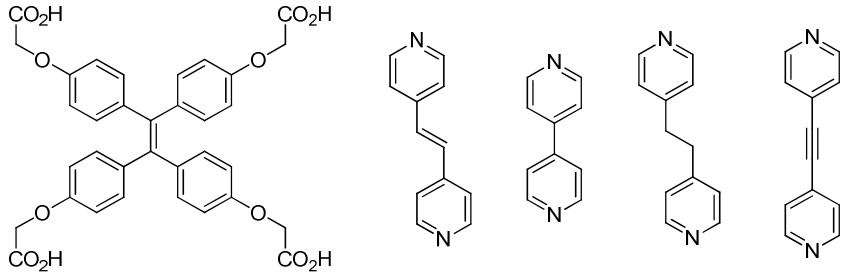

Figure 2.2 Components used for crystallization.

An electron rich TPE derivative functionalized with four carboxylic acid groups was identified as a suitable initial target for exploration of solid state charge transfer behavior. The synthesis of this compound is shown in Scheme 2.1. Commercially available 4,4'-dimethoxybenzophenone (**2.6**) served as starting material. Ketone **2.6** underwent McMurry reaction in the presence of $TiCl_4$ and Zn to yield tetraanisylethylene **2.7**.[29] Demethylation with BBr_3 gave the tetraphenol **2.8**.[29] Phenol **2.8** was then alkylated with ethyl bromoacetate to produce tetraester **2.9.** Saponification of the ester groups using KOH and re-acidified with 50% aqueous HCl afforded desired tetraacid **TCA** (**2.2**) as a pale yellow solid.[42]

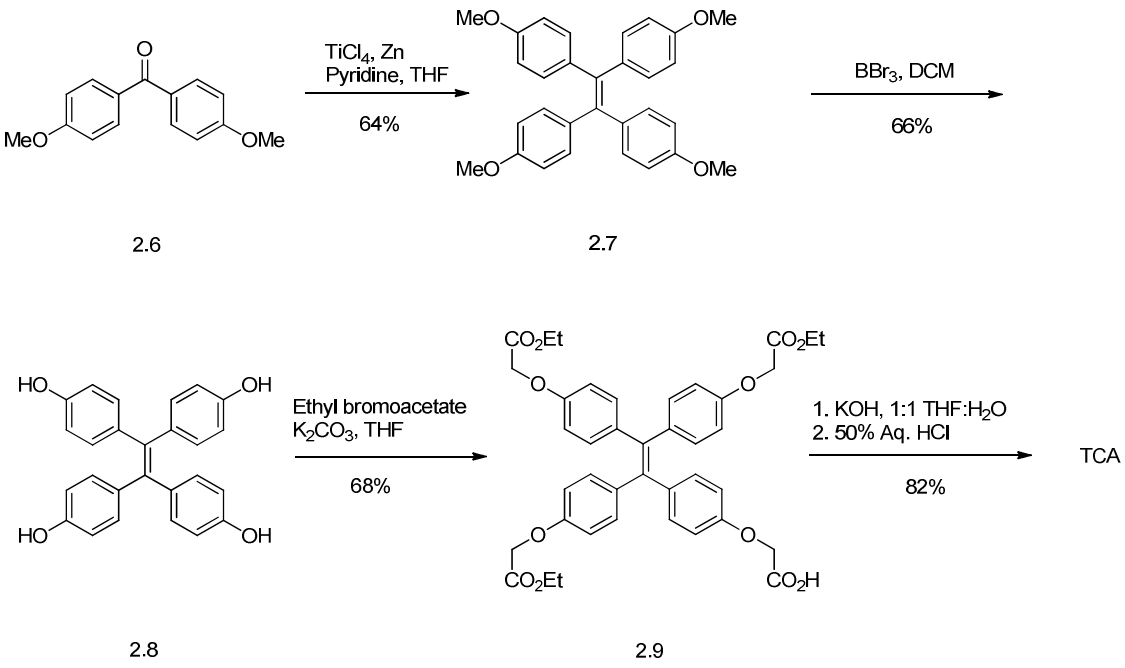

Scheme 2.1 Synthesis of tetraacid **TCA**.

With **TCA** in hand, we first attempted to prepare crystalline composites with recognized electron acceptors, such as TCNQ, DDQ and TCNE. Ultimately, these efforts

failed to produce single crystals. Moreover, visual evidence for charge transfer interactions was also not apparent. Given the difficulties encountered in attempting to combine **TCA** and various quinones within crystalline networks, we decided to examine the structure of **TCA** itself in order to gain insight into important solid state features of this putative supramolecular building block. Unfortunately, we have been unable to grow single crystals of **TCA**, despite repeated attempts under various conditions that included a variety of solvent combinations (a limiting factor, however, is the low solubility of **TCA** in solvents other than methanol and DMSO) and solvothermal crystallizations. We also tried to capitalize on acidic properties of **TCA** via crystallization in the presence of various alicyclic, aliphatic and aromatic diamines. Deposition of crystalline ammonium carboxylate salts, however, was not observed. Greater success was realized when we switched to pyridine based bases as crystallizing components, and several ordered crystalline composites were obtained using various bis(pyridine)s as described below.

TCA was crystallized with four different bis(pyridine)s, **BPE**, **Bpy, BPA**[43] and **BPEt** (Figure 2.1). Unlike previous efforts to obtain crystals of **TCA**, formation of bis(pyridine) composites were easily accomplished by mixing an acetone solution of bis(pyridine) with a methanol solution of **TCA** in a 2:1 molar ratio. After thoroughly mixing, the solution was allowed to slowly evaporate to yield crystals suitable for X-ray diffraction after 3-4 days.[42]

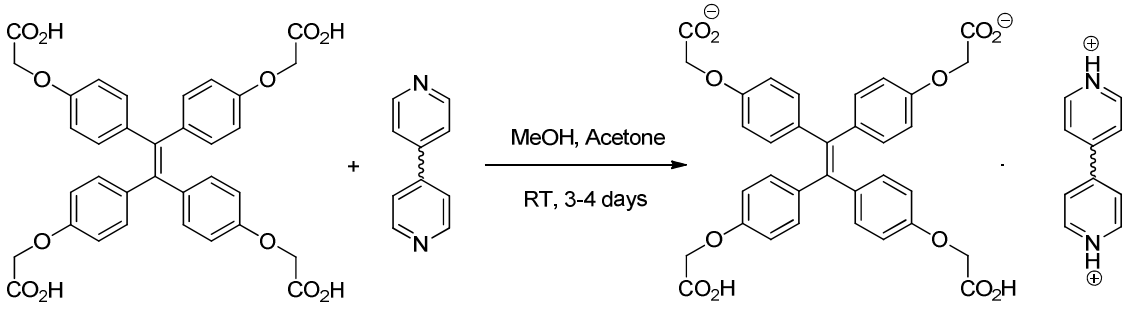

2.2

(TCA)

Scheme 2.2 Preparation of organic semiconducting crystals.

Contrary to expectations and starting molar ratios, crystals that were obtained exhibited a 1:1 stoichiometry between **TCA** and bis(pyridine). Examination of crystal structures (discussed below) revealed that two of the four carboxylic acid groups on each TPE were deprotonated by bis(pyridine) reagent. Thus, the remaining carboxylic acids may experience a decrease in acidity, in turn contributing to the observed **TCA**:bis(pyridine) stoichiometry. The structure of **TCA·BPE** shown in Figure 2.3a illustrates many features common to all four structures.

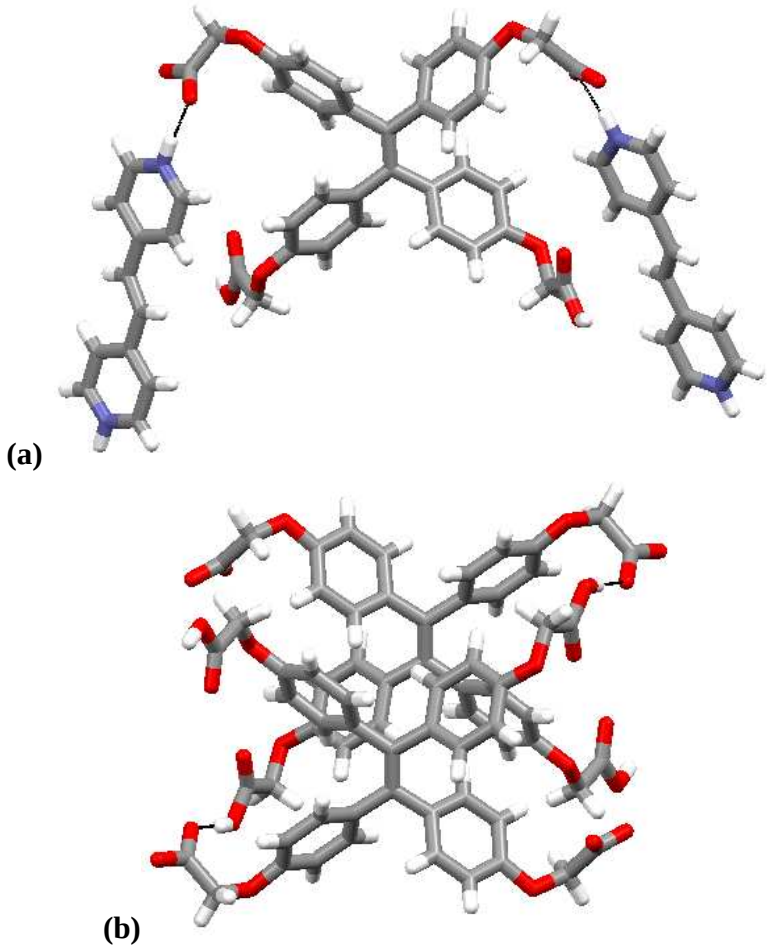

Figure 2.3 (a) Repeating unit of pyridinium dicarboxylate in **TCA·BPE** (b) Stacking of **TCA** mediated by $CO_2H\cdots{}^{-}O_2C$ hydrogen bonding.

Molecules of **TCA** adopt a propeller-like conformation which is common to many TPE-containing molecules in the solid state.[9] Two geminal carboxylic acid residues (with respect to the central olefin) are deprotonated and both nitrogen atoms the BPE units are protonated, resulting in bis(pyridinium) dicarboxylate as the repeating unit. This is concluded from the position of hydrogen atoms (which were crystallographically located) and similar C-O bond lengths in carboxylate residues. In addition, the C-N-C angle in each pyridine ring experiences a slight flattening upon protonation, and the observed values for this angle (~120°-121°) are slightly larger than corresponding free base

(~116°-117°).[44] Thus, both carboxylate residues are engaged in charge assisted hydrogen bonding with pyridinium N-H groups as indicated by the black dashed lines (Figure 2.3a). The two remaining carboxylic acid residues in each TPE are involved in hydrogen bonding interactions with carboxylate units of adjacent layers as shown in Figure 2.3b. One carboxylic acid residue interacts with a molecule above and the other interacts with a molecule below also resulting in head-to-tail stacking of individual molecules of **TCA**. All four structures have disordered solvate molecules (methanol and acetone, location indicated in Figure 2.4a) within the crystalline matrix, but these do not appear to participate in any interactions with either **TCA** or bis(pyridine)s.

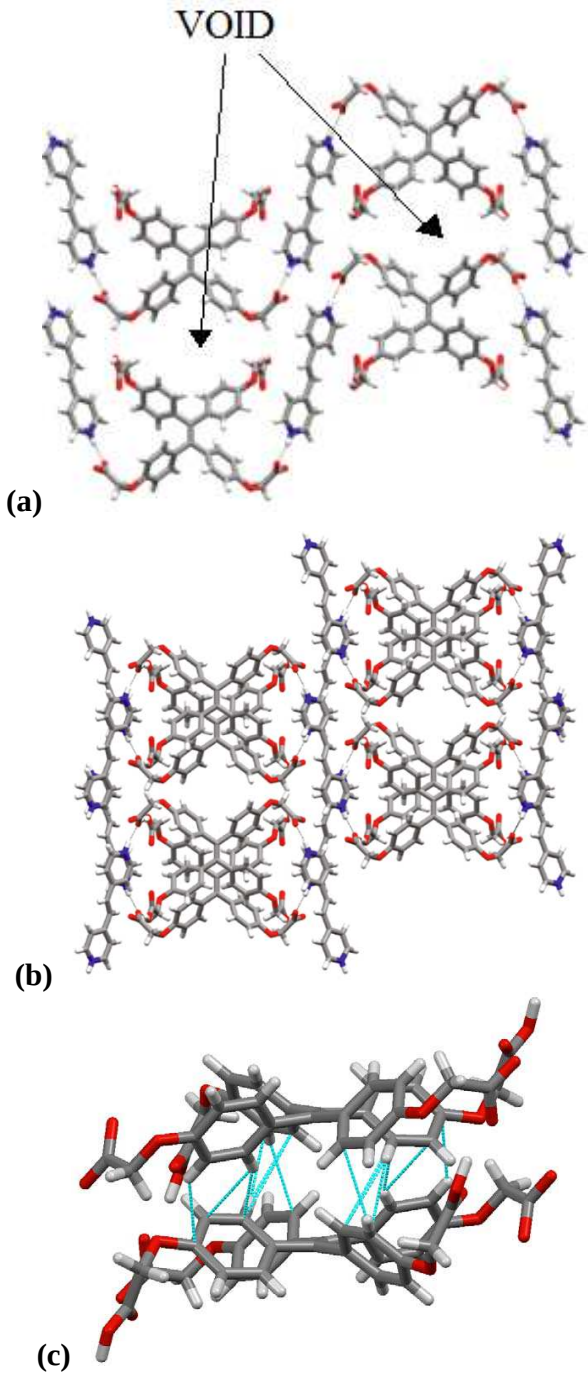

Figure 2.4 (a) 2D layers formed via charge assisted hydrogen bonding in **TCA·BPE** (b) Stacking of 2D layers mediated by $CO_2H\cdots^{-}O_2C$ hydrogen bonding in **TCA·BPE** (c) Edge to face arene contacts in columns of **TCA**. Disordered solvates omitted for clarity.

In the crystal structure of **TCA·BPE**, each molecule of **TCA** bridges two molecules of **BPE**. This results in generation of 2D layers that are mediated by charge assisted hydrogen bonding interactions as shown in Figure 2.4a. Hydrogen bonding interactions between carboxylate anion groups and carboxylic acid residues helps to mediate stacking of these 2D layers (Figure 2.4b). This stacking motif is further reinforced by edge-to-face arene stacking of **TCA** molecules (Figure 2.4c). Solvent molecules occupy void space between two adjacent molecules of **TCA** as indicated in Figure 2.4a.

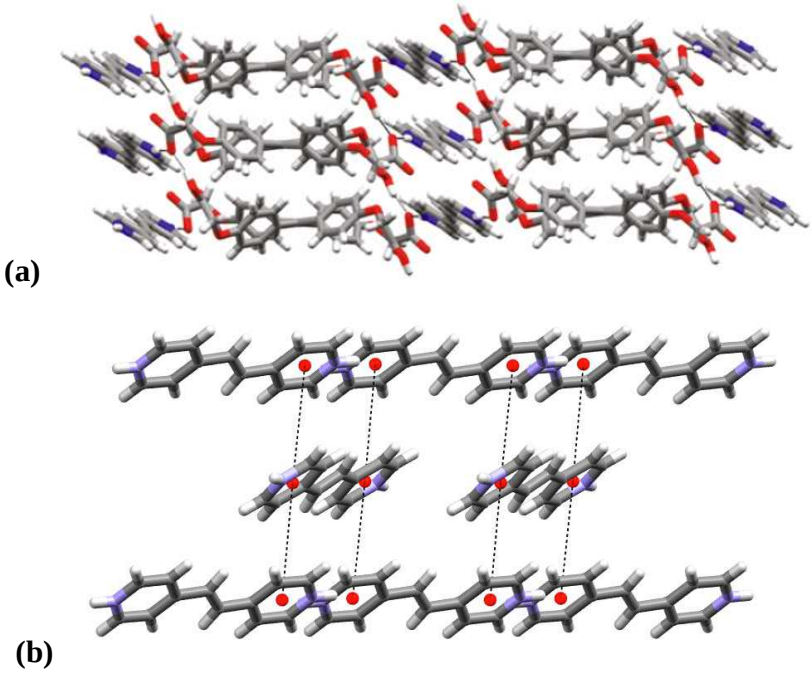

Figure 2.5 (a) View of **TCA·BPE** illustrating segregated columns of **TCA** and **BPE** (b) Stacking of **BPE** molecules in **TCA·BPE**.

As a consequence of these stacking interactions, individual 2D layers are aligned 180° in slightly offset fashion to produce an *abab*-type pattern. This results in well-defined segregated columns of **TCA** and **BPE** as shown in Figure 2.5a. Individual

molecules of **BPE** are arranged in a cofacial fashion with centroid-centroid distance of 4.646 Å (Figure 2.5b). This cofacial alignment may indicate the presence of π stacking interactions between **BPE** arenes. As will be discussed later, these interactions may play an important role in defining the conducting properties of the **TCA·BPE** crystalline assembly.

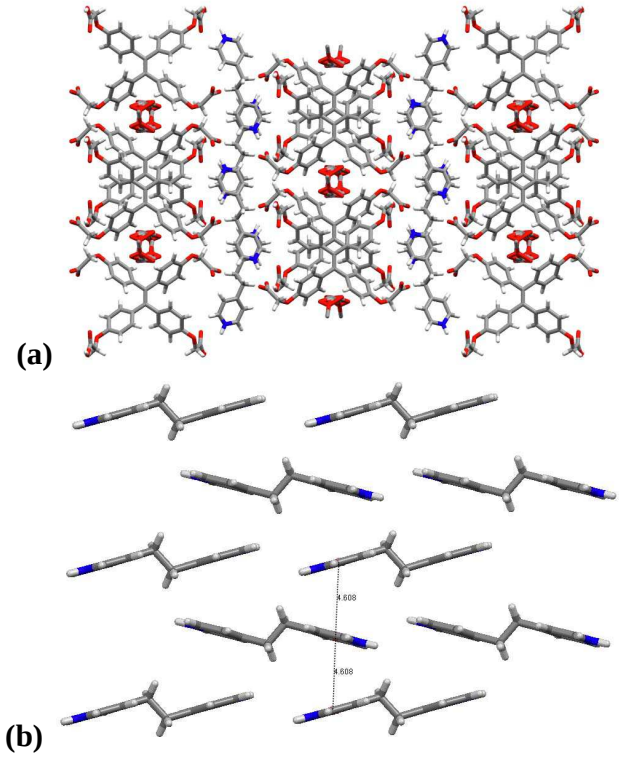

Figure 2.6 (a) Packing of **TCA·BPEt** (b) **BPEt** layers in **TCA·BPEt**.

The single crystal structure of **TCA·BPEt** was found to be isostructural with **TCA·BPE**. Similar to **TCA·BPE**, **TCA·BP*Et al.*** so displays formation of 2D layers of anionic carboxylate and bis(pyridinium) components facilitated by charge assisted hydrogen bonding. These 2D layers are stacked mediated by $CO_2H\cdots O_2C$ hydrogen bonding interactions (Figure 2.6a) as well as edge-to-face arene interactions. This results

in segregated regions of **BPEt** and **TCA**. Individual molecules of **BPEt** are aligned cofacially as shown in Figure 2.6b. The only difference between **TCA·BPE** and **TCA·BPEt** structures is the presence of a π bond linking the two pyridinium rings. In other words, pyridinium groups in **TCA·BPEt** are not conjugated, and this appears to exert a significant influence over the conductivity of the material (which will be discussed in a later section).

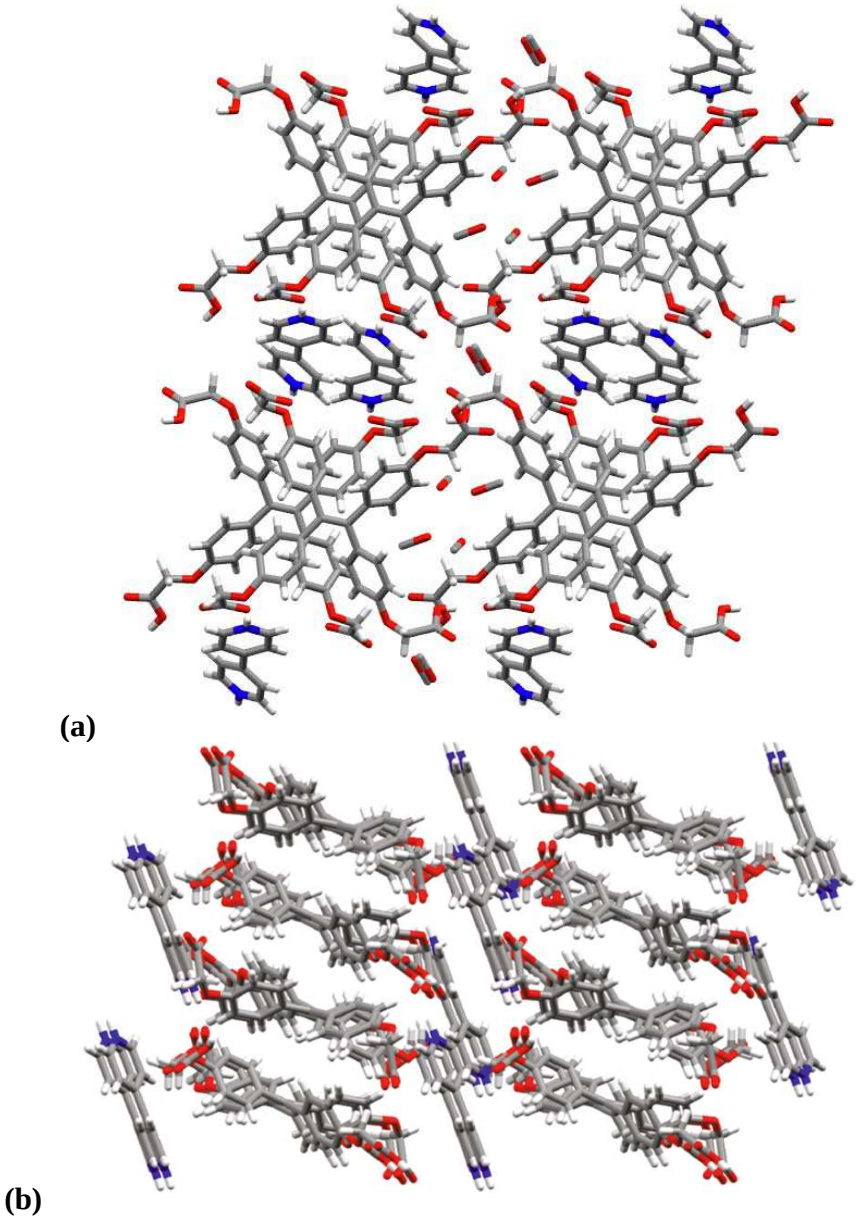

Figure 2.7 (a) View of **TCA·Bpy** (b) View of **TCA·Bpy** illustrating columns of **TCA** flanked by layers of **Bpy**.

The structure of **TCA·Bpy** possesses features similar to **TCA·BPE** and **TCA·BPEt** but differs in the overall packing arrangement of the components. Once again, bis(pyridinium) units bridge molecules of **TCA** via charge assisted hydrogen

bonding. Additionally, $CO_2H\cdots O_2C$ hydrogen bonding interactions are also evident (Figure 2.7a). However, in this case, molecules of **Bpy** and **TCA** are arranged in step-like fashion, rather than distinct layers as was the case in the **TCA·BPE** and **TCA·BPEt** crystals (Figure 2.7b). Despite the different packing arrangement, segregated columns of **Bpy** and **TCA** are clearly evident. These columns are separated by layers of **Bpy** molecules oriented with their long axis roughly parallel to **TCA** stacking direction. This packing results in cofacial stacking of bis(pyridinium) rings that are separated by 4.366 Å. Bpy stacks run through the crystalline matrix perpendicular to the charge assisted hydrogen bond network between **TCA** and **Bpy** (Figure 2.8). As will be discussed later, this cofacial stacking of **Bpy** arene rings may play an important role in determining the conducting properties of this crystalline assembly.

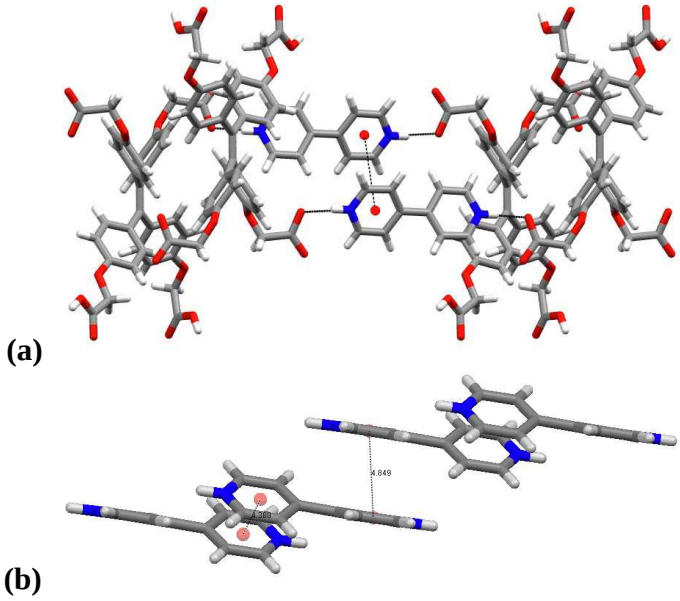

Figure 2.8 (a) Partial packing of **TCA·Bpy** showing cofacial arrangement of pyridinium (b) **Bpy** layers in **TCA·Bpy**. Methanol solvates omitted for clarity.

The single crystal structure of **TCA·BPA** was found to be isostructural to **TCA·Bpy**. Similar to **TCA·Bpy**,in the structure of **TCA·BPA** individual molecules of **TCA** and **BPA** are arranged via charge assisted hydrogen bonding. Additionally, $CO_2H\cdots O_2C$ hydrogen bonding interactions are also evident. Segregated columns of **BPA** and **TCA** are seen. This packing results in cofacial stacking of bis(pyridinium) rings that are separated by 3.386 Å.

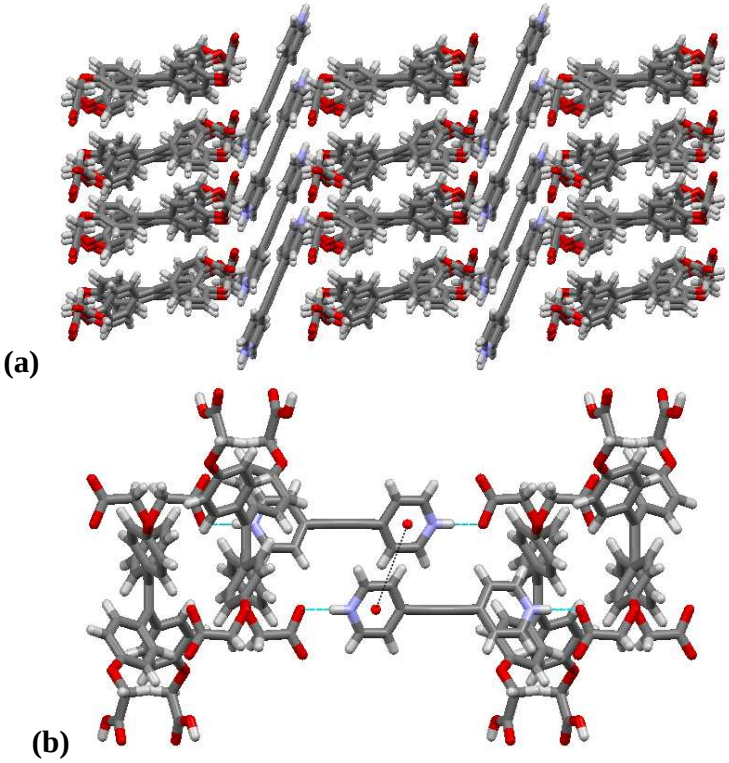

Figure 2.9 (a) View of **TCA·BPA** illustrating columns of **TCA** flanked by layers of **BPA** (b) Partial packing of **TCA·BPA** showing cofacial arrangement of pyridinium. Solvate molecules omitted for clarity.

Interestingly, the color of these crystals varied from pink for **TCA·BPE**, to orange for **TCA·Bpy** to yellow for **TCA·BPEt** to red for **TCA·BPA** as compared to colorless or pale yellow starting materials. This change in color indicates some type of

charge-transfer phenomenon occurring, presumably between electron-rich **TCA** and electron deficient bis(pyridine). These charge transfer interactions are expected to be enhanced by proton transfer which results in **TCA** being converted to a dicarboxylate and the bis(pyridine)s being converted to bis(pyridinium) cations. However, this charge transfer was not apparent from crystal structure data. For example, if **TCA** acquires radical cation character, the central olefin is expected to elongate, which did not happen. In all four crystals, this bond length ranged between 1.358 and 1.363 Å, which was comparable to the C=C bond length reported for tetraanisylethylene (1.359 Å) but significantly shorter than bond length reported for the corresponding radical cation (1.417 Å).[9]

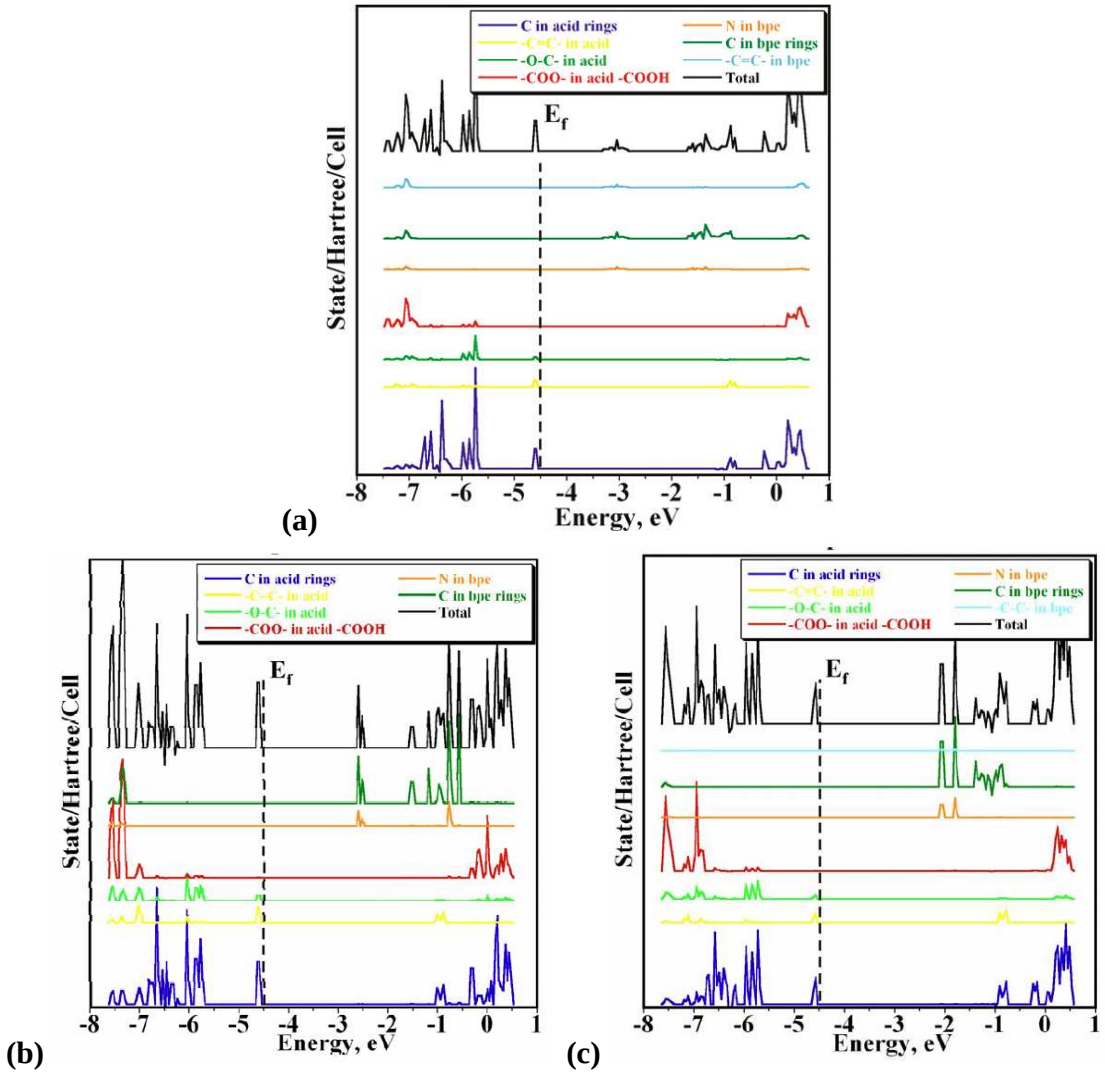

Figure 2.10 DOS calculations for (a) **TCA·BPE** (b) **TCA·Bpy** and (c) **TCA·BPEt**. Fermi energy (E_F, dashed line) corresponds to the energy of the HOCO.

The color changes observed during crystallization of the composites prompted us to examine the apparent charge transfer interactions in more detail. The X-ray diffraction structure data obtained for **TCA·BPE**, **TCA·BPA, TCA·BPEt**, and **TCA·Bpy** were subjected to further quantum chemical refinement. These DFT calculations were performed by our collaborator Dr. Jonas Baltrusaitis. Periodic *ab initio* solid state program suite CRYSTAL'09 was used in all calculations.[45] This program uses the

functions localized on atoms as the basis for expansion of the crystalline orbitals via the linear combination of atomic orbitals (LCAO) technique.

For these calculations, one molecule of **TCA** and one molecule of bis(pyridine) was considered as a unit and geometry was optimized. Optimized atomic positions were subjected to density of state (DOS) calculations to identify crystalline orbitals involved in the charge transfer process. Calculated atom and total density of states for **TCA·BPE**, **TCA·Bpy**, and **TCA·BPEt** are shown in Figure 2.10a, 2.10b and 2.10c, respectively. In these figures, Fermi energy (E_F) is defined as the top of the topmost occupied (valence) band with the bandgap defined as the energy difference between the topmost occupied and bottom virtual (conduction) crystalline bands. Atomic projections of densities of states shown in the figures represent a sum of contributions of: (1) all carbon atoms, (2) C=C bonds, (3) -O-C-, and (4) -COO- functional groups in acid molecules (**TCA**) and (5) nitrogen, (6) carbon atoms in bis(pyridine) rings and (7) –C-C- or –C=C- (except for **Bpy**) functional groups in bis(pyridine) molecules. In this way, the charge donors (e.g., atoms or functional groups in a certain molecule contributing to the topmost occupied crystalline bands) and charge acceptors (e.g., atoms or functional groups contributing to the bottom virtual crystalline bands) can be identified. Hydrogen atom contributions were found to be negligible in the -8 to 1 eV region and thus are not shown. In all four compounds, major contributors to the top of the valence bands were carbon atoms in aromatic rings of **TCA**, as well as –C=C and –O-C- functional groups in the acid molecules. E_F in all cases was located at ~-4.5 eV. The bottom of the conduction band and its main contributors, however, varied between all four compounds. In **TCA·BPEt** and **TCA·Bpy** major contributors were nitrogen and carbon atoms in bis(pyridine) rings. The sp^3 hybridized –C-C- bond in **TCA·BPEt** did not affect the position of the bottom of the conduction band. A very different picture of the bottom conduction band emerged from **TCA·BPE** projected density of states, where sp^2 hybridized –C=C- bond facilitated charge transfer by shifting bottom of conduction band to ~ -3.5 eV. This effect was also

readily seen from the calculated bandgap values for **TCA·BPEt**, **TCA·Bpy** and **TCA·BPE** of 2.47, 1.99, and 1.28 eV, respectively. Thus, appearance of conjugation and empty π orbitals in the –C=C- functional group significantly changed the magnitude of the crystal bandgap. Preliminary calculations performed on **TCA·BPA** indicate an even smaller band gap of 0.77 eV, but this material has not been further characterized due to difficulties encountered in preparing bulk crystalline samples.

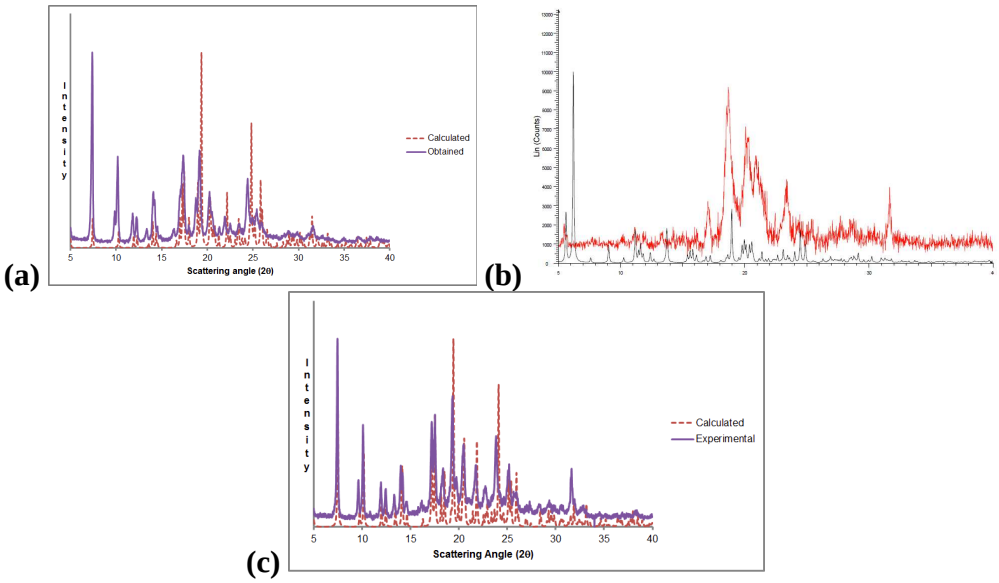

Figure 2.11 Comparision of calculated and experimental powder XRD pattern obtained from bulk samples of (a) **TCA·BPE** (b) **TCA·Bpy** and (c) **TCA·BPEt**.

The calculated band gaps of our composites are comparable to the band gaps found in established semiconductors (like 1.11 eV for Si and 0.67 eV for Ge). Given this situation, we wondered if these composites would also exhibit semiconducting behavior. In order to investigate conducting properties, nano-crystalline materials were prepared by mixing equimolar solutions of **TCA** and bis(pyridine)s and allowing the solvent to evaporate slowly. Samples prepared in this manner were found to be homogeneous and

colors of bulk samples matched the colors of the corresponding single crystals where **TCA·BPE** sample was pink, **TCA·Bpy** sample was orange and **TCA·BPEt** sample was yellow. An exception was encountered in the case of **TCA·BPA**. A stable bulk sample of this material has not been successfully prepared using the procedure outlined above. The morphologies of bulk samples were compared to single crystals by powder XRD, and were found to be identical in each case as shown in Figure 2.11. In the case of **TCA·Bpy** PXRD, slight differences in the two spectra are attributed to loss of included solvent. In general, crystals of **TCA·Bpy** were more fragile than the other two samples and drying in air or brief exposure to vacuum resulted in partial conversion to amorphous material.

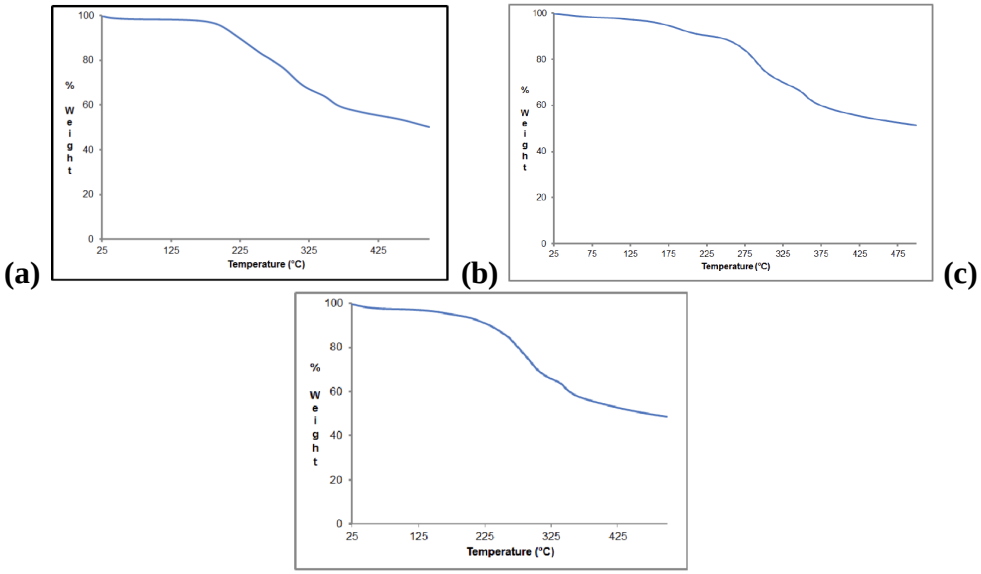

Figure 2.12 TGA trace of (a) **TCA·BPE** (b) **TCA·Bpy** and (c) **TCA·BPEt**.

Thermal stability of the bulk samples was determined by thermogravimetric analysis (TGA). TGA traces for all three samples are shown in Figure 2.12. In the case of **TCA·BPE**, the percentage of sample mass remaining at 203 ºC (94.3%) corresponds to complete loss of methanol and acetone solvates indicated in the single crystal X-ray data.

Similarly, solvent loss in samples of **TCA·Bpy** and **TCA·BPEt** was found to occur at 245 ºC (89.1%) and 179 ºC (94.8%) respectively.

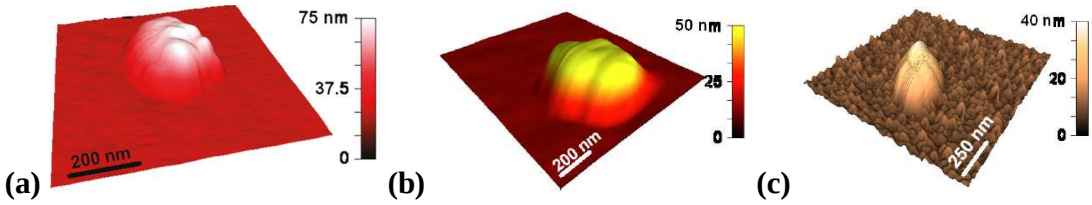

Figure 2.13 Representative 3D crystal image for (a) **TCA·BPE** (b) **TCA·Bpy** and (c) **TCA·BPEt**.

The electrical properties of these crystalline assemblies were then measured using conducting probe atomic force microscopy (CP-AFM). This was performed by our collaborators Dr. Alexei Tivanski and Ms. Lindsay Ditzler. The sample substrates were prepared by thermally depositing Au on mica. Crystals were suspended in hexanes and deposited on the Au substrate. Samples were allowed to dry for 20 minutes to allow solvent to evaporate and then immediately used for the conductivity measurements. All measurements were performed in an insulating bicyclohexyl solution to reduce water contamination and decrease the adhesion forces caused by capillary forces between the AFM probe and sample due to water layer formation on the tip-surface interface. Crystals were imaged to obtain height of individual crystals (Figure 2.13). Crystals with heights between 20 and 300 nm were used for the *I-V* measurements. For these experiments the force of the AFM tip upon the crystals was held constant at 50 nN. This force was found to be sufficient to ensure a stable electrical contact resulting in reproducible *I-V* measurements without physically damaging the crystals. The voltage was swept over various ranges, depending on the crystal thickness. For thinner crystals, a smaller volatage range was used to prevent saturation of the current. A combination of large

applied forces and high current density sometimes resulted in irreversible changes in crystal morphology. For that reason, crystals were imaged after the conductive measurements to be sure that the crystals remained intact throughout the experiment.

Representative I-V curves are shown in Figure 2.14 for **TCA·BPE**, **TCA·Bpy**, and **TCA·BPEt**. It is important to note that the I-V curve for **TCA·BPE** has been divided by a factor of 100 to be displayed on the same scale as the curves for the other two samples. From the representative data shown in Figure 2.14, it is clear that crystals of **TCA·BPE** are highly conductive, while **TCA·Bpy** is moderately conductive and **TCA·BPEt** showed no measurable current throughout the voltage bias range of the measurement considering detection limits of the instrument (10 pA).

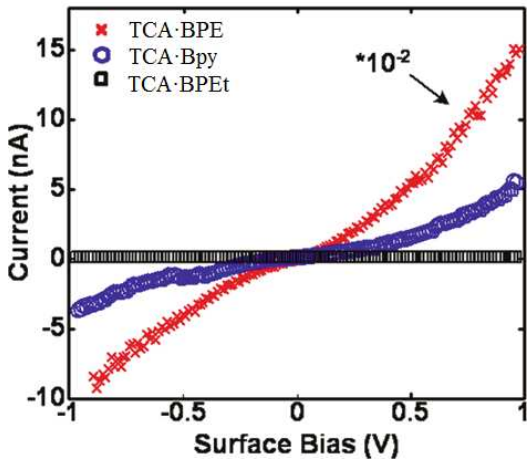

Figure 2.14 Representative I-V curves for **TCA·BPE** (red crosses), **TCA·Bpy** (blue circles) and **TCA·BPEt** (black squares). The TCA·BPE is scaled down by a factor of 100 as indicated.

The resistivity (ρ) of **TCA·BPE** and **TCA·Bpy** was calculated using the slope of the near linear Ohmic region of the I-V curves (bias range ±0.15V). These values, along with crystal height (measured directly from AFM images) and estimated contact area, were used to calculate resistivity (ρ) using the formula $\rho=R(a/h)$ where a is contact area

and h is height of the crystal. The Hertzian elastic contact model was used to estimate the AFM tip-surface contact area.[46]

$$a^2 = \left(\frac{Fr}{K}\right)^{2/3}$$

Here, a is contact area, r is radius of tip (150 nm), F is the loading force (50 nN), and K is an effective modulus equaling

$$K = \frac{4}{3}\left[\frac{1-\nu_{Tip}^2}{E_{Tip}} + \frac{1-\nu_S^2}{E_S}\right]^{-1}$$

where E_S, υ_S, E_{Tip} and υ_{Tip} are the Young's modulus and Poisson's ratio of the sample and the AFM tip respectively. The Poisson ratio for most materials is between 0.25 and 0.5,[46] and thus assuming $\upsilon_{Tip} \approx \upsilon_S \approx 0.33$, an effective modulus can be approximated as $K = 1.5E_{Tip}E_S/(E_{Tip}+E_S)$. The elastic modulus of the diamond tip is 1220 GPa.[47] The E_S for similar organic materials was assumed to be 350 MPa.[48] Using the parameters above, the contact area between diamond-coated AFM tip and crystal is estimated to be 1850 ±50 nm^2.

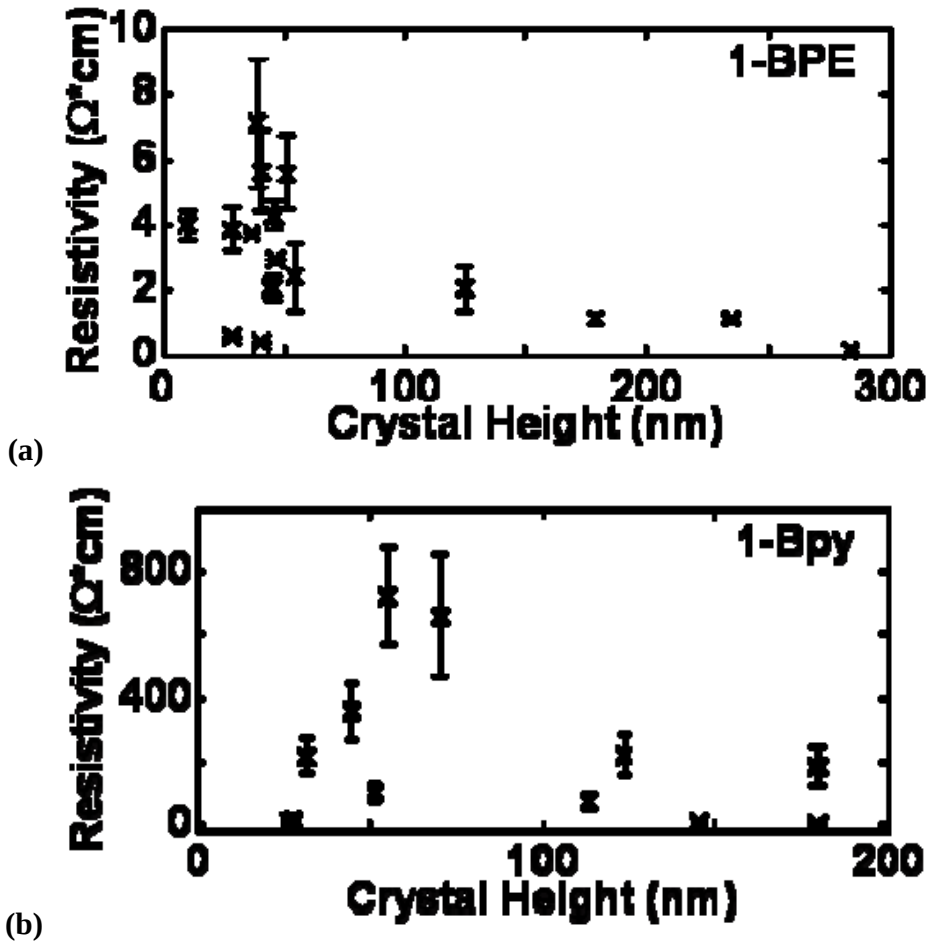

Figure 2.15 Plot of resistivity vs. crystal height for (a) **TCA·BPE** and (b) **TCA·Bpy**.

The distribution of resistivity values as determined above as a function of crystal height for **TCA·BPE** and **TCA·Bpy** are shown in Figure 2.15a and 2.15b respectively. Each data point in Figure 2.15 represents a crystal that was subjected to electrical measurements. The error bars indicate the range of resistivity determined from 15 separate I-V measurements. The deviations in I-V measurements can be due to orientation of the crystals and differences in morphology of the crystals resulting in varied degree of contact with the tip surface. Crystals of **TCA·BPEt** showed virtually no current over the bias range scanned, hence measurements were performed on a relatively

lower number of samples. Conductivity (σ, the reciprocal of resistivity) was calculated for each sample and this data is shown in Table 2.1.

An important parameter in semiconductors is the effective mobility, which is a measure of how fast electrons (or holes) move through the material. In general, higher effective mobilities mean better semiconductors. From the data in hand, we initially attempted to calculate effective mobilites by applying the space charge limited current model.[49,50] In this model, a plot of I vs. V^2 should be approximately linear and the charge mobility (μ) can be calculated from the slope. In the case of both **TCA·BPE** and **TCA·Bpy** plots of I vs V^2 were significantly nonlinear, rendering the SCLC model inappropriate for mobility determination. Instead we calculated charge mobilites using a simple empirical model developed by Brown *et al*. that relates charge mobility to conductivity ($\mu = \sigma^{0.76}$).[51,52] Data for effective mobilities is also shown in table 2.1.

Table 2.1 Physical and electrical properties of TCA·Bis(pyridine) crystals.

Crystal	Color	Band gap (eV)	ρ (Ω·cm)	σ ($S \cdot cm^{-1}$)	μ_{eff} ($cm^2/V \cdot s$)
TCA·BPE	Pink	1.28	3.6±0.9	0.28±0.06	0.38±0.05
TCA·Bpy	Orange	1.99	213±70	$(4.7\pm1.3)\times10^{-3}$	$(1.7\pm0.4)\times10^{-2}$
TCA·BPEt	Yellow	2.47	$>2.4\times10^{6}$	not calculated	not calculated
TCA·BPA	Red	0.77			

The results obtained from CP-AFM conductivity measurements clearly show that **TCA·BPE** and **TCA·Bpy** function as crystalline organic semiconductors, whereas **TCA·BPEt** acts as insulator. Effective mobilities for the two conducting samples are comparable to known organic semiconducting crystalline materials like thiophene and TTF.[53-55] Moreover, our results also demonstrate an ability to tune the conducting properties as a function of bis(pyridine) component. The most conjugated bis(pyridine)

reagent (**BPE**) afforded crystals with **TCA** exhibiting a conductivity approximately 2 orders of magnitude greater than that for crystals obtained from **Bpy**, while crystals derived from **TCA** and non-conjugated **BPEt** were comparatively non-conducting. These conducting properties correlate nicely with the band gaps obtained via quantum chemical calculations.

Currently the relative contributions of **TCA** and the bis(pyridine) moieties in governing charge mobility are not known. The high conductivity exhibited by **TCA·BPE** and the absence of conductivity in **TCA·BPEt** despite their isostructural crystalline networks suggests a vital role for the bis(pyridine) units as principal charge carriers. In the case of **TCA·BPE** as well as **TCA·Bpy**, pyridinium rings are arranged in cofacial orientations and π-conjugation between these rings may facilitate charge transport across layers. Alternatively, **TCA** may also contribute in some degree to the conducting properties of these assemblies as a consequence of intermolecular arene edge-to-face interactions and/or participation in extended H-bonded networks. In order to study charge transport in detail, the sample must be connected in transistor configuration and then AFM measurements have to be performed.

2.4 Conclusion

Principles of crystal engineering have been applied toward construction of supramolecular assemblies between an acid functionalized tetraphenylethylene **TCA** and four different bis(pyridine)s, **BPE**, **Bpy, BPA** and **BPEt**. Each assembly was structurally characterized by X-ray diffraction. Charge transfer interactions were observed and were studied in detail by quantum chemical calculations. Density of state (DOS) calculations were performed on experimental X-ray data after optimization of geometry. These calculations determined crystal band structure and band gap. Changes in crystal color and in conjugation of the bis(pyridine) component both correlated with calculated band gap energies. Conducting properties of these materials were investigated by conducting

probe-AFM. Two of these crystals displayed charge carrying capacity and conductivities as well as effective mobilities in the range of established organic semiconductors. Conducting properties of these crystals can be modulated as a function of bis(pyridine) component where mobilities increased with increased conjugation in bis(pyridine). This study not only opens exciting opportunities for construction of new tunable electroactive organic materials but also illustrates the potential of tetraarylethylenes as attractive supramolecular building blocks.

CHAPTER III

AGGREGATION-INDUCED EMISSION PROPERTIES AND SOLID STATE STRUCTURES OF TETRAPYRIDYL TETRAPHENYLETHYLENES

3.1 Introduction

Fluorescence is a form of photoluminescence in which atoms or molecules are excited to a singlet excited state by absorption of electromagnetic radiation. The excited species then relax back to the ground state, giving up their excess energy as photons emitted at longer wavelengths than the initially absorbed light.[56] In 1954, Förster and Kasper discovered that the fluorescence of pyrene was weakened with an increase in its solution concentration.[57] It was soon recognized that this was a general phenomenon for many aromatic molecules.[58,59] This concentration quenching effect was found to be caused by formation of sandwich-shaped excimers and exciplexes aided by collisional interactions between the aromatic molecules in excited and ground states.[60] The ubiquitous concentration quenching effect has forced researchers to study and utilize fluorophores as isolated single molecules in very dilute solutions. Even in dilute solutions, concentration quenching can still occur as aggregation can increase local fluorophore concentration. This problem is even more pronounced in the solid state as molecules are located in immediate vicinity. This can produce intermolecular interactions (such a π-π stacking interactions) that result in excited state decay via non-radiative pathways. This phenomenon is sometimes referred to as aggregation-caused quenching (ACQ) (Figure 3.1).

In 2001, Tang, *et al.* discovered a system involving 1-methyl-1,2,3,4,5-pentaphenylsilole, where luminogen aggregation played a constructive role in the light emission process.[61,62] A series of silole molecules were observed to be non-luminescent in solution phase but became emissive in aggregated states, either as nanoparticle

suspensions in poor solvents or as thin films in the solid state (Figure 3.1). As non-luminescent silole molecules were induced to emit by aggregate formation, the term 'aggregation-induced emission' (AIE) was coined.[62]

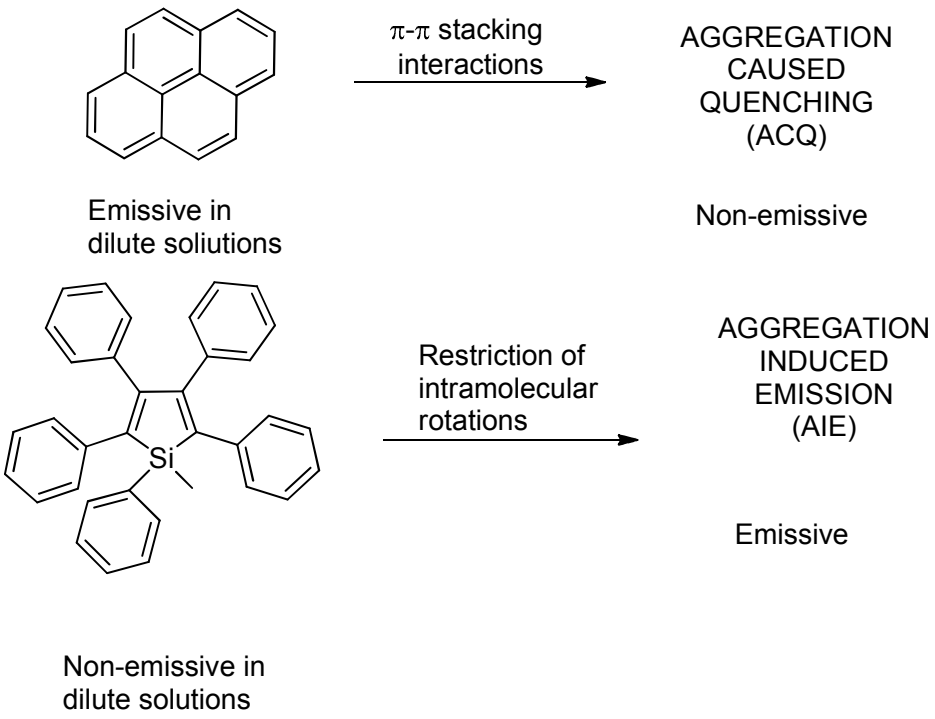

Figure 3.1 Phenomenon of aggregation caused quenching (ACQ) and aggregation-induced emission (AIE).

Tetraphenylethylenes have been observed to fluoresce when aggregated as solids or in solutions in which the TPE's are sparingly soluble. It is believed that restriction of intramolecular motion, principally aryl-alkene bond rotations, provide the physical basis for the observed photoluminescence.[63] Derivatives of TPE have been incorporated into organic polymers and oligomers with the resulting materials displaying fluorescence profiles that can be perturbed according to the density of TPE units within the polymer/oligomer and the environment surrounding the bulk material.[64] Alternatively,

discrete fluorescent sensors for biomolecules and metal ions have been prepared by attachment of specific ligands to TPE scaffolds using flexible spacers.[65]

3.2 Objective

We are interested in harnessing AIE properties of novel TPE derivatives based on organic and metal-organic precursors. Ultimately, we aim to utilize the fluorescence response of these materials to signal supramolecular functions ranging from chemical sequestration to catalysis. As a first approach to molecules that fit this design criteria, two rigid tetra(pyridyl)-substituted TPE derivatives **3.1** and **3.2** have been prepared.[30,66]

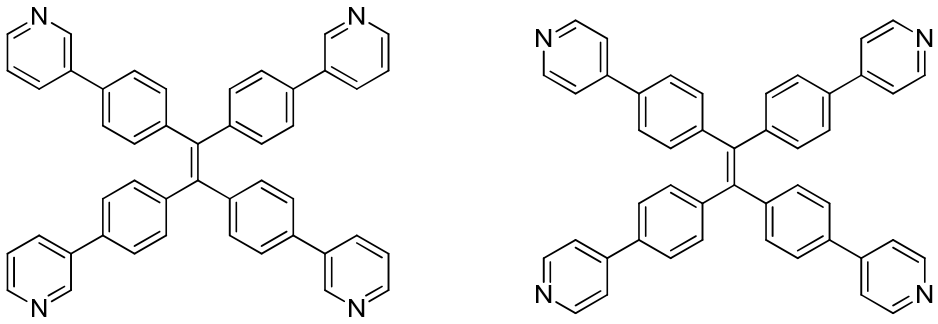

3.1 3.2

Figure 3.2 Compounds used in this study.

The AIE properties of both compounds have been examined in the solid state as well as in organic/aqueous solution mixtures. The Lewis basic residues lining on periphery of these compounds potentially offer a means to modulate the fluorescence response of these materials in aqueous solutions as a function of pH. Additionally, both **3.1** and **3.2** have been structurally characterized by X-ray diffraction. An attempt to crystallize these TPE derivate with $Fe(ClO_4)_3 \cdot H_2O$ resulted in conversion of these compounds to their respective tetrapyridinium tetra-perchlorate salts. These salts were isolated as single crystals and their structures were determined by X-ray diffraction.

3.3 Results and discussion

A straightforward route was used for preparation of **3.1** and **3.2** as shown in Scheme 1. Tetra(bromophenyl) ethylene[18] **3.4** was prepared from TPE by bromination with neat bromine as described by Schultz, *et al.* The key transformation involved four fold Suzuki coupling between **3.4** and either 3- or 4-pyridyl boronic acid.[30] Both products proved to be readily soluble in organic solvents and purification was easily accomplished by flash column chromatography to provide **3.1** and **3.2** as pale yellow solids.[66]

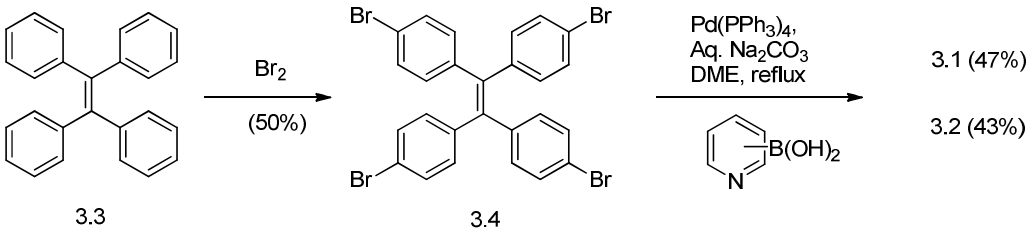

Scheme 3.1 Synthesis of **3.1** and **3.2**.

3.3.1 Aggregation-induced emission properties of **3.1** and **3.2**

Both **3.1** and **3.2** were markedly fluorescent in the solid state as revealed qualitatively using a hand-held UV lamp. Both pyridyl TPE's **3.1** and **3.2** were dissolved in dichloromethane and deposited on a glass slide to form films which were subjected to solid state fluorescence using an excitation wavelength of 375 nm. The solid state spectra of **3.1** and **3.2** were found to be virtually identical with each compound displaying a broad emission centered at ~510 nm as shown in Figure 3.3. The emission maxima correspond to green color which agrees with visual inspection of the compounds under a hand held UV light.

(a)

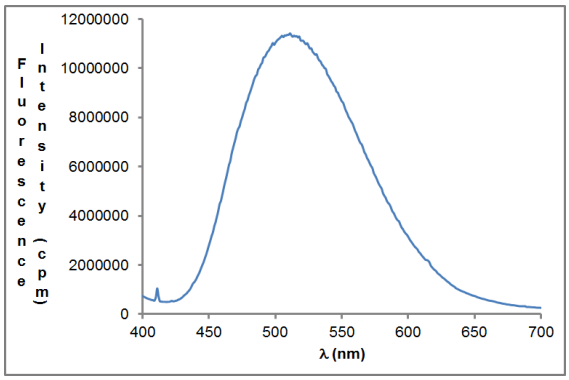

(b)

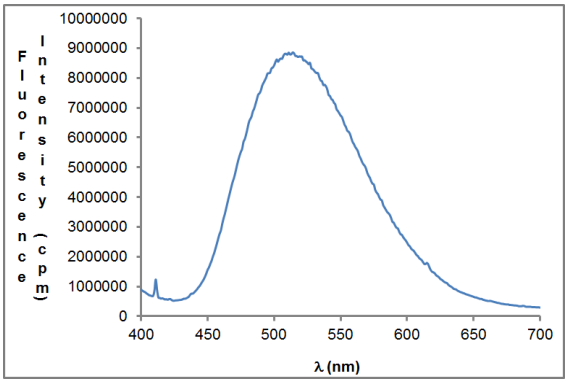

Figure 3.3 (a) Solid state fluorescence spectrum of **3.1** and (b) **3.2**. Excitation wavelength = 375 nm.

In THF solution, **3.1** was completely non-luminescent. Gradual addition of water (a solvent in which **3.1** is insoluble) had little effect on fluorescence spectra until 9:1 H_2O:THF was obtained (Figure 3.4a). In this mixture, a pronounced fluorescence signal was observed centered at ~510 nm, identical to the solid state fluorescence. This is attributed to the formation of nano-aggregate assemblies caused by the decreased solubility of **3.1** in the predominantly aqueous environment, similar to behavior observed by other organic compounds that display AIE properties.[11] In the case of **3.2**, weak fluorescence was observed in THF and aqueous THF solutions up to 80 vol% water. This emission was significantly enhanced and slightly red shifted on going to 90 vol% water in

THF. Here the emission maxima is positioned at ~465 nm as shown in Figure 3.4b which is slightly blue shifted from the emission observed in the solid state (~510 nm). The origin of the blue shift observed in solution phase aggregates of **3.2** relative to the solid state is not known with certainty, but likely involves formation of distinctly different aggregate assemblies arising from variation in intermolecular contacts between pyridyl and phenyl rings. These studies imply that both pyridyl TPE's **3.1** and **3.2** are AIE active compounds, similar to TPE and other AIE compounds containing TPE cores.[24]

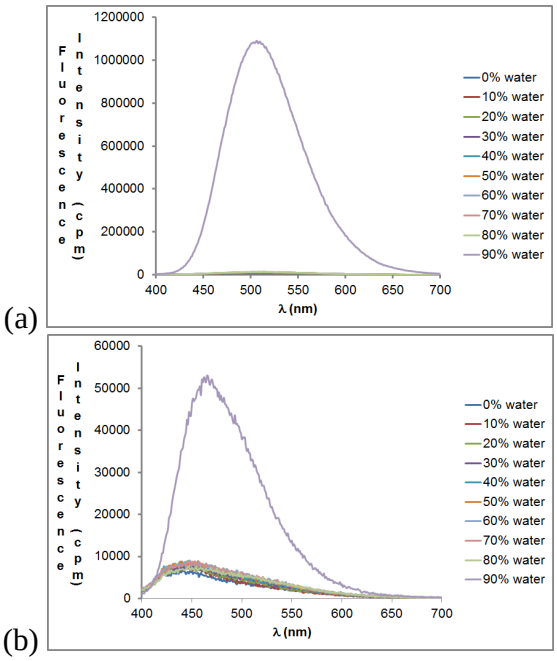

Figure 3.4 (a) Fluorescence spectra of **3.1** in THF and THF:H_2O mixtures (vol %). [**3.1**] = 15.9 μM (b) Fluorescence spectra of **3.2** in THF and THF:H_2O mixtures. [**3.2**] = 8.7 μM. Excitation wavelength = 375 nm.

In order to utilize peripheral Lewis basic sites on **3.1** and **3.2**, fluorescence response was investigated as a function of pH. Both **3.1** and **3.2** were found to be soluble in dilute aqueous HCl solutions of pH ~1.6. In these solutions, pH was increased by addition of small aliquots of concentrated NaOH solutions. As expected starting acidic

solutions were non-luminescent. At low pH, a sufficient number of pyridyl residues are protonated so as to render these compounds completely soluble in water. For both pyridyl TPE's **3.1** and **3.2**, fluorescence response was not observed until pH ~4.0 and reached maxima at pH ~10 (Figure 3.5). In both cases, emission maxima was situated at ~510 nm which is similar to the emission maxima in the solid state. Thus, emission of both **3.1** and **3.2** was found to be switchable as a function of pH.

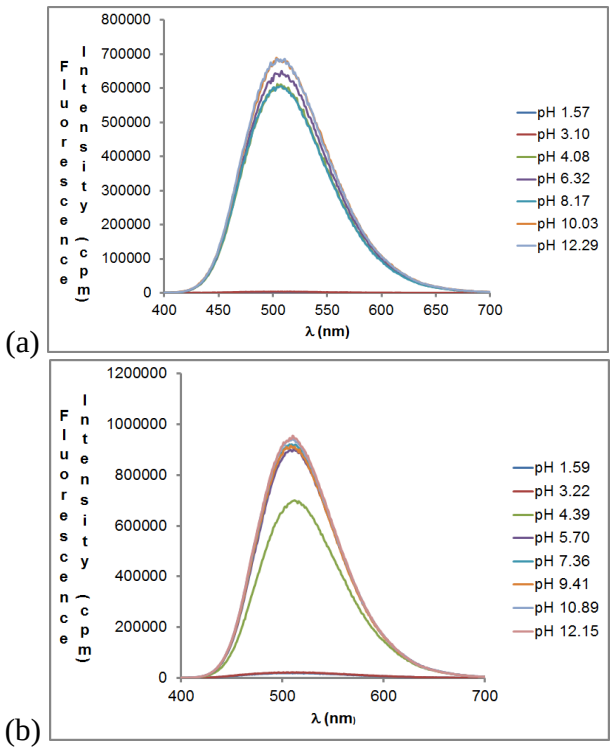

Figure 3.5 (a) Fluorescence spectra of **3.1** in aqueous solutions as a function of pH. [**3.1**] = 35 μM. (b) Fluorescence spectra of **3.2** in aqueous solution as a function of pH. [**3.2**] = 48 μM. Excitation wavelength = 375 nm.

3.3.2 Solid state structures of **3.1** and **3.2**

Two different single-crystal samples of **3.1** from ethyl acetate (EtOAc) and N,N-dimethyl formamide (DMF)/ N,N-dimethyl acetamide (DMA) and one sample of **3.2**

from N-methyl pyrrolidinone (NMP) were obtained by slow evaporation of the indicated solvents.

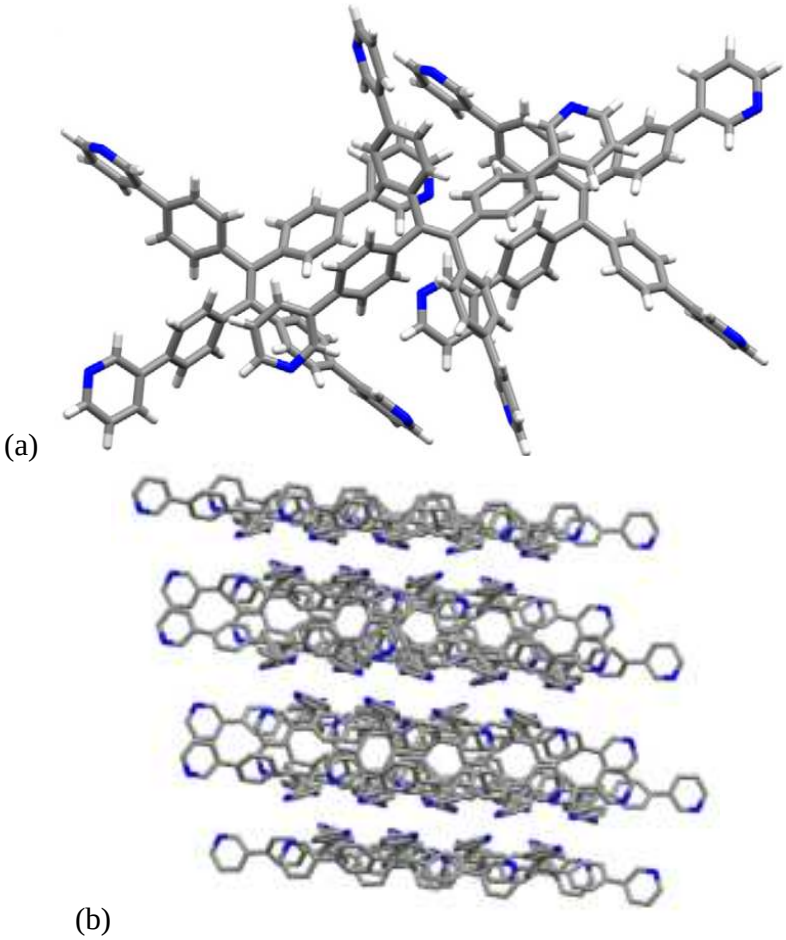

Figure 3.6 (a) Three unique molecules of **3.1** in the unit cell grown from EtOAc. (b) Extended packing of **3.1**. Disordered EtOAc omitted for clarity

Crystals of **3.1** obtained from slow evaporation of EtOAc solution were found to contain three unique molecules of **3.1** in the unit cell along with a disordered solvate molecule (Figure 3.6a). All of the molecules exhibited a propeller like conformation of the TPE core as is typically found in tetraarylethylenes.[9] Differences in the three

molecules were slight and involved the torsion angles between the phenyl and pyridine rings. Pyridine rings on periphery were not perfectly planer, and the C-N-C angle in all pyridine rings was found to be ~116°. Extended packing down *b* reveals distinct helical arrangement of **3.1** (Figure 3.6b) mediated by edge-to-face arene interactions. In this structure, disordered EtOAc solvates were also present participating in O···H polar interactions with **3.1**.

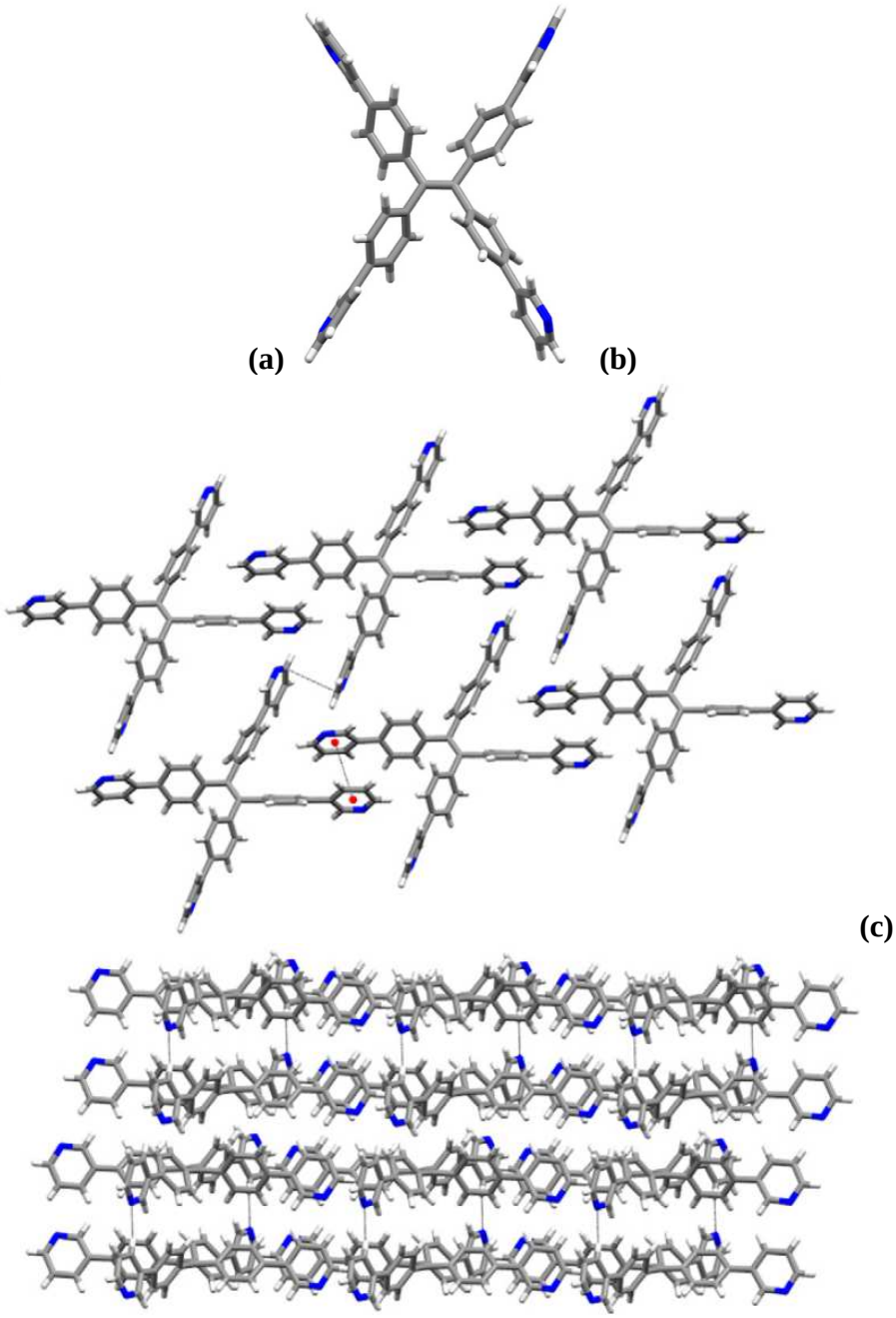

Figure 3.7 (a)Molecular structure of **3.1** in crystals obtained from DMF/DMA solution. (b) Favorable local dipolar alignment in layers of **3.1**. (c) Offset stacking of adjacent layers in **3.1** via H-bonds. Solvents omitted for clarity.

In the crystals of **3.1** obtained from a mixture of DMF and DMA, a single molecule of **3.1** is found in the unit cell along with disordered DMA solvate. As expected, the molecule also features a propeller-like conformation of the TPE core. Here vicinally disposed pyridine rings (with respect to central olefin) are oriented with their pyridine nitrogen atoms facing in opposite directions (Figure 3.7a) and geminally located pyridine rings have nitrogen atoms facing in same direction. Pyridine rings on periphery were not totally flat, and the C-N-C angle in all pyridyne rings was found to be ~116°. Individual molecules of **3.1** are arranged in 2D layers that are mediated by intermolecular arene interactions between pyridine rings (Figure 3.7b). Adjacent pyridine rings are aligned co-facially with ~4.0 Å separation with their local dipole moments opposed. The propeller shape of the TPE core results in offset stacking of adjacent layers to produce an *abab* arrangement down the *a* axis (Figure 3.7c). Stacking interactions appear to be reinforced by aryl C-H$\cdots$N$_{py}$ hydrogen bonding (H$\cdots$N distance – 2.45 Å).

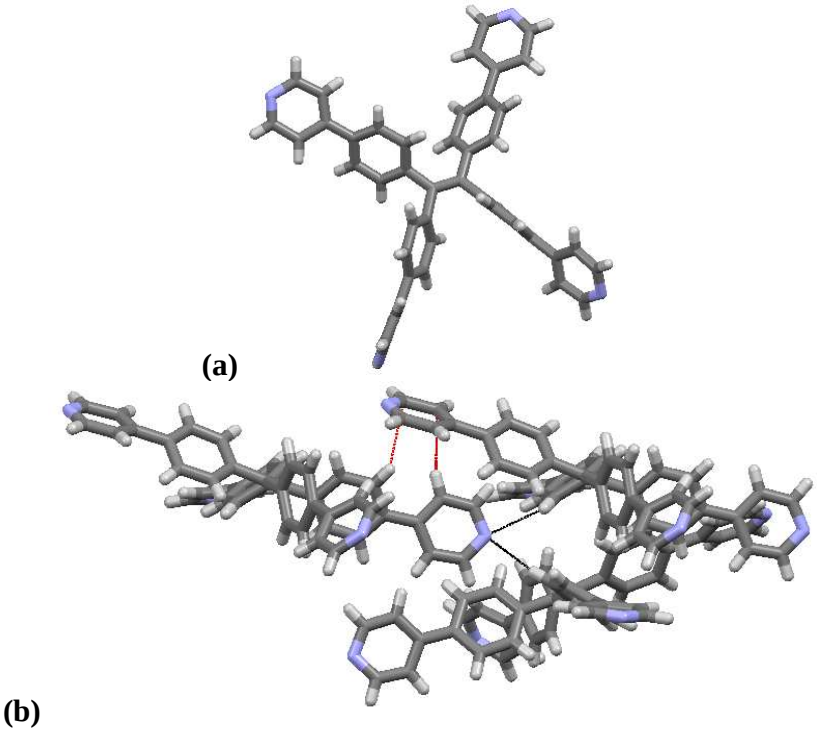

(a)

(b)

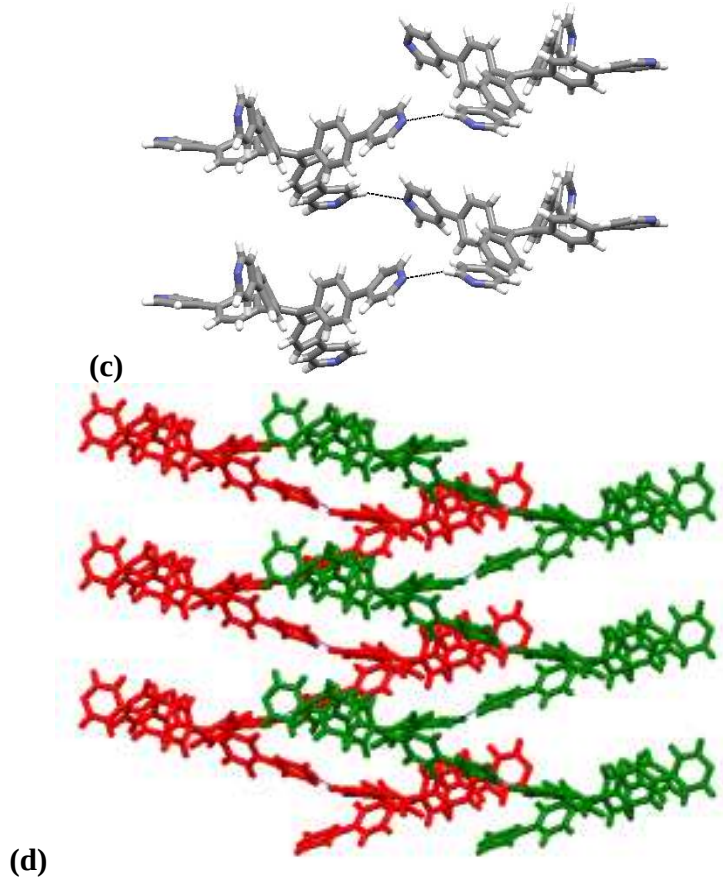

Figure 3.8 (a) Molecular structure of **3.2** (b) Bifurcated H···N_{py} hydrogen bonding interactions along with edge-to-face arene stacking interactions (c) Helical arrangement of molecules of **3.2** (d) Two non-interpenetrating helices of **3.2** moving in same direction.

Crystals of tetrapyridyl TPE **3.2** were obtained from slow evaporation of N-methyl pyrrolidinone (NMP) and EtOAc. The unit cell contained one unique molecule of **3.2** with three molecules of NMP solvate. NMP solvate molecules occupy void space in between molecules. Along with edge-to-face stacking of arene rings and polar interactions between individual molecules of **3.2** and NMP solvate, aryl H···N_{py} hydrogen bonding interactions were observed. Two diagonally opposite nitrogen atom on the molecule of **3.2** participate in C-H···N_{py} hydrogen bonding interactions. One nitrogen atom participates in bifurcated hydrogen bonding interactions shown as black dotted lines

in Figure 3.8b whereas edge-to-face arene interactions are shown as red dotted lines. Non-bifurcated hydrogen bonding interactions results in arrangement of individual molecules of **3.2** arranged in helical fashion (Figure 3.8c). Two non-inteterpenetrating helices of **3.2** move in same direction as shown in Figure 3.8d.

3.3.3 Generation and characterization of tetrapyridinium perchlorate salts of **3.1** and **3.2**

Both tetrapyridyl TPE derivatives **3.1** and **3.2** were found to form stable pyridinium perchlorate salts **3.5** and **3.6** upon treatment with highly acidic ferric perchlorate hydrate (Scheme 2). Combining the tetrapyridyl TPE with four equivalent of $Fe(ClO_4)_3 \cdot xH_2O$ in methanol at room temperature, followed by slow evaporation of the solvent resulted in formation of crystalline salts.[44] The crystal structures revealed that all four pyridine moieties were protonated under these conditions resulting in inclusion of four perchlorate counterions per each TPE in the crystal structure. In addition, water molecules of hydration and, in the case of **3.5**, a methanol of solvation, were also detected in the crystalline lattice and appear to play important roles as hydrogen bonding linkers between pyridinium cations and perchlorate anions. The tetraphenylethylene core adopts a propeller like arrangement, as has been observed in other TPE crystal structures.[9]

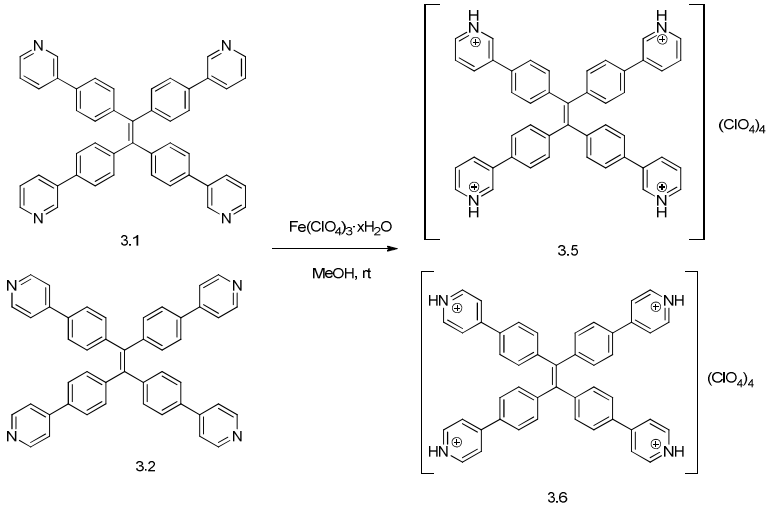

Scheme 3.2 Generation of tetrapyridinium salts **3.5** and **3.6** from tetrapyridyl TPE's **3.1** and **3.2**

Crystals of **3.5** were obtained as hydrates along with a methanol solvent molecule (Figure 3.9). Pyridinium C-N-C angles (~120°) are slightly flattened with respect to the free base form (~116°).[66] All four pyridinium N-H groups in **3.5** are engaged in hydrogen bonding interactions. Two of these interactions involve direct hydrogen bonds to perchlorate ions while the remaining two N-H groups are connected to perchlorate ions via water bridges. The methanol solvate is also associated to one of the perchlorate anions via H-bonding.

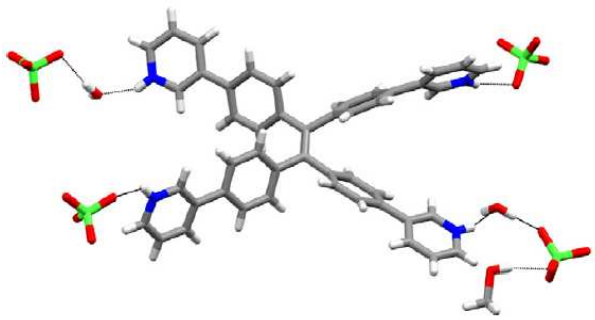

Figure 3.9 Molecular structure and principal pyridinium N-H hydrogen bonding interactions in **3.5**.

Individual molecules in **3.5** are connected in helical stacks via hydrogen bonding bridges composed of two perchlorate anions and one water (Figure 3.9). One dimensional stacks are connected to adjacent helical bundles via additional solvate/hydrate hydrogen bonds to N-H pyridinium moieties so as to extend packing in two dimensions (Figure 3.10a). These linked helical stacks are then aligned in parallel in the three dimensional lattice (Figure 3.10b). The net result is the presence of tetrapyridyl tetraphenylethylene stacks surrounded by perchlorate anions and molecules of hydration/solvation.

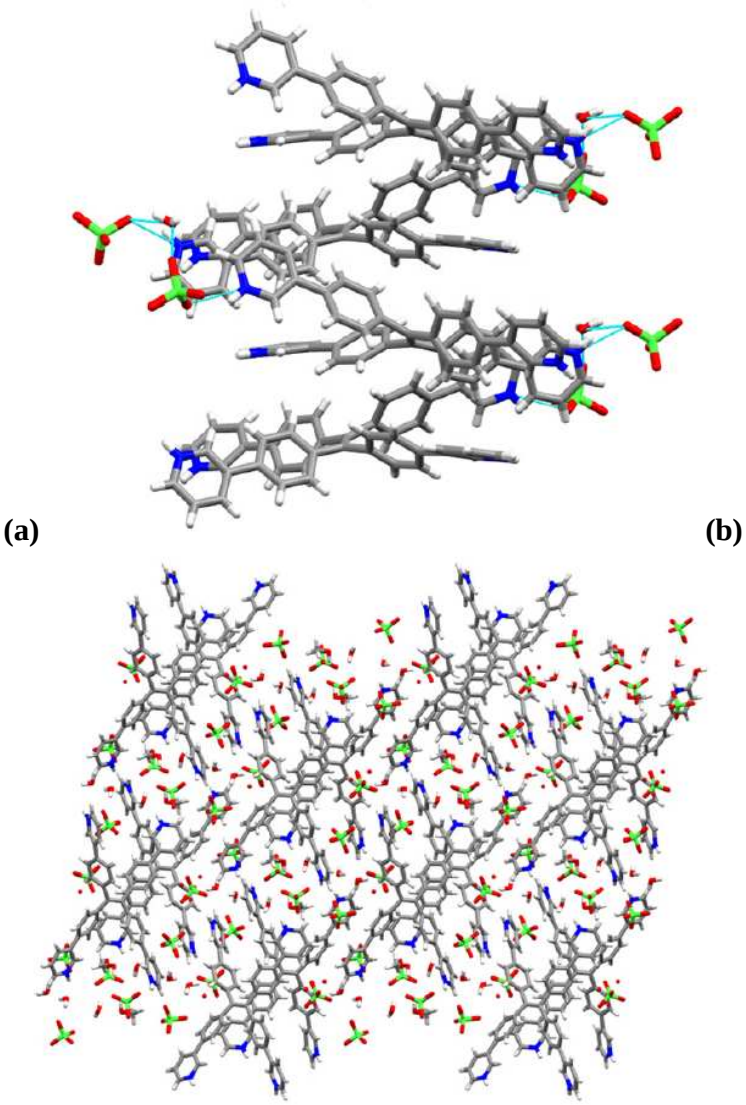

Figure 3.10 (a) Helical stacking arrangement of tetrapyridinium cations in **3.5** viewed perpendicular to the helical axis. (b) View of extended packing in **3.5**.

In the crystal structure of **3.6**, in addition to perchlorate anions, 2.17 molecules of water were also detected in the unit cell (Figure 3.11a). The pyridinium N-H groups are all engaged in hydrogen bonding interactions involving one water molecule and five perchlorate ions. Two geminally placed pyridine groups (with respect to the central olefin) engage in bifurcated hydrogen bonding with two separate perchlorate anions. The

final pyridinium participates in a single hydrogen bonding interaction with a perchlorate anion.

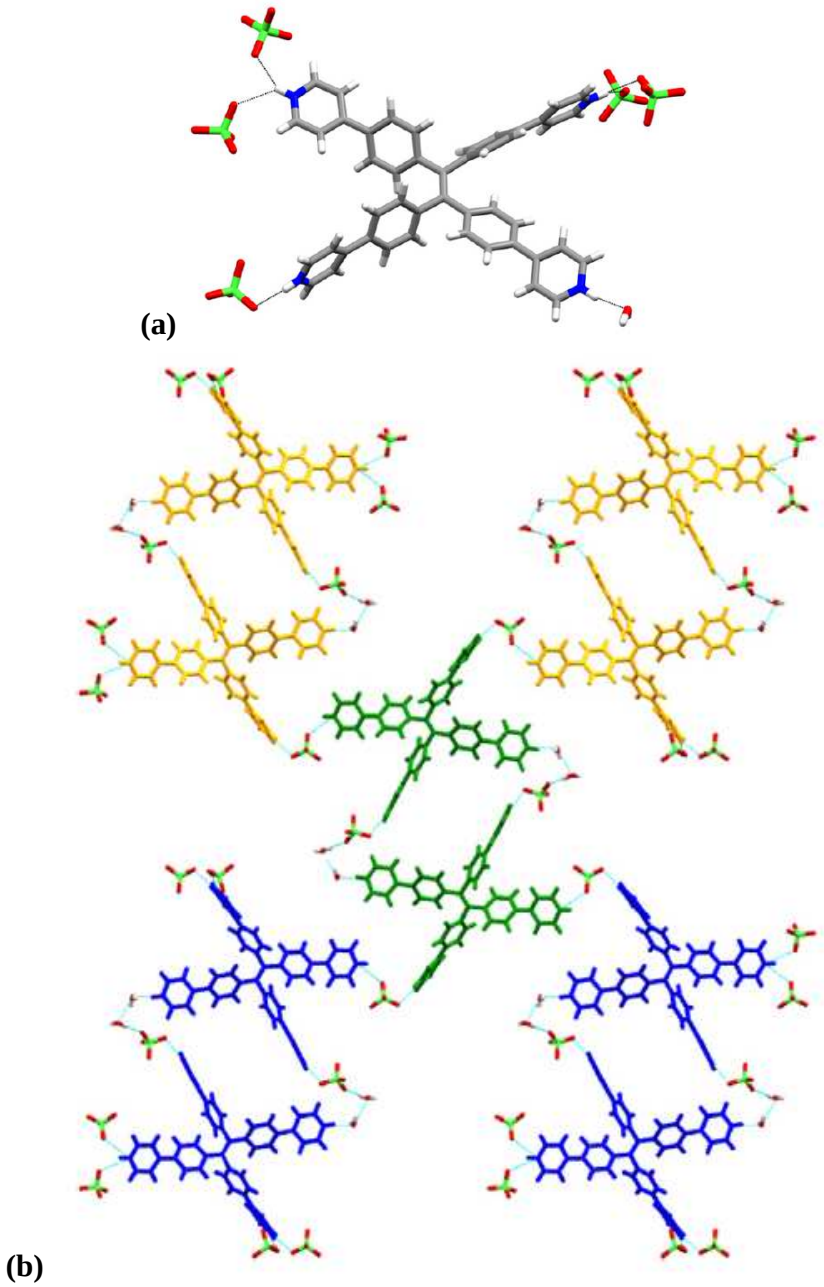

Figure 3.11 (a) Molecular structure of **3.6**. (b) 2-D layer arrangement of tetrapyridinium cations in **3.6**.

Individual molecules of **3.6** are arranged in the *b*, *c* plane via an extensive hydrogen bonding network involving pyridinium N-H groups, water molecules of hydration and perchlorate anions. Geminally disposed pyridyl groups (with respect to central alkene) are connected by complementary hydrogen bonding network involving two water molecules and a perchlorate anion. These dimers are color coded in Figure 3.11b. Dimeric units are further connected via additional bridging perchlorate ions resulting in formation of 2D layers. This layer motif is further reinforced through face to face π-π stacking interactions.

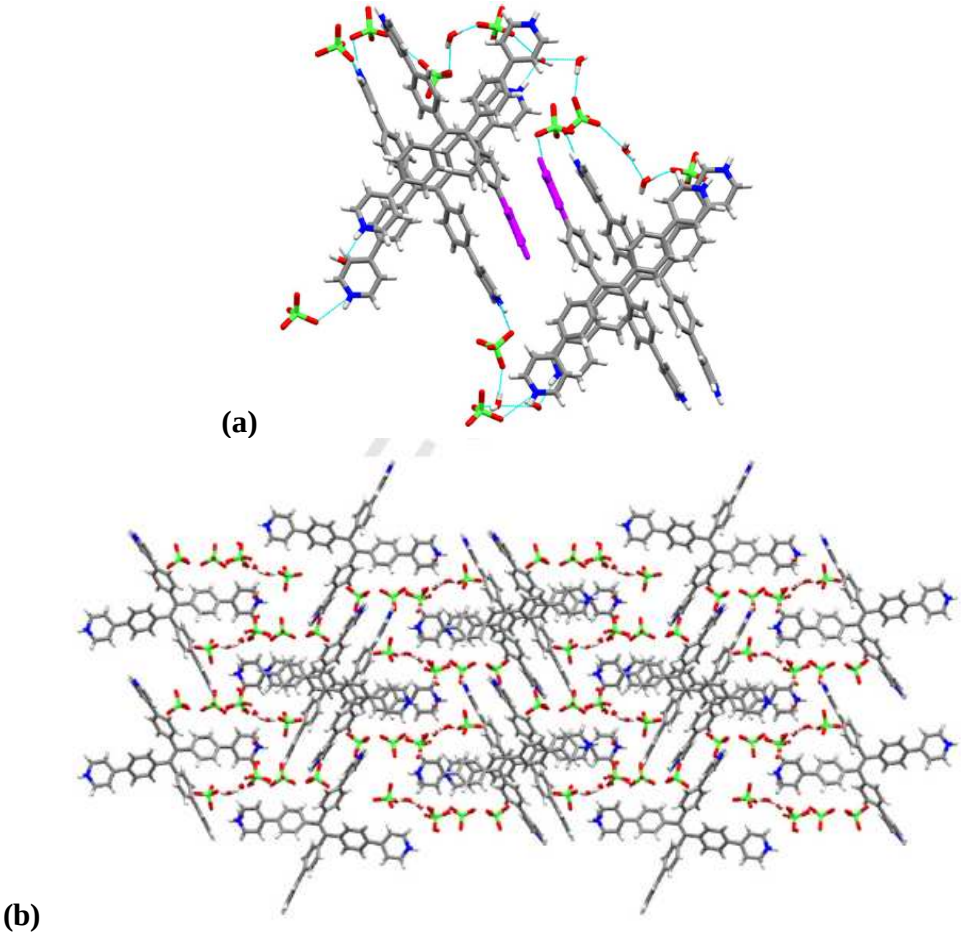

Figure 3.12 (a) Offset stacking of tetrapyridinium cations in **3.6**. (b) Extended packing of **3.6**.

The two dimensional layers are linked in the third dimension through additional pyridinium-H_2O-perchlorate hydrogen bonding which results in stacking of TPE derivatives in a slightly offset manner (Figure 3.12a). Overall, the combination of tetrapyridinium cations and perchlorate anions produces stacks of tetrapyridinium units surrounded by perchlorate anions along with water of hydration (Figure 3.12b).

Both these structures have many features in common, most notably the presence of helical tetrapyridyl cations. Along with structures other tetraphenylethylene derivatives, these structures indicate a general propensity of for adoption of this general motif[42] where the stacks of hydrophobic TPE's are surrounded by hydrophilic components of pyridinium cations along with perchlorate anions.

3.4 Summary

Two tetrapyridyl tetraphenylethylene derivatives were successfully prepared and characterized. A four-fold Suzuki coupling between tetrabromo TPE and pyridyl boronic acids provided the key step in the synthesis. The photoluminescence properties of both pyridyl TPE's were investigated in the solid state as well as in solution. Fluorescence of these compounds in solution was found to be tunable as a function of solvent mixture (THF and H_2O) and pH where emission was turned on between pH 3 and 4.

Both tetrapyridyl TPE's were characterized in the solid state via X-ray diffraction. Crystal structures reveal extensive edge-to-face arene interactions along with C-H$\cdots$N$_{py}$ hydrogen bonding interactions. Both tetrapyridyl TPE's were converted to their respective perchlorate salts upon exposure to $Fe(ClO_4)_3$, which were structurally characterized. In both cases, extensive hydrogen bonding was observed involving pyridinium N-H groups, perchlorate anions and included water molecules. Additionally, both structures feature hydrophobic regions formed by stacking of tetraarylethylene cations in helical fashion and polar pyridinium N-H groups are directed away from these stacks in hydrophilic regions formed by perchlorate anions and water molecules of

hydration. Coupled with the switchable aggregation-induced emission properties of pyridyl TPE’s, a variety of photoluminescent materials may be available via this strategy.

CHAPTER IV

INFLUENCE OF HALOGEN BONDING INTERACTIONS IN CRYSTALLINE NETWORKS OF TETRAARYLETHYLENE HALOBENZOYL ESTERS

4.1 Introduction

Halogen bonding is a non-covalent interaction that takes place between halogen atoms, functioning as electrophilic species, and neutral or anionic electron donors.[67,68] In organic halides, halogen atoms feature an anisotropic distribution of electron resulting in a region of positive potential called the 'sigma hole' located along the axis of the C-X bond.[69] It is this region of positive electrostatic potential that imparts electrophilic character upon halogens in organohalides. Halogen bonding interactions are weaker than hydrogen bonds but they are highly directional. The strength of halogen bonding interactions can be altered by modifying nearby substituents on the carbon skeleton to increase the electrophilicity of halogen atoms, resulting in greater propensity to form halogen bonds.[70] Halogen atoms show 'amphiphilic character' i.e. they function as electron deficient sites when they form contacts at the pole but can also function as electron rich sites on forming contacts at the equator.[71] Experimental data from solid, liquid, and gas phases confirm theoretical predictions that the strength of halogen bond donors increases in the order of Cl<Br<I.[72] Hybridization of the carbon atom to which the halogen is attached also plays a role due to different electronics. Hence the order C(sp)-X>C(sp^2)-X>C(sp^3)-X is followed.[73]

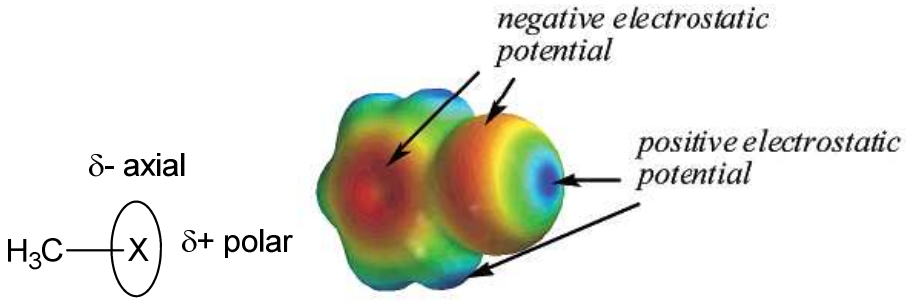

Figure 4.1 Illustration of sigma hole along C-X bond

Halogen bonding has an impact on all research fields where control of intermolecular recognition and self-assembly processes is important. In a molecule halogens can effectively function as 'sticky sites' that direct molecular association in a supramolecular assembly. Coupled with their presence along the periphery of organic molecules, halogens engaged in bonding may play an important role where the design and manipulation of aggregation phenomena are important. For example, halogen bonding interactions have been exploited in mediating solid state assemblies of supramolecular architectures[71], liquid crystals,[74] organic semiconductors,[75] magnetic materials,[76] NLO materials[77] and as templates for solid state synthesis.[78] Halogen bonding has also been observed in solution phase in the context of synthetic molecular receptors.[79] Halogen bonding interactions have also been implicated in certain biological systems.[80]

4.2 Objective

Despite their significance, there are many fundamental aspects of halogen bonding that are currently poorly understood. For example, the relative importance of various halogen bonding interactions in polyfunctional organohalides have not been established. In order to gain insight into this issue, we designed a series of tritopic and tetra-topic haloarenes connected via conformationally flexible ester linkages. We

envisioned that these substrates would allow us to determine the relative preference of X···X vs. X···O=C vs. X·π halogen bonding interactions via single crystal X-ray diffractometry.[81,82] Moreover, the conformational flexibility of the substrates would allow energetically significant non-covalent interactions to be maintained within a series of organohalides despite differences in the relative size of halogen atoms.

4.3 Results and discussion

The first family of multitopic and flexible haloarenes we prepared were based on a trimesic acid platform, and the synthesis of tris(4-iodophenoxy) trimesoate is shown in Scheme 4.1.[83] The triiodo substrate **4.2** possesses an attractive element of C3 symmetry and is structurally similar to halogenated triaroylbenzenes previously examined in our group.[81,82]

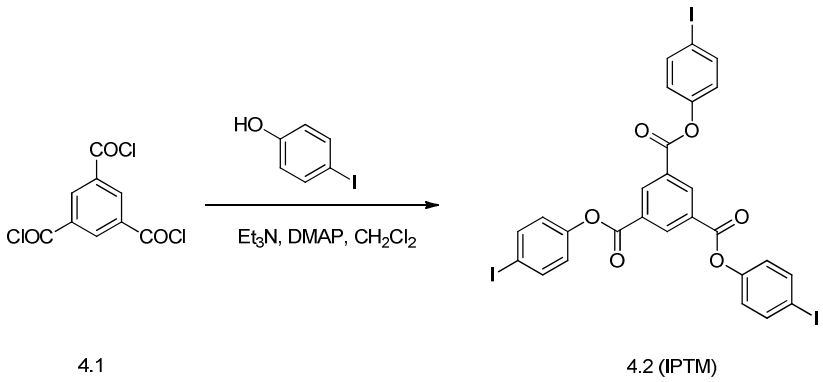

Scheme 4.1 Synthesis of 4-iodophenoxy trimesoate.

Crystals of **4.2** obtained from $CHCl_3$ exhibited a hexagonal morphology and the structure was found to be an inclusion complex of stoichiometry **4.2·(CHCl$_3$)$_3$**. Molecules of **4.2** adopt an approximately symmetrical conformation. The most striking feature of the structure is the manner in which three iodophenoxy ester moieties from

three independent molecules come together in a triangular array seemingly facilitated by roughly trigonal symmetry of **4.2**, templating effects of the included solvent and bifurcated I···O and I··π interactions (Figure 4.2a). This triangular motif serves to position adjacent molecules of **4.2** laterally to form 2D layers. These 2D layers stack such that the central 1,3,5-tricarbonylbenzene rings are positioned above and below the bifurcated halogen bonding moieties. This arrangement produces large hexagonal channels (distance across openings ~13 Å) that are filled with included chloroform solvates as shown in Figure 4.2b. The porosity of the network was determined to be 37.4%.[84]

Compound **4.2** was also crystallized via slow evaporation of pyridine solution, which again resulted in a channel type inclusion complex of stoichiometry **4.2·(py)$_3$**. Here **4.2** self-assembles to form two dimensional layers that stack in an *abab* pattern resulting in generation of hexagonal channels which are filled with pyridine solvate (Figure 4.2c). Here this motif is reinforced by bifurcated I···O and I··π interactions. While there is considerable precedent for pyridyl N···I halogen bonds, no such halogen bonding interactions were observed. The porosity of this structure was determined to be 39.7%. A similar structure was obtained from benzene with disordered benzene molecules taking place of pyridine solvates in the channels.

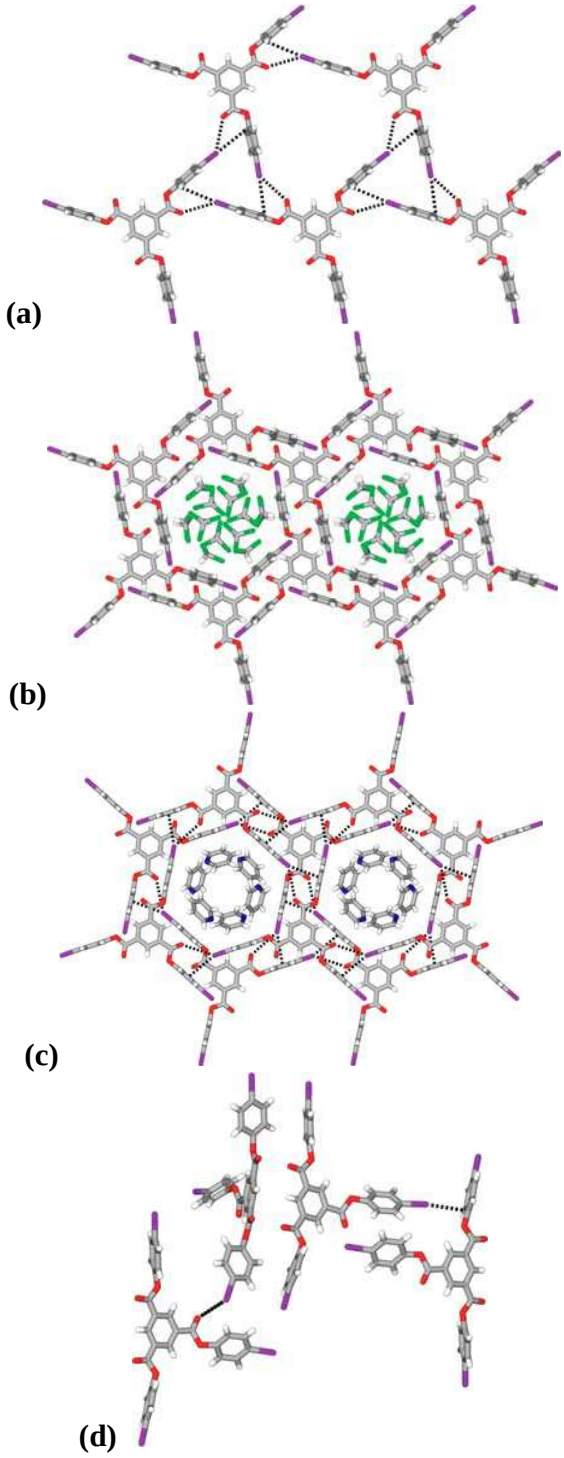

Figure 4.2 (a) 2D layers in **4.2·(CHCl$_3$)$_3$**. Triangular motif mediated by bifurcated I···O and I··π interactions (b) Extended packing in **4.2·(CHCl$_3$)$_3$** (c) Honeycomb network of **4.2·(py)$_3$** mediated by bifurcated I···O and I··π interactions (d) Close-packed structure of **4.2**.

Extensive characterization of these channel-type inclusion complexes proved difficult due to their fragility when removed from the crystallization solvent. In fact, continued contact with the mother liquor resulted in transformation of the large blocks characteristic of the inclusion complexes into needle like crystals. These crystals were characterized by X-ray diffraction and found to be identical to crystals grown from dichloromethane and other solvents like methanol and acetone. This modification of **4.2** exists as a close-packed structure of as shown in Figure 4.2d. Molecules in the asymmetric unit are part of helical chains that intertwine to achieve close packing. It appears that the hexagonal inclusion complexes obtained are metastable products which are eventually replaced by the thermodynamically favored close-packed form.

Halogen bonding, though generally recognized as weaker than conventional hydrogen bonding, may be capable of exerting a similar influence over the crystallization process. In the system described above, the combination of trigonal host **4.2** and appropriate solvent guests produced inclusion complexes with nanometer-sized channels mediated by mutually reinforcing halogen bonding and symmetry interactions. Spontaneous conversion of this solid state network into a solvate-free close-packed structure provides evidence that the open porous framework is thermodynamically less stable. One can envision, however, that in the presence of stronger halogen bonding interactions the thermodynamic preference for close packing may be inverted in favor of porous architectures (analogous to hydrogen bonded networks). Consequently, as the phenomenon of halogen bonding becomes better understood, the engineering of strong and directional halogen bonding interactions should emerge as valuable design elements in the fabrication of functional organic materials such as porous solids.

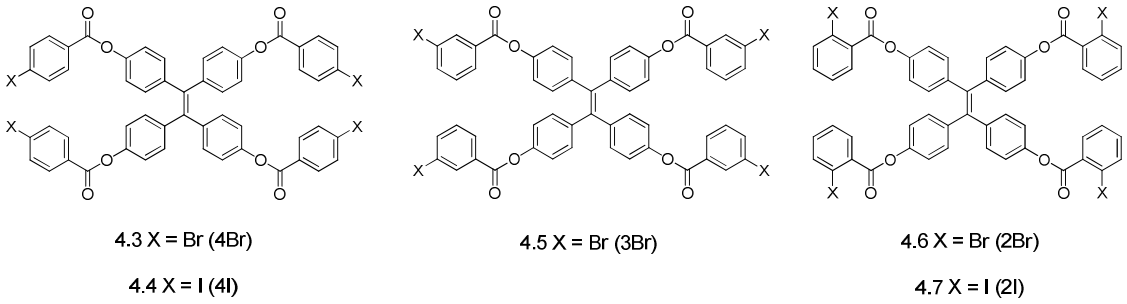

Figure 4.3 Tetraarylethylene halobenzoyl esters examined for halogen bonding.

As an extension of our investigations into tritopic haloarenes and consistent with our desire to exploit tetraarylethylenes in supramolecular chemistry (including applications in crystal engineering), we next prepared a series of halobenzoate esters (**4.3** to **4.7**) arrayed on a TPE scaffold. The synthesis of these substrates is illustrated in Scheme 4.2. The TPE derivatives **4.3** to **4.7** feature haloarene substituents symmetrically appended to the periphery of a common TPE core via ester linkages. Thus, these compounds allow us to explore the halogen bonding preferences in structurally similar but electronically different substrates. It is anticipated that the ester group will activate halogens at the 4- and 2- positions toward halogen bonding while halogens at 3-position will remain unactivated.

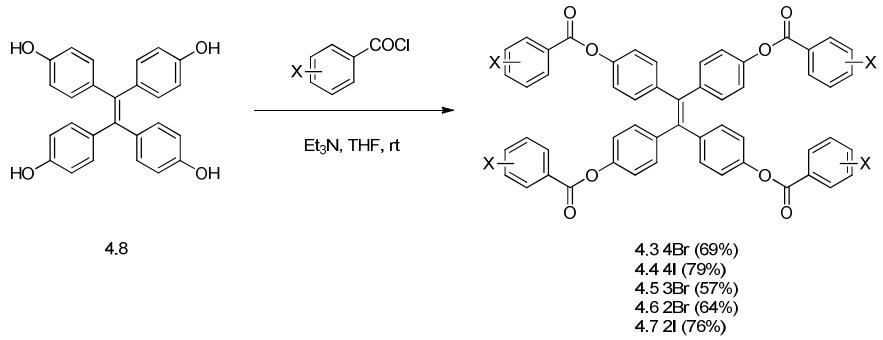

Scheme 4.2 Synthesis of tetraarylethylene halobenzoyl esters **4.3** to **4.7.**

The TPE esters **4.3**-**4.7** were all prepared from the known tetraphenol **4.8** via acylation with a halobenzoyl chloride in THF (Scheme 4.2). All products were found to be sparingly soluble in common organic solvents and this characteristic initially hampered efforts to obtain X-ray quality crystals. Eventually, nine different crystals were obtained from slow evaporation of DMF or pyridine solutions. Of the nine crystalline samples, seven were found to contain included molecules of solvation. Analysis of these structures (described below) led to identification of various halogen bonding motifs operative in this system, and the parameters of these interactions are summarized in Table 4.1.

Table 4.1 Selected halogen bonding contact distances and angles in **4.3-4.7**.

Crystal	Contact	Length (Å)	Contact	Angle (°)
4.3·(py)	Br···O	3.302	C-Br···O	166.22
	Br··π	3.623	C-Br··π	141.05
4.4·(py)	I···O	3.401	C-I···O	163.68
	I··π	3.574	C-I··π	142.88
4.3·(DMF)$_2$	Br···O	3.526	C-Br···O	125.71
	Br··π	3.595	C-Br··π	160.48
4.4·(DMF)$_2$	I···O	3.522	C-I···O	126.91
	I··π	3.552	C-I··π	160.10
4.4·(py)$_3$	I···O	3.380	C-I···O	152.49
	I··π	3.564, 3.649	C-I··π	154.15, 171.11,
	I···I	3.795	C-I···I	168.24, 96.73
4.5·(py)	Br··π	3.458	C-Br··π	151.73
	Br···Br	3.751	C-Br···Br	135.39
4.5·(DMF)	Br···O	3.407	C-Br···O	163.60
4.6	Br··π	3.510	C-Br··π	164.73
	Br···Br	3.607	C-Br···Br	89.11, 158.98
4.7	I···O	3.322	C-I···O	149.53
	I··π	3.976, 3.332, 3.563	C-I··π	134.92, 170.40, 146.78

The inclusion complexes **4.3·(py)** and **4.4·(py)** obtained from slow evaporation of pyridine solutions were found to be virtually isostructural. In each case TPE molecules adopt propeller like conformations typical of tetraphenylethylenes in the solid state.[9] Individual molecules of **4.3** and **4.4** are engaged in two types of halogen bonding interactions resulting in formation of 1D chains. As shown in Figures 4.4a and 4.4b, these chain motifs are mediated by complementary X···O=Cand X··π halogen bonding. In the case of halogen-π interactions, the closest X··π_{arene} interaction is to the midpoint of an arene π bond rather than the arene centroid.[85,86] One dimensional chains are extended into 2D layers via a combination of arene edge-to-face interactions between adjacent halobenzoyl moieties and additional X··π contacts as shown in Figure 4.4c. Disordered pyridine solvate molecules are housed within cavities formed at the chain-chain interface.

As mentioned previously, there is considerable precedent for pyridyl N···X halogen bonds,[67,68,71] however pyridine solvates appear to be serving a space filling role instead of participating in any intermolecular interactions in these structures.

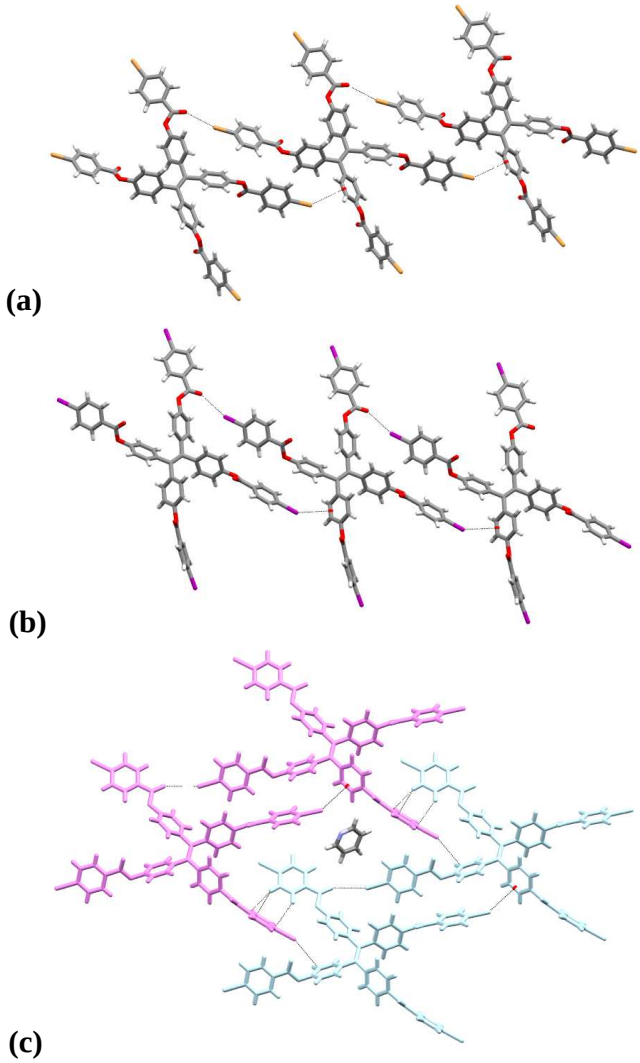

Figure 4.4 (a) 1D chains present in **4.3·(py)** (b) 1D chains present in **4.4·(py)** (c) 2D layers formed from interdigitation of 1D chains along with pyridine solvate molecule in **4.4·(py)**.

While halogen bonding appears to play an important role in 2D organization of **4.3·(py)** and **4.4·(py)**, stacking of individual layers in the third dimension is mediated by an extensive network of edge-to-face arene contacts as shown in Figure 4.5. In these structures, 2D layers are stacked in an *abab* pattern. Arene rings in the TPE core interact with arene rings from adjacent TPE cores, while peripheral halobenzoyl rings interact with peripheral halobenzoyl rings in adjacent layers.

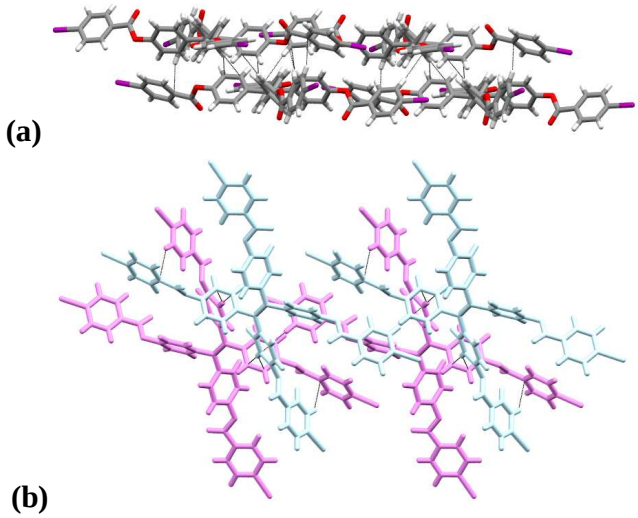

Figure 4.5 Stacked 2D sheets in **4.4·(py)** (b) Two different layers of **4.4·(py)**.

Single crystals of **4.3** and **4.4** obtained from slow evaporation of DMF exhibited a similar arrangement of 1D chains organized into 2D sheets with included solvent molecules occupying cavities at the inter chain interface as shown in Figure 4.6a. A linear network of I···O=C and I···π_{arene} halogen bonding interactions similar to those found in the pyridine solvates result in ribbon like chains of individual molecules. These chains are arranged in 2D layers via edge-to-face π-stacking of aromatic rings. Additional polar interactions with DMF solvates appear to further reinforce this layered structure. The 2D layers stack in *abab* pattern mediated by edge-to-face π-stacking interactions. As a

consequence of these interactions, individual 2D layers are aligned in slightly offset fashion producing rhomboid channels of 13 × 7 Å filled with DMF solvates as shown in Figure 4.6b. The presence of these channels produces a relatively porous network with approximately 41% solvent accessible void space as examined using PLATON calculations.[84] The DMF inclusion complex obtained from **4.3** exhibited a similar overall network architecture with Br···O=C and Br···π_{arene} interactions similar to the inclusion complex with iodo analogue **4.4**.

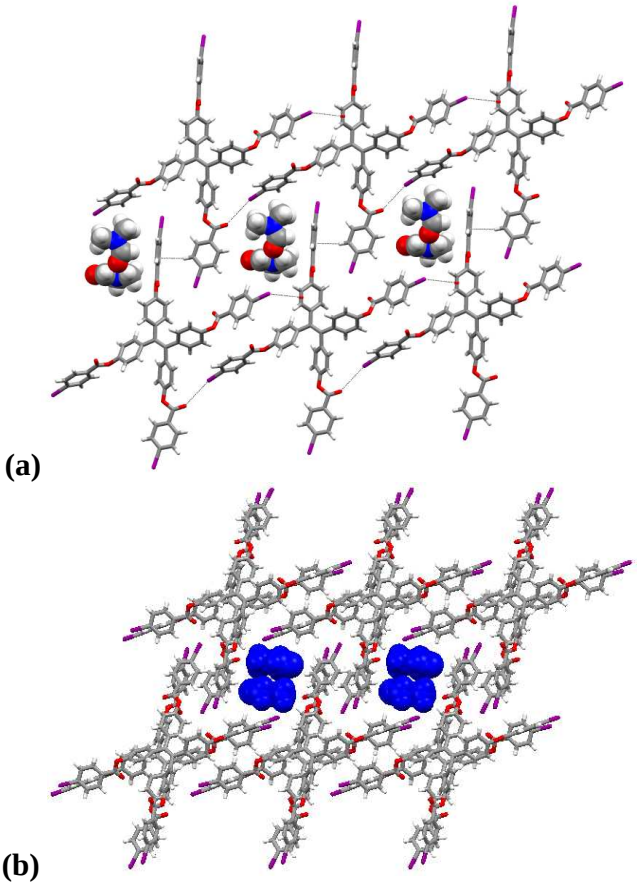

Figure 4.6 (a) 2D sheets formed by parallel alignments of chains in **4.4·(DMF)$_2$** (b) Rhomboid channels in **4.4·(DMF)$_2$** occupied with DMF molecules.

An attempt was made to prepare co-crystalline networks with **4.4** and various compounds with two halogen bond acceptor groups (dimethyl malonate, methyl nicotinate, diethyl maleate and several bis(pyridine)s) in DMF or pyridine solvents. While no co-crystals were obtained, a new pyridine inclusion complex of **4.4** was obtained with stoichiometry of **4.4·(py)$_3$**. This structure was unique in the way that all four haloarene groups in **4.4·(py)$_3$** were engaged in some form of halogen bonding resulting in linking of each molecule of **4.4** to five other molecules as shown in Figure 4.7a. Two iodo groups are involved in distinct I$\cdots\pi_{arene}$ interactions with two different molecules if **4.4** whereas a third iodine participates in a halogen bond to a carbonyl group and the fourth iodine functions as a halogen bond donor toward another iodine on adjacent molecule of **4.4**. TGA analysis of **4.4·(py)** and **4.4·(py)$_3$** could not be performed due to the fragility of the crystals, but based on calculated densities it appears that the **4.4·(py)** is the more close packed structure (D_{calc} is 1.775 vs. 1.663). It is possible that **4.4·(py)$_3$** complex represents a metastable state along the path to **4.4·(py)** complex and halogen bonding interactions in **4.4·(py)$_3$** are displaced by edge-to-face arene contacts in **4.4·(py)**. This would indicate that disruption of the halogen bonding network observed in **4.4·(py)$_3$** is offset by other intermolecular attractions (like edge-to-face arene contacts) to produce a more favorable solid state assembly.

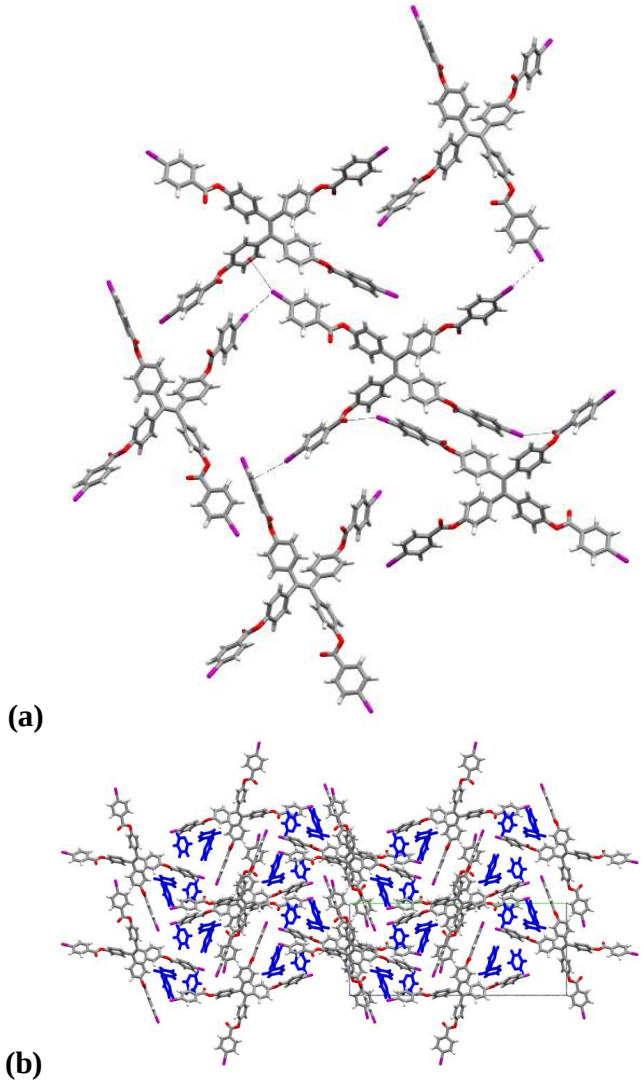

Figure 4.7 (a) Halogen bonding interactions in **4.4·(py)$_3$** (b) Extended packing in **4.4·(py)$_3$**.

In order to investigate the effect of substitution pattern on halogen bonding interactions, TPE derivatives **4.5**, **4.6** and **4.7** were synthesized and characterized. As was case with **4.3** and **4.4**, two different inclusion complexes of **4.5** were obtained from DMF and pyridine solutions. In **4.5·(DMF)**, only one halogen bond between a bromine and the carbonyl group of DMF is observed as shown in Figure 4.8a. Apart from this halogen

bond, edge-to-face arene contacts are also observed. These interactions generate 2D sheets as shown in Figure 4.8b. The structure of **4.5·(py)** also features 2D sheets that stack in an *abab* pattern as shown in Figure 4.8c. This structure also features inversion related Br···Br contacts (Type I halogen bonding),however these contacts are not attractive interactions. Thus, moving the bromine substituents in the peripheral arene rings from the electronically activated para-positions to unactivated meta-positions appears to have dramatic effects in the propensity for solid state halogen bonding. While steric factors may also play a role, the observation that o-halobenzoate esters display halogen bonding interactions reminiscent of their 4-substituted analogues (as discussed below) further indicates the influence of electronics in this system.

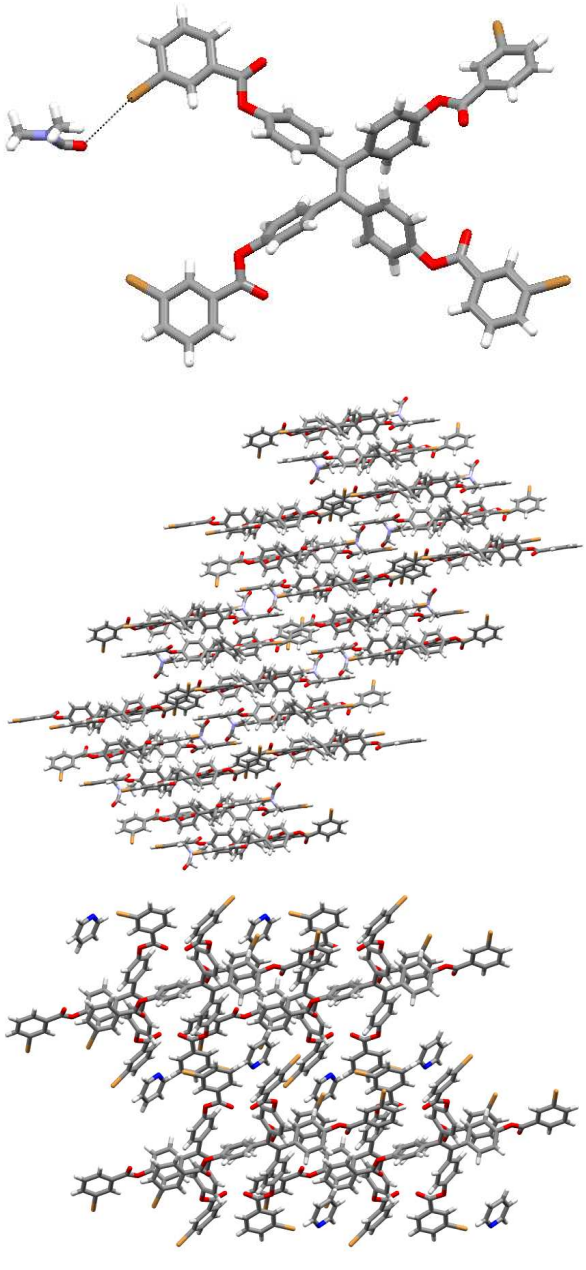

Figure 4.8 (a) Halogen bonding interactions between **4.5** and DMF solvate in **4.5·(DMF)** (b) Extended packing in **4.5·(DMF)** (c) Extended packing in **4.5·(py)**.

The final set of compounds examined in this study included TPE frameworks with ortho-substituted bromo or iodobenzoyl rings. Again crystals of **4.6** and **4.7** were obtained from slow evaporation of pyridine or DMF solutions. In this instance each

compound gave the same close-packed structure without any included solvate irrespective of crystallization solvent.

In the structure of **4.6**, two types of halogen bonding interactions appear to be significant. Individual molecules of **4.6** are organized into 1D ribbons via attractive Type II halogen bonding between aryl bromides as shown in Figure 4.9a. To achieve close packing, each 1D ribbon is connected in slightly offset manner to adjacent ribbons via Br···π contacts along with C-H···O interactions. This results in one bromine in each molecule being engaged in amphiphilic bifurcated halogen bonding by acting as a halogen bond donor toward an arene π system and a halogen bond acceptor in a Type II Br···Br interaction.[87]

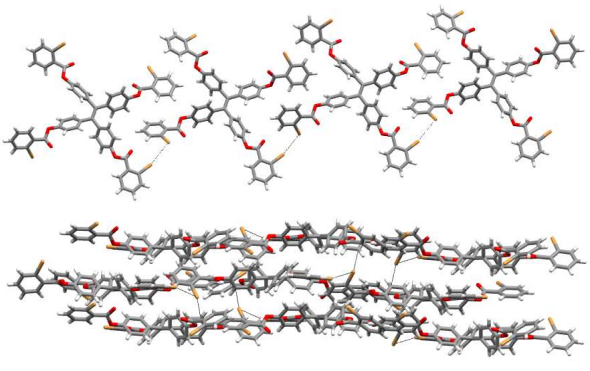

Figure 4.9 (a) Type II halogen bonding in **4.6** (b) Stacked sheets of **4.6**.

Compound **4.7** adopts a slightly different packing arrangement in which ribbons are aligned to form sheets. Along with I···π halogen bonding, C-H···O interactions are observed as shown in Figure 4.10a. In one ribbon, a bifurcated halogen bonding interaction is observed wherein iodine acts as a halogen bond donor simultaneously to O from an ester and an arene ring. These sheets are stacked in an *abab* pattern with additional inter-layer I···π interactions as shown in Figure 4.10b.

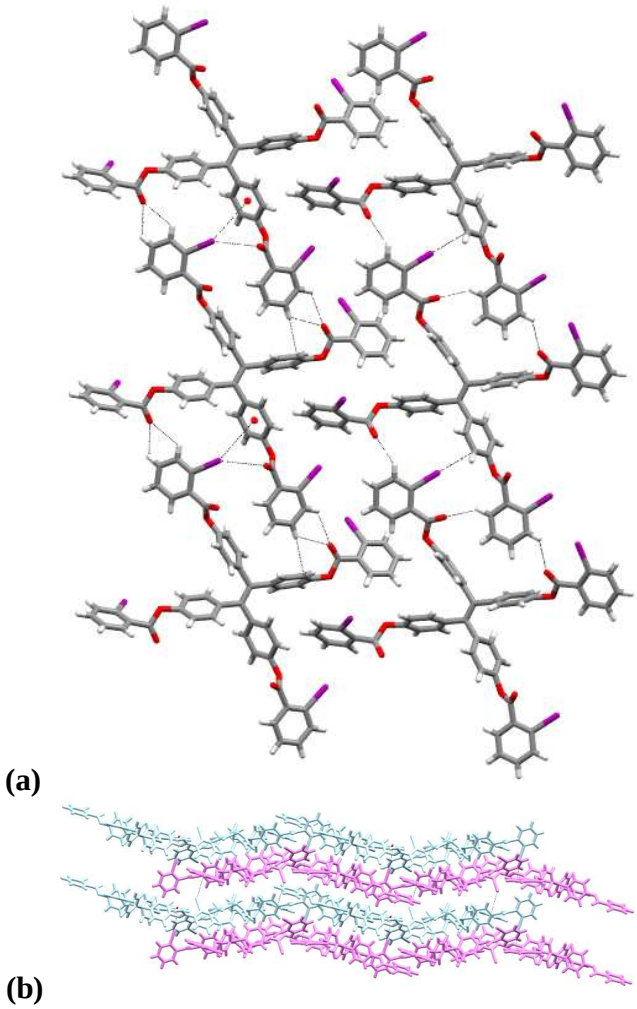

Figure 4.10 (a) 2D sheets in **4.7** (b) Stacked sheets of **4.7** with *abab* pattern.

The substrates in this study were designed to probe the interplay between specific types of halogen bonding interactions and molecular structure in similar but electronically distinct systems. Six basic halogen bonding synthons were observed as shown in Scheme 4.2. Table 4.3 provides a summary of halogen bonding synthons observed in compounds **4.3**-**4.7**. Although all the structures (except **4.4·(py)$_3$**) exhibited similar extended stacks of 2D layers, consistent trends in halogen bonding as a function of halogen or substitution pattern were not observed. Only in 1:1 solvent inclusion

complexes of 4-halobenzoyl esters were similar halogen bonding motifs present irrespective of structure. However, the halogen bonding interactions in all these structures were all confined to 2D sheet assemblies formed from parallel alignment of 1D ribbons. In all structures, extensive arene edge-to-face contacts appear to dominate over halogen bonding interactions. Given the abundance of π systems in all substrates, perhaps it is not surprising that when halogen bonding was observed, halogen···π synthon II was the most common, followed by X···O=C synthon I. Moreover, inmost of the structures, not all of the four peripheral halogens participate in halogen bonding interactions. Presumably this can be attributed to other competing interactions present in the system, most commonly edge-to-face stacking of arene rings.

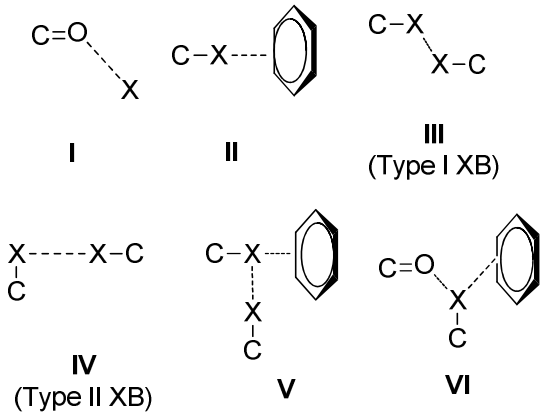

Scheme 4.3 Halogen bonding synthons exhibited in **4.3-4.7**.

Table 4.2 Summary of solid state halogen bonding interactions (synthons I-VI) observed in the TPE derivatives.

	I	**II**	**III**	**IV**	**V**	**VI**
4.3·(py)	+++	+++	---	---	---	---
4.4·(py)	+++	+++	---	---	---	---
4.3·(DMF)	+++	+++	---	---	---	---
4.4·(DMF)	+++	+++	---	---	---	---
4.4·(py)$_3$	---	+++	---	---	+++	---
4.5·(py)	+++	---	---	---	---	---
4.5·(DMF)	---	+++	+++	----	---	---
4.6	---	+++	---	+++	+++	---
4.7	---	+++	---	---	----	+++

Tetraphenylethylene and many TPE derivatives exhibit aggregation-induced emission.[23] In dilute solutions TPE's are generally non-fluorescent, but upon addition of poor solvent aggregation occurs which results in a fluorescence signal. The physical reason behind this phenomenon is restriction in intramolecular motion in solid or aggregated states. Sold state samples of TPE's **4.3** to **4.7** were fluorescent as seen with a hand-held UV light. Single crystals of **4.3** and **4.4** were further examined using confocal microscopy (Figure 4.11). As seen, the wavelength of solid state emission appears to be independent of halogen or solvent used for crystallization. This may indicate that AIE in this system is a molecular phenomenon that is not significantly influenced by extended solid state packing.

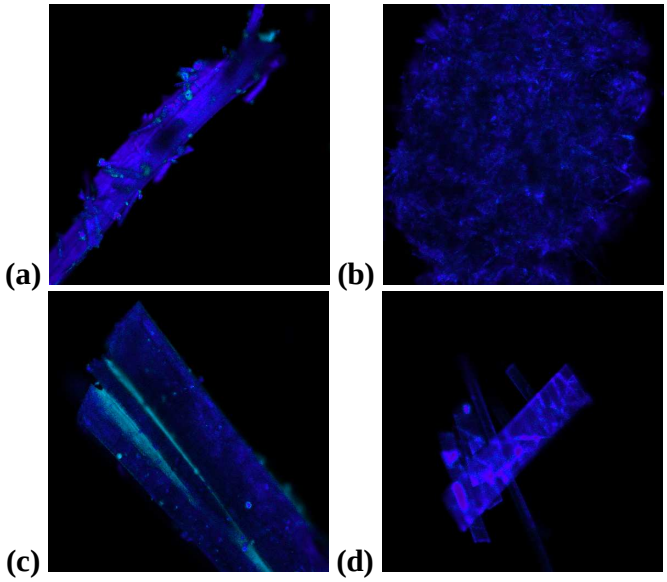

Figure 4.11 Solid state fluorescence confocal microscope image of (a) **4.3·(py)** (b) **4.3·(DMF)$_2$** (c) **4.4·(py)** (d) **4.4·(DMF)$_2$**.

Solution phase fluorescence studies were also performed in DMF and DMF water mixtures. All compounds **4.3-4.7** were found to be non-emissive in DMF solution. A change in fluorescence was observed as a function of % of water in solution. For **4.3**, **4.4** and **4.5**, fluorescence was turned on upon addition of 20% water and reached maxima at 60% water in DMF. Emission maxima for all these compounds were observed at ~470 nm. For **4.6** and **4.7**, no or little fluorescence was observed until solutions reached 80% (vol) water and a strong fluorescence signal was observed in of 90% water/DMF with maxima centered at ~500 nm.

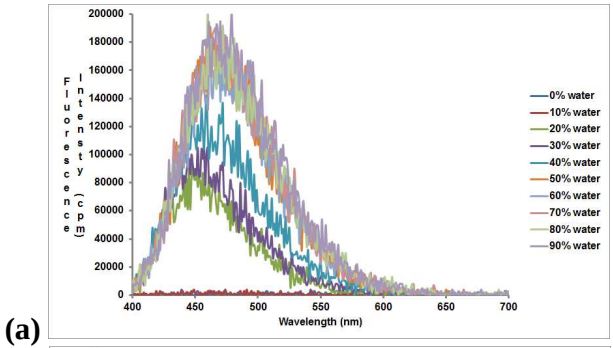
Fluorescence Intensity (cps)
Wavelength (nm)
0% water
10% water
20% water
30% water
40% water
50% water
60% water
70% water
80% water
90% water

(a)

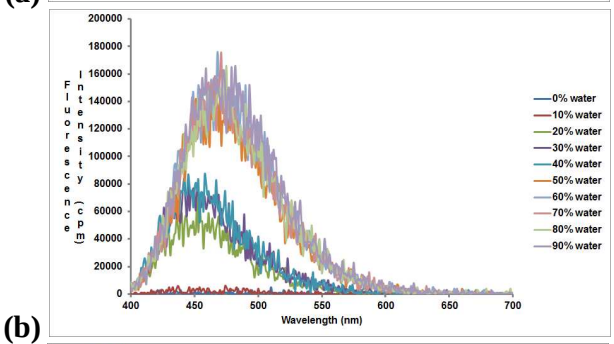
Fluorescence Intensity (cps)
Wavelength (nm)
0% water
10% water
20% water
30% water
40% water
50% water
60% water
70% water
80% water
90% water

(b)

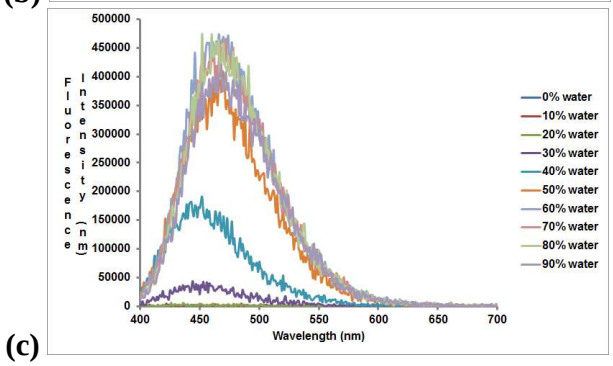
Fluorescence Intensity (cps)
Wavelength (nm)
0% water
10% water
20% water
30% water
40% water
50% water
60% water
70% water
80% water
90% water

(c)

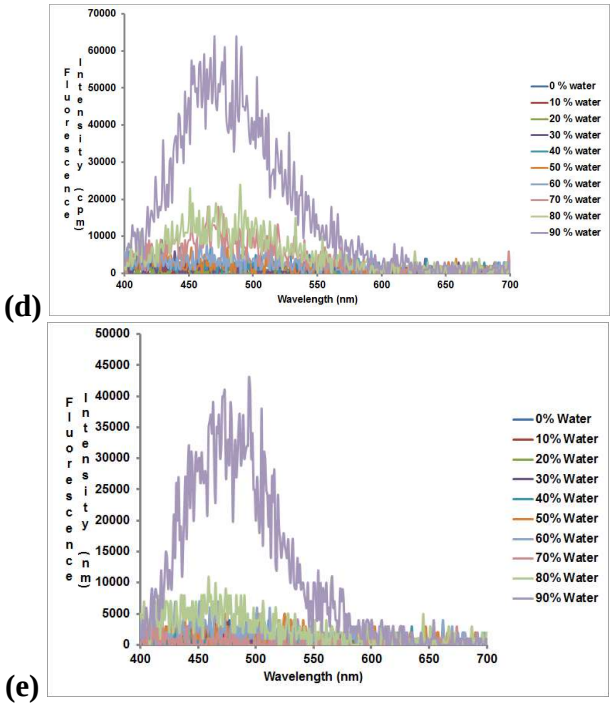

Figure 4.12 Fluorescence spectra of (a) **4.3** (b) **4.4** (c) **4.5** (d) **4.6** (e) **4.7** in DMF-water solvent system.

The differences in fluorescence and aggregation profiles of **4.3**-**4.5** as compared to **4.6**-**4.7** can be attributed to different solubilities in aqueous DMF. Difference in emission maxima can be attributed to positioning of halogen resulting in difference in aggregation.

4.4 Conclusion

This study was designed to assay the importance of specific halogen bonding interactions in conformationally flexible tritopic and tetratopic haloarenes. Bifurcated X···O=C and X··π halogen bonds in haloarene **4.2** assist in formation of unique iodo-arene trimers leading to nanoscale hexagonal channels in chloroform, pyridine and benzene inclusion complexes. These inclusion complexes were found to be metastable

state en route to thermodynamically favored close packed structure displaying both X···O=C and X··π interactions.

Halogen bonding was also examined in substrates **4.3-4.7** which lacked strong hydrogen bonding groups in order to maximize the influence of halogen bonding interactions. However, only the 4-halobenzoyl substituted compounds **4.3** and **4.4** displayed a high correlation between molecular structure and preferred halogen bonding motifs (X···O=C and X··π). In general, halogen bonding interactions observed in **4.3-4.7** appear to reinforce a common stacked-sheet packing motif in cooperation with edge-to-face arene interactions and C-H···O⁄π hydrogen bonding. Compared to **4.2** (and other tritopic haloarenes), compounds **4.3-4.7** display much less tendency to form X···X type halogen bonds.

CHAPTER V

APPLICATION OF TETRAARYLETHYLENES AS SUPRAMOLECULAR BUILDING BLOCKS IN METAL ORGANIC FRAMEWORKS AND ORGANIC CO-CRYSTALS

5.1 Introduction

Crystal engineering is the design and synthesis of molecular solid-state structures with desired properties, based on an understanding and exploitation of non-covalent interactions.[88] Two widely used strategies in crystal engineering are based on applications of hydrogen bonding and metal-ligand coordinate bonding.[89] Thus, supramolecular assemblies can be prepared from purely organic components or by combination of inorganic and organic precursors.

The terms metal-organic framework (MOF) or coordination polymer are often used to describe crystalline compounds consisting of metal ions or clusters coordinated to often rigid organic molecules. A metal-organic framework is composed of two major components: a metal ion or cluster of metal ions and an organic molecule called a linker. The organic units are typically di-, tri-, or tetravalent ligands.[90] The choice of metal and linker has significant effects on the dimensionality and properties of the MOF. For example, the metal's coordination preference influences the size and shape of pores by dictating how many ligands can bind to the metal and in which orientation.[91] Many MOFs prepared are porous and this property has been widely exploited in design of functional materials, especially materials for gas storage (e.g. H_2, CO, CO_2).[92-97] Fewer studies have targeted alternative applications of MOFs such as chemical sensing or catalysis.[98-101]

5.2 Objective

Three different TPE derivatives **5.1**, **5.2** and **5.3** have been synthesized as described in Chapter 2 and 3.[42,66] Compound **5.1** has carboxylic acid groups on the periphery whereas **5.2** and **5.3** have pyridine rings on the periphery. Here outer groups on all three compounds have the potential to act as ligands for metal ions or metal clusters. There is also precedent for pyridines to act as halogen bond acceptors due to their Lewis basicity. Thus, the TPE derivatives shown in Figure 5.1 all have possible applications as linker in organic co-crystals as well as in metal organic frameworks. Moreover, crystalline assemblies prepared from **5.1**-**5.3** should be photoluminescent due to the AIE phenomenon.[23] Frameworks with luminescent properties are envisioned to be well suited for applications related to chemical sensing and catalysis.[98-101] Consequently, a study was initiated to test the feasibility of using these TPE derivatives as metal ligating linkers in new MOF structures. Additionally, **5.2** and **5.3** were examined as halogen bond acceptors in combination with polytopic halogen bond donors. The aim in each case was to use the bulk and rigidity of TPE components to fashion open coordination and halogen bonding networks.

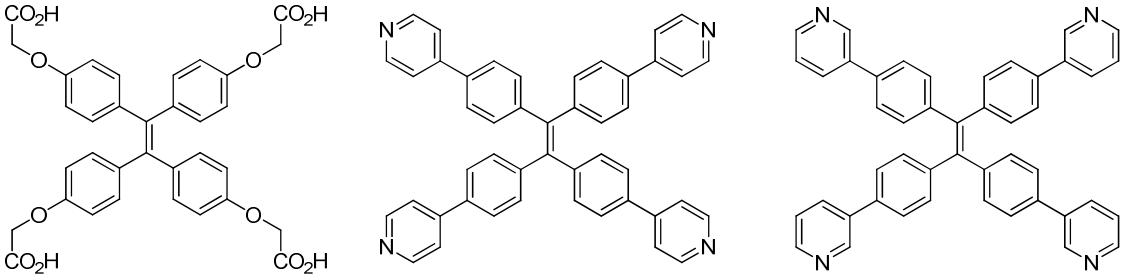

5.1 5.2 5.3

Figure 5.1 TPE derivatives used as supramolecular building blocks

5.3 Results and discussion

5.3.1 Chiral complex of **5.1** with zinc (II)

Although the molecular flexibility of the acid **5.1** complicates rational design of coordination polymers, we nonetheless envisioned **5.1** as a roughly square-planar tetratopic ligand toward appropriate metal ions.[42] Zinc was first examined as a potential metal component, and we were able to obtain Zn^{2+} complex **5.4** as colorless plates simply by mixing **5.1** with $Zn(ClO_4)_2 \cdot 6H_2O$ in 1:2 molar ratio in methanol and allowing the solvent to evaporate slowly at room temperature. Contrary to expectation, the stoichiometry of the isolated complex was 1:1, similar to the semiconducting assemblies obtained from **5.1** and bis(pyridine)s.[42] Each octahedrally-coordinated zinc ion is ligated by carboxylate units from **5.1** along with methanol and water solvates.

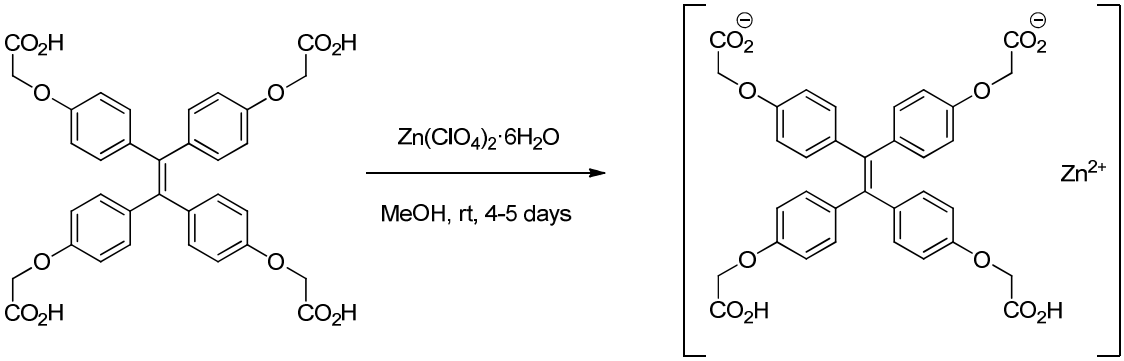

Scheme 5.1 Synthesis of complex **5.4**

In the complex **5.4**, Zn^{2+} ions link individual molecules of **5.1** via monodentate carboxylate/carboxylic acid coordination. The overall structure is complex due to its non-centrosymmetric nature with space group $P2_1$ and the presence of coordinated and included solvent molecules (water and methanol). Each Zn center is surrounded by 0.5

molecules of methanol and 2.5 molecules water ligands that are not only disordered but also have partial occupancy. The last coordination site on the octahedral Zn^{2+} center is occupied by free carboxylic acid residue from **5.1** as a neutral ligand.

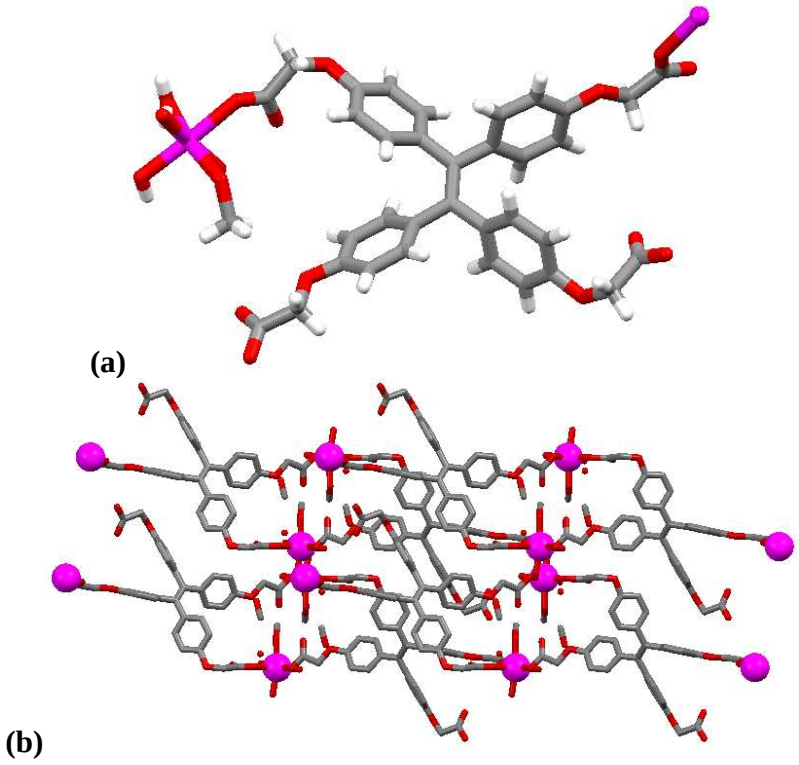

Figure 5.2 (a) Structure of complex **5.4** (b) Extended packing in **5.4**.

In the extended packing of **5.4**, it is observed that each molecule of **5.1** bridges two Zn^{2+} ions. This results in segregated regions of **5.1** and Zn with individual molecules arranged in step like fashion (Figure 5.2b). Segregated columns of **5.1** and Zn are clearly evident. These columns are separated by layers of Zn ions oriented with their axial ligands roughly parallel to the **5.1** stacking direction. Attempts to grow similar complexes from other metal salts such as $Ni(ClO_4)_2$, $Cu(ClO_4)_2$, $Fe(ClO_4)_3$, $Co(ClO_4)_2$ were not successful under similar crystallization conditions.

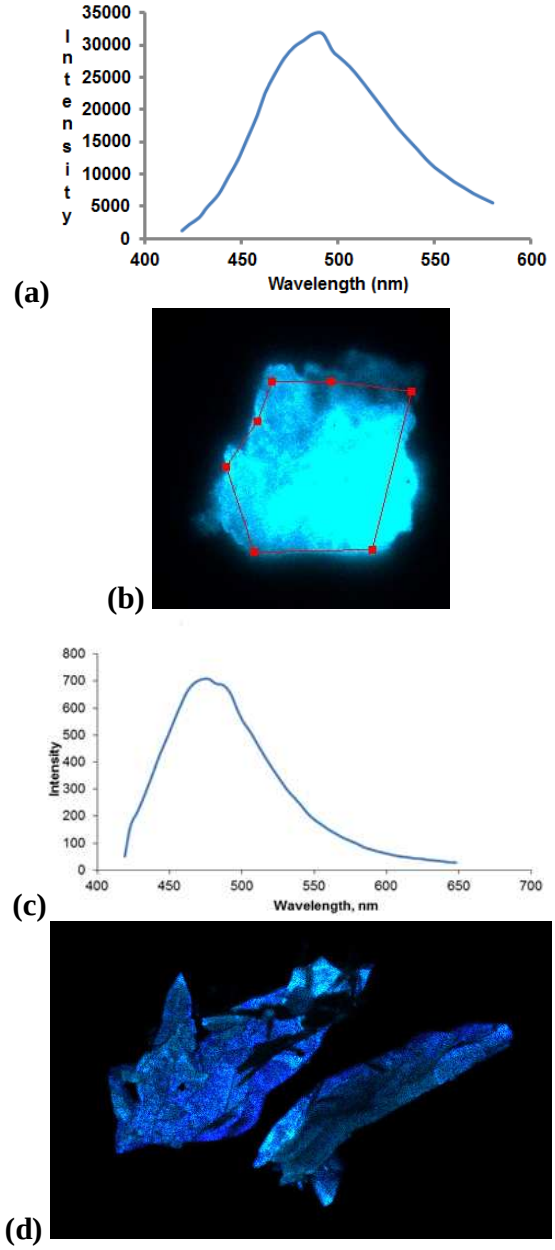

Figure 5.3 (a) Solid state fluorescence spectrum of **5.1** (b) Confocal fluorescence microscopy image of **5.1** (c) Solid state fluorescence spectrum of **5.4** (d) Confocal fluorescence microscopy image of **5.5**. For all measurements, excitation wavelength is 405 nm.

As is the case with many TPE derivatives, both acid **5.1** and Zn complex **5.4** were found to be fluorescent in the solid state under UV irradiation.[24] Solid state fluorescence

on crystalline samples was performed using confocal fluorescence microscopy and image of each sample along with the spectrum was obtained. As seen in Figure 5.3a, acid **5.1** gives broad fluorescence spectrum centered ~495 nm. On the other hand, emission maxima blue shifts in case of the Zn complex **5.4** where spectrum is centered at ~475 nm (Figure 5.3c). This phenomenon can also be visually seen by the images obtained from this study (Figures 5.3b and 5.3d).

5.3.2 Porous metal organic framework prepared from **5.2** and $ZnCl_2$

Compound **5.2** was envisioned to be a planar tetradentate ligand with four pyridine nitrogen atoms located in the same plane as the central alkene as observed in the crystal structure of **5.2** described in Chapter 3. Complex **5.5** has been synthesized under solvothermal conditions by mixing tetrapyridyl TPE **5.2** with $ZnCl_2$ in a mixture of DMF and DMA. The reaction was heated to 135 °C in a programmable oven at 1 °C/min and maintained at this temperature for 24 hours, followed by cooling to room temperature at 0.1 °C/min. X-ray quality crystals of **5.5** were obtained as colorless bars.

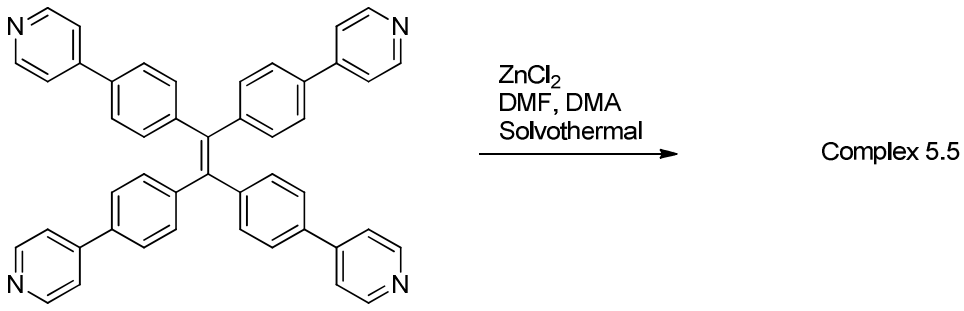

5.2

Scheme 5.1 Synthesis of complex **5.5**

An X-ray diffraction study on the complex **5.5** reveals the expected topology. An *abab* type layered structure was obtained with octahedrally coordinated zinc centers. The four equatorial positions of each zinc ion are occupied by pyridine residues from four different molecules of **5.2**, and axially ligated chloride ions complete the Zn^{2+} coordination sphere (Figure 5.4a). As shown in Figure 5.4b, all four pyridine units of **5.2** coordinate to Zn^{2+} ions. The co-planar geometry of the pyridine groups in **5.2** with respect to the central alkene coupled with octahedral zinc centers results in formation of 2D layers as shown in Figure 5.4c. The coordination sphere surrounding the invidual zinc ions is similar to that encountered in classical Werner complexes of general formula $M(py)_4X_2$ where X is halide or pseudohalide anion, and M is a divalent metal ion.[102] Molecular complexes of this type are interesting as they frequently crystallize with specific solvates (so-called Werner clathrates) and have been investigated for selective solid state guest inclusion. Examples of tetrapyridyl MX_2 complexes are very scarce.[103] MacGillivray *et al.* have reported a metal organic framework of $Zn(NO_3)_2$ with a tetrapyridyl ligand tpcb (1,2-tetrakis(4-pyridyl)cyclobutane) which binds metal atoms via the two different pyridyl groups to give a 2D MOF based exclusively on 4-connected nodes.[55] Metal organic network. **5.5** can be viewed as a polymeric array of Werner complexes and may represent the prototype for a family of structurally related metal ions.

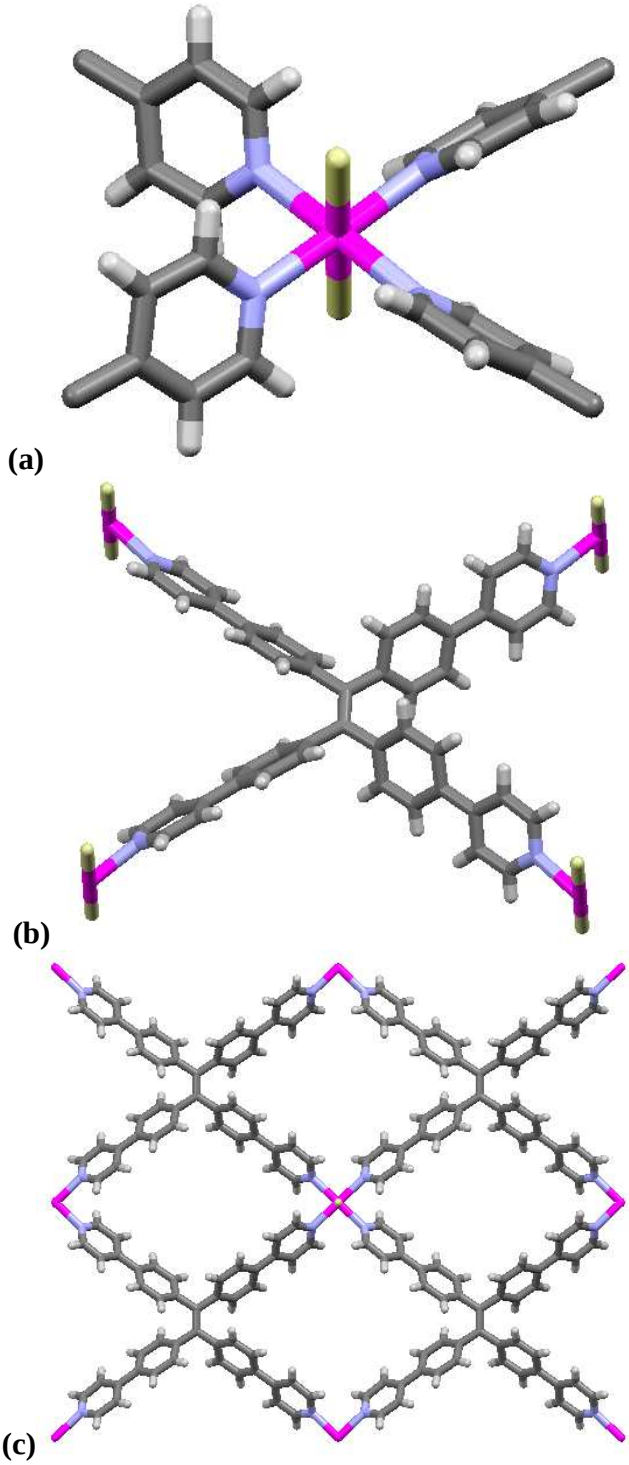

Figure 5.4 (a) Octahedrally coordinated Zn center in **5.5** (b) Four pyridine groups of **5.2** ligating to Zn centers in the complex **5.5** (c) 2D layers of the complex **5.5**.

The 2D layers in **5.5** are arranged is an *abab* type stacking pattern with interlayer interactions featuring chloride ligands positioned directly above and below the central alkene of **5.2** at a distance of ~3.49 Å as shown in Figure 5.5a. The absence of interpenetration and the layered structure results in generation of large channels with 2D openings of ~17 × 14 Å (Figure 5.5b). These voids are filled with disordered DMA solvates as shown in Figures 5.5c and 5.5d. The solvent molecules participate in polar interactions with pyridine rings in **5.2**. The calculated solvent-accessible void space in this crystal was found to be 42% using PLATON[84].

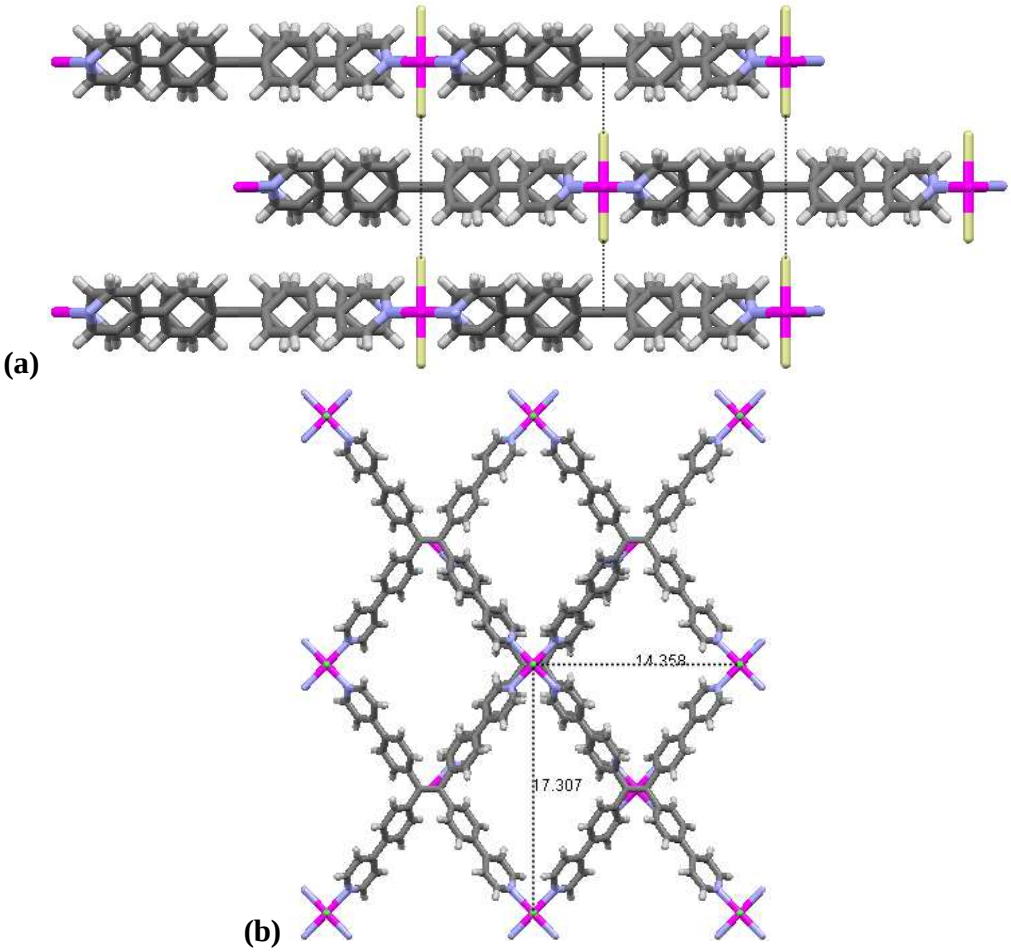

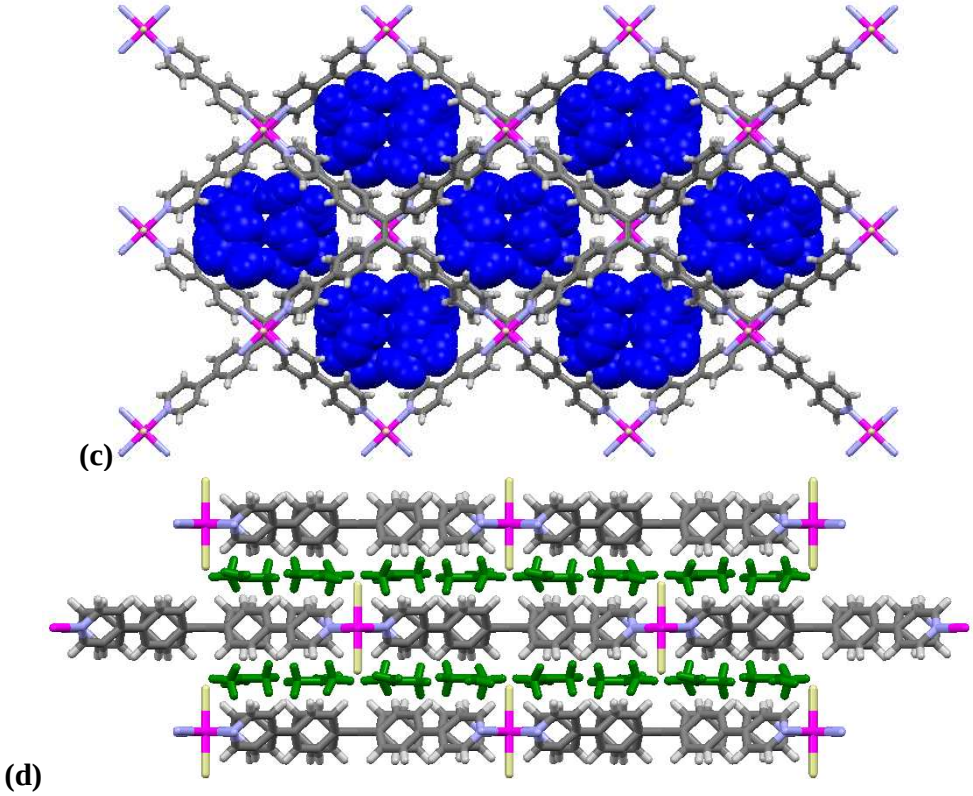

Figure 5.5 (a) 2D layers stacked in **5.5** (b) Extended packing in **5.5** showing channels with dimension of of ~17 × 14 Å (c) Extended packing in **5.5** showing presence of DMA solvent in channels (d) Solvent occupying interlayer space in **5.5**.

As is the case with many TPE derivatives, the coordination polymer **5.5** was found to be fluorescent under UV irradiation. A preliminary TGA study showed that the sample loses DMA solvates between ~150 °C to ~180 °C to afford thermally stable species up to ~350 °C. We have not yet been able to obtain bulk sample to determine crystal morphology after solvent evacuation or to study porosity and gas adsorption of the sample. Nonetheless, the successful preparation of **5.5** satisfies one of the main objectives of this study as the feasibility of incorporating metal-ligating TPE's into topologically intriguing coordination polymers has been demonstrated. Notably, exposure of 3-pyridyl TPE **5.3** to $ZnCl_2$ under identical reaction conditions failed to produce crystalline

material. Thus, the geometry of **5.2** may be crucial for coordination polymers modeled after Werner clathrate hosts. It is anticipated that additional examples of similar coordination networks should be available from **5.2** and other M^{2+} halides. It is further expected that the presence of a suitable 'solvent' to act as a template for clathrate assembly will be important as well. Applications of solvothermal conditions to prepare crystals from same ligand with other metal dihalides such as $CuCl_2$, $NiCl_2$, $CdCl_2$ and $CoCl_2$ were not successful.

5.3.3 Organic co-crystals prepared from tetrapyridyl TPE **5.3** and iodoperfluorobenzenes

Halogen bonding interactions between pyridine and haloarenes are well precedented in the literature.[67] Toward this end, we utilized both tetrapyridyl TPE's **5.2** and **5.3** to form co-crystalline assemblies with iodoperfluoroarenes. Two different iodoperfluoroarenes were used in this study; 1,4-diiodotetrafluorobenzene and 1,2-diiodotetrafluorobenzene. The fluoro groups (which do not participate in halogen bonding interactions) serve to activate the iodoarene substituents for halogen bonding by virtue of their electron withdrawing ability. Both **5.2** and **5.3** were subjected to crystallization with these two iodoperfluorobenzenes and two different single crystalline samples were obtained. Both structures featured short C-I$\cdots$$N_{py}$ halogen bonds and both were obtained as close packed co-crystals, in other words, solvents were not included in **5.6** or **5.7**. Both structures also bear remarkably similar bulk topologies, despite differences in individual packing motifs.

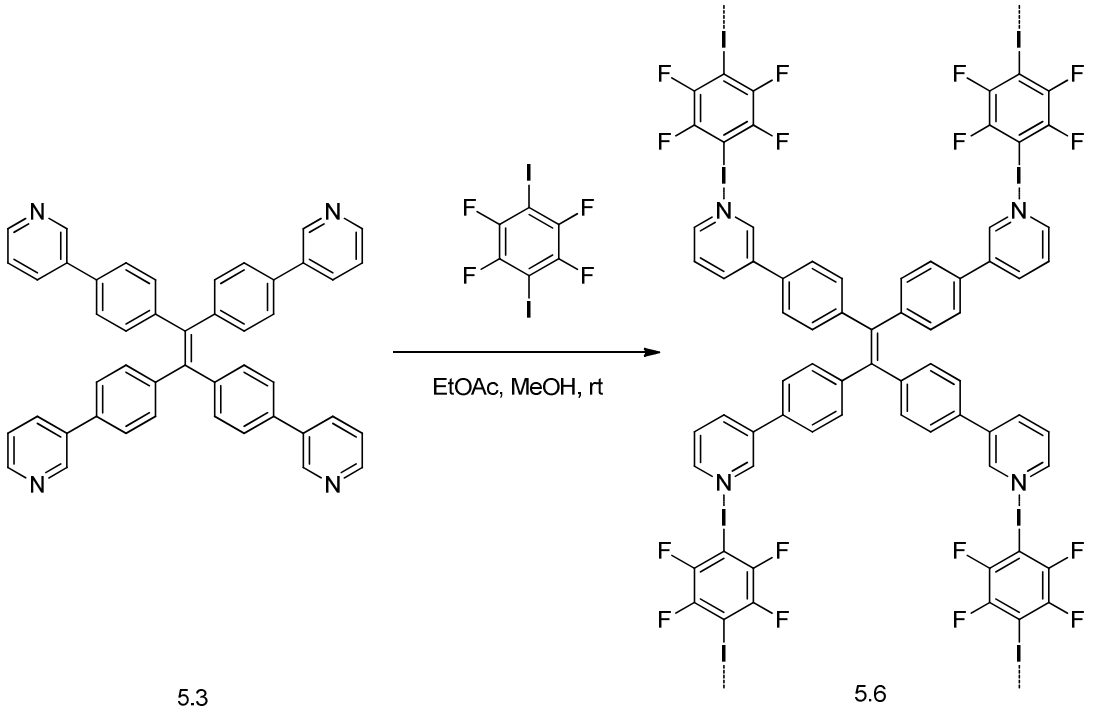

5.3 5.6

Scheme 5.2 Synthesis of **5.6**

Compound **5.6** was obtained via slow evaporation of solutions of **5.3** and 1,4-diiodotetrafluorobenzene in methanol and ethyl acetate solvent mixture (Scheme 5.4). As envisioned, a 1:2 stoichiometry between **5.3** and 1,4-diiodotetrafluorobenzene was observed with C-I···N_{py} halogen bond interactions being present (Figure 5.7a). Each molecule of **5.3** interacts with 4 molecules of 1,4-diiodotetrafluorobenzene. The I···N distances were 2.768 Å to 2.959 Å which are in the range of some of the shortest I···N halogen bonds reported in neutral complexes.[104]

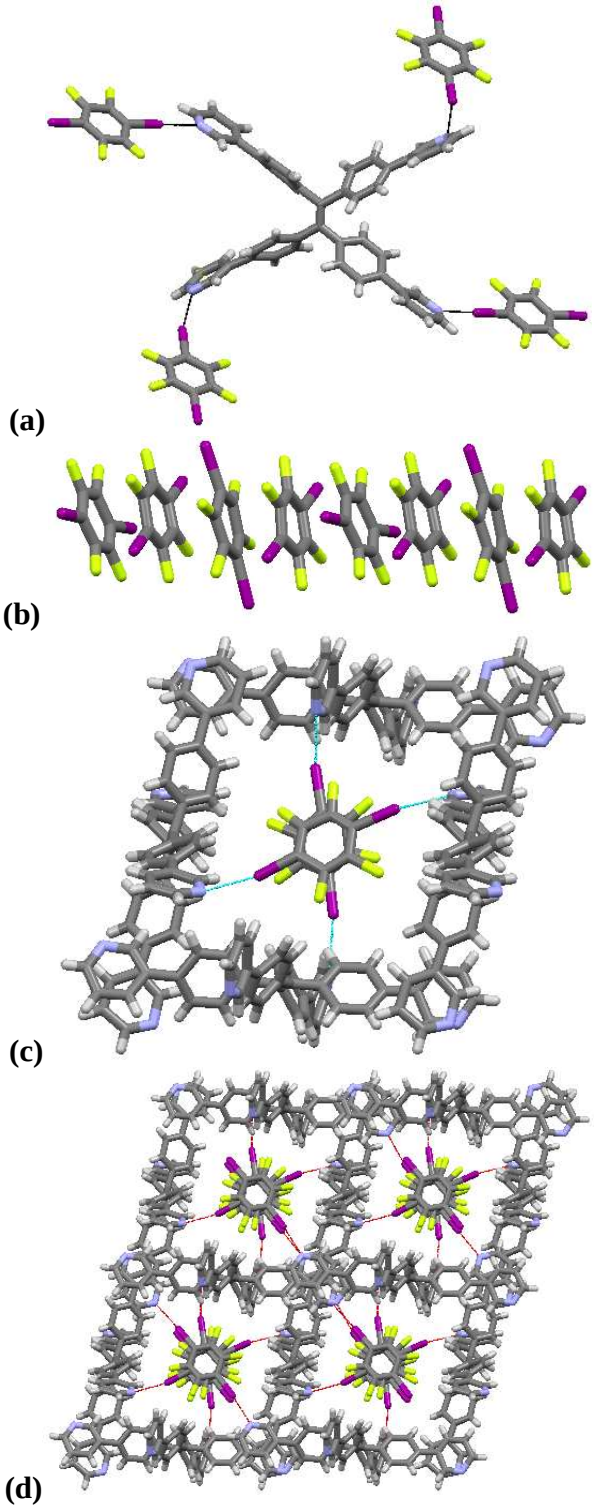

Figure 5.6 (a) C-I$\cdots$N$_{py}$ halogen bonds observed in **5.6** (b) Stacks of 1,4-diiodotetrafluorobenzene in **5.6** (c) (d) Extended packing in **5.6**.

In this structure, diiodotetrafluorobenzene molecules are cofacially stacked with centroid distances ranging between ~3.6 Å to ~3.8 Å (Figure 5.6b). Adjacent arene rings are rotated with respect to one another such that every fifth arene is in the same orientation. Individual molecules of **5.3** are oriented in such a way that both molecules in contact with one iodoarene are arranged in mutually perpendicular directions. This results in propagation of molecules of **5.3** in two different directions, ultimately resulting in rhomboid channels as shown in Figure 5.6c. The extended packing illustrated in Figure 5.6d shows that these rhomboid channels extend throughout the crystalline matrix and house the cofacially stacked iodoarenes.

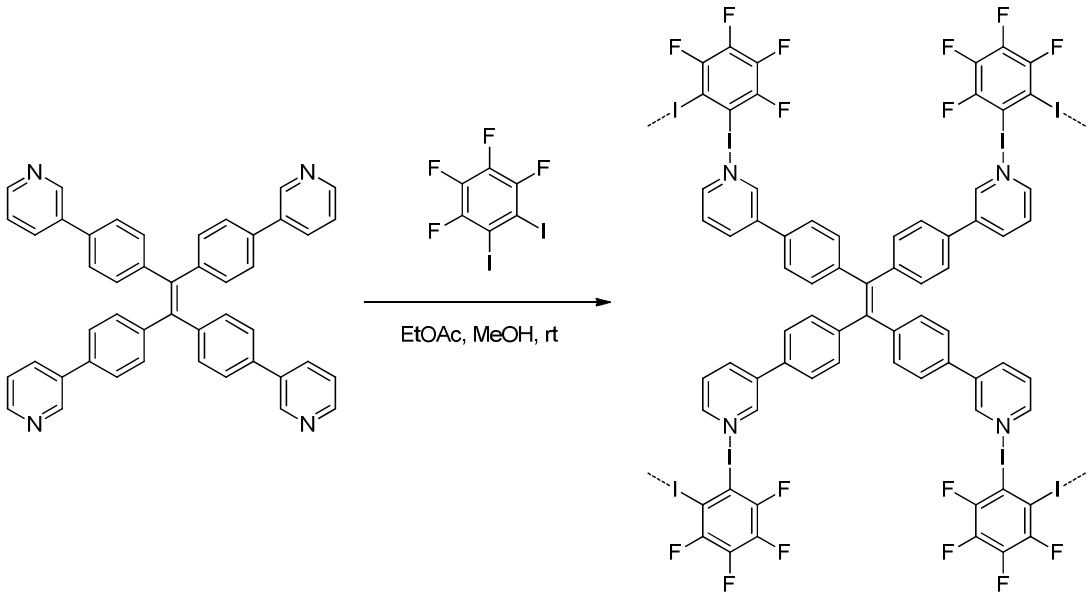

5.3 5.7

Scheme 5.3 Synthesis of **5.7**

Compound **5.7** was obtained via slow evaporation of solutions of **5.3** and 1,2-diiodotetrafluorobenzene in methanol and ethyl acetate solvent mixture (Scheme 5.4). As envisioned, a 1:2 stoichiometry of **5.3**: 1,2-diiodotetrafluorobenzene was observed with

C-I···N_{py} halogen bond interactions being present (Figure 5.7a). Similar to the situation encountered in co-crystal **5.6** each molecule of **5.3** interacts with 4 molecules of 1,2-diiodotetrafluorobenzene. The I···N distances were~2.9 Å to 3.1 Å. Once again, diiodotetrafluorobenzene molecules are cofacially stacked with centroid distances ~3.6 Å to ~3.8 Å, Figure 5.7b).

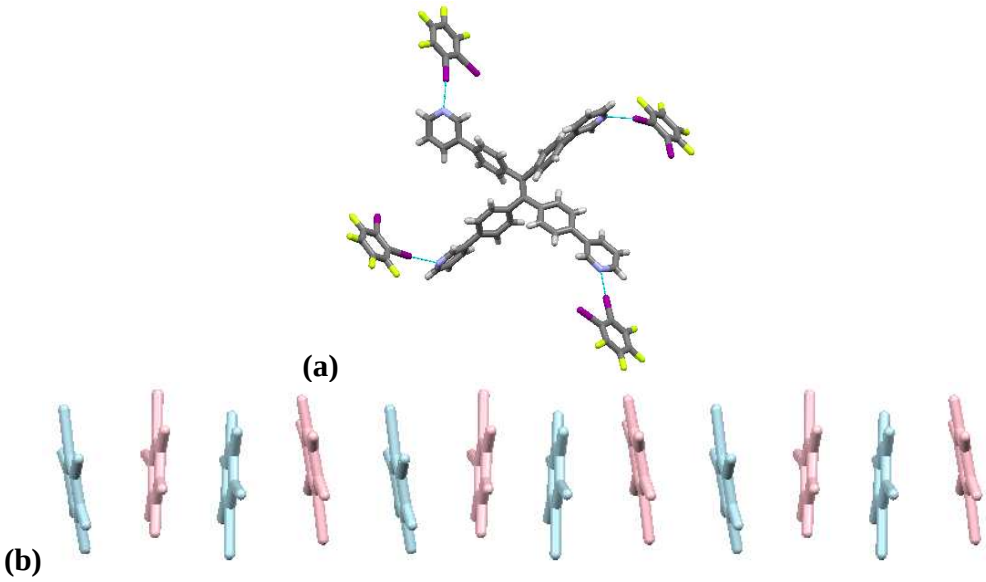

(a)

(b)

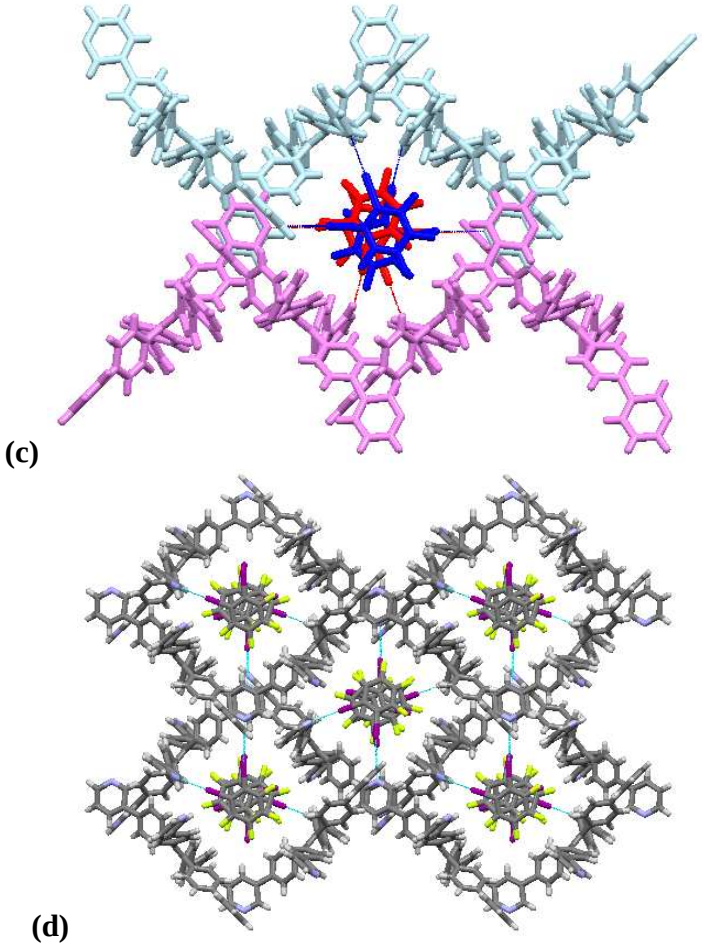

Figure 5.7 (a) C-I$\cdots$N$_{py}$ halogen bonds observed in **5.7** (b) Color coded stacks of 1,2-diiodotetrafluorobenzene in **5.7** (c) (d) Extended packing in **5.7**.

The overall structure of **5.7** consists of two distinct non interpenetrating networks that include haloarenes along with molecules of **5.3** (Figure 5.7c). Alternate molecules of iodoarenes are part of alternate networks as shown in Figure 5.7b. Interestingly, these networks pack in such way so as to produce rhomboid channels in which layers of iodoarene halogen bond donors reside. Thus, at first glance **5.6** and **5.7** appear to have virtually identical solid state structures even though there are significant differences in individual network architectures.

The extent of halogen bonding in **5.6** and **5.7** emphasizes the fact that electrophilicity of the iodo halogen bond donor has been enhanced by presence of more fluorine atoms on the arene rings. This results in participation of both iodine atoms in each arene in halogen bonding interactions with nitrogen atoms of pyridine. We briefly examined whether halogen bonding was operative in solution using fluorescence spectroscopy. We speculated that halogen bonding interactions may lead to multimolecular aggregates that might be fluorescent (i.e. AIE). In the event, however, we found no indication of fluorescence in THF solutions of **5.3** and diiodoarenes at concentrations as high as 48 μM. Only upon addition of H_2O was fluorescence was observed and this is attributed to aggregation of the TPE derivative in aqueous solution.[66]

5.4 Summary

The three TPE derivatives **5.1**, **5.2** and **5.3** have been successfully used as supramolecular building blocks in construction of metal-organic frameworks and organic co-crystals via coordinate bonds and halogen bonds. Compounds **5.1** are **5.2** have been used as linkers in metal organic frameworks. The Zn^{2+} complex **5.4** formed from tetraacid **5.1** and $Zn(ClO_4)_2$ displays structural characteristics similar to organic semiconducting assemblies obtained from **5.1** and various bis(pyridine)s in that segregated regions of TPE stacks and Zn^{2+} ions are present. Additional coordination of water and methanol as exchangeable ligands on the Zn centers results in a non-centrosymmetric structure. This property can potentially be exploited in application of **5.4** as asymmetric catalyst.

In the MOF **5.4** obtained from solvothermal crystallization of **5.2** with $ZnCl_2$, a layered structure is observed with generation of large channels with 2D openings of ~17×14 Å which were occupied by solvent molecules. Future work includes performing solvent exchange experiments as well as gas absorption studies on this material and inspecting the effect of solvent on fluorescence. Halogen bonded assemblies **5.6** and **5.7**

display seemingly strong N···I halogen bonding interactions as judged by the short N···I contact distances. All four pyridines of **5.3** and both iodine atoms of 1,4- or 1,2-diiodotetrafluorobenzene participate in halogen bonding interactions. Both structures show the presence of cofacially stacked haloarenes surrounded by a square grid network of **5.3**. This results in formation of rhomboid channels in which stacks of diiodotetrafluorobenzene reside.

CHAPTER VI

SUMMARY AND FUTURE DIRECTIONS

6.1 Summary

The initial objective of the research described in the previous chapters was to utilize tetraphenylethylene (TPE) derivatives as supramolecular building blocks for functional materials. Toward this end, synthesis and applications of various TPE derivatives was described.

Principles of crystal engineering were applied toward the construction of supramolecular assemblies between an acid-functionalized tetraphenylethylene derivative and four different bis(pyridine)s. Each assembly was structurally characterized, and charge transfer interactions within each sample were visually apparent. Quantum chemical calculations were used to determine crystal band structure and band gap magnitude, and electrical properties of the materials were measured using conducting probe atomic force microscopy (CP-AFM). The crystals displayed charge-carrier capability, and the magnitude of semiconductivity varied systematically as a function of conjugation in the bis(pyridine) component. Crystals incorporating 4,4'-bis(pyridyl)ethylene and 4,4'-bipyridine displayed conductivities comparable to those of established organic semiconductors (μ_{eff} = 0.38 and 1.7 × 10^{-2} $cm^2/V \cdot s$, respectively).

Two tetrapyridyl-substituted tetraphenylethylenes were prepared via Suzuki coupling between tetrabromo tetraphenylethylene and 3- or 4-pyridine boronic acid. Both compounds exhibit aggregation-induced emission as determined by solid state fluorescence spectroscopy and solution phase fluorescence measurements performed in aqueous/organic solvent mixtures. Solution phase fluorescence was also found to be switchable as a function of pH. Both compounds were structurally characterized by X-ray crystallography. Upon treatment with $Fe(ClO_4)_3 \cdot xH_2O$, these compounds were converted to their tetraperchlorate salts. These tetra-perchlorates were isolated as single crystals and

their structures were determined by X-ray diffractometry. In both cases extensive hydrogen bonding networks were observed involving pyridinium N–H groups, perchlorate anions, and included water molecules. Additionally, both structures feature hydrophobic crystalline regions formed from stacking of tetraarylethylene cations in helical fashion.

Solid state halogen bonding interactions have been examined in structurally similar tetratopic haloarenes bearing a common tetraphenylethylene core. This study was designed with the aim of providing insight into the relative importance of fundamental solid state halogen bonding interactions. A total of nine crystal structures from five different tetraarylethylene substrates were obtained. While distinct and unique X···O and X··π halogen bonding interactions were identified in each structure, all structures displayed nominally similar packing arrangements generally consisting of 1D ribbons aligned to generate non-interpenetrating 2D sheets. This feature may be a consequence of extensive edge-to-face arene-arene interactions found in each structure and may indicate a greater structure-determining role for aryl interactions relative to halogen bonding contacts in this system.

The last part of this work involved utilizing different TPE derivatives as building blocks in metal organic frameworks and organic co-crystalline assemblies. Tetraacid derivative of TPE was treated with Zn^{2+} to yield a zinc complex which crystallized in a non-centrosymmetric space group. Two different tetrapyridyl derivatives of TPE were used as building blocks in a porous metal organic framework with $ZnCl_2$ and an organic co-crystalline assembly with diiodotetrafluorobenzenes mediated by N···I halogen bonding interactions. In each system intriguing features were evident. Zn^{2+} MOF possesses relatively large channels that may permit selective solvate ingress and egress while the halogen bonded co-crystals exhibited insulated columnar stacks of iodoarene components. These initial findings establish a basis for future work aimed at capitalizing upon these unique structural features for design of novel functional materials.

6.2 Future directions

We have demonstrated that TPE is an attractive supramolecular building block and TPE derivatives can be used as functional materials for variety of applications. To extend this study, a variety of TPE derivatives can be prepared and used in design of functional materials.

6.2.1 Organic semiconducting assemblies based on TPE framework

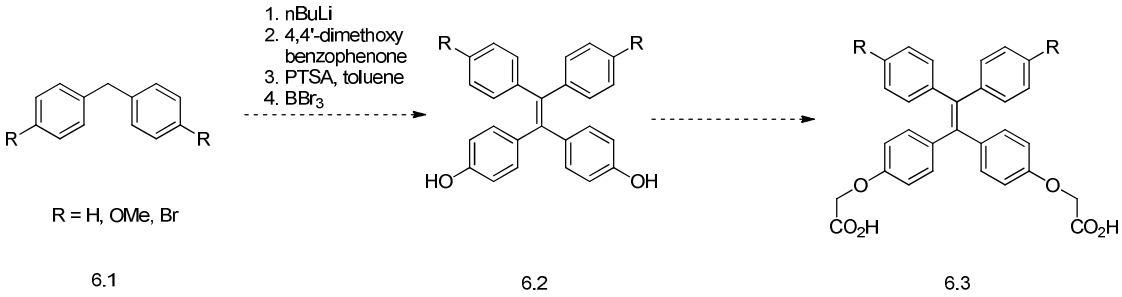

Scheme 6.1 Synthesis of dicarboxylic acid **6.1**.

There are two variables in our design of organic semiconducting assemblies; the carboxylic acid component and the bis(pyridine). The importance of four carboxylic acid residues and the effect of electron donating groups on the acid molecule can be examined by synthesis of diacid **6.3** from previously known phenol intermediates **6.2**[105] as shown in Scheme 6.1. Additionally, other variants in the bis(pyridine) can be examined by use of various previously known bis(pyridine)s **6.4**-**6.7**.[106-109] Compound **6.7** is of particular interest due to presence of electronically active naphthalene diimide group as the core.

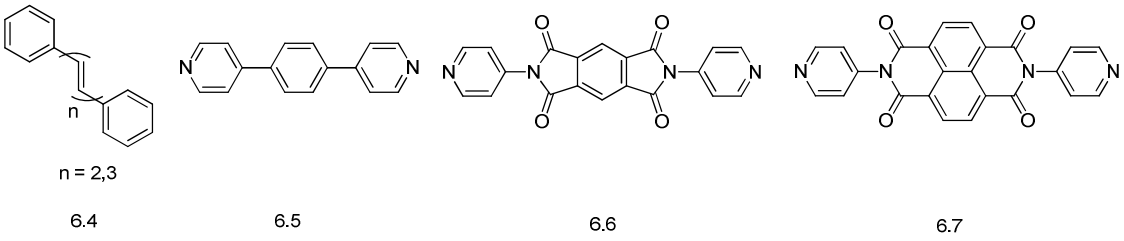

Figure 6.1. Examples of other bis(pyridine) units to be synthesized and used.

A different approach is to combine both participating units on the same molecule. Scheme 6.2 displays synthesis of two such compounds along this approach. One side of the TPE core is functionalized with pyridine units and the other side has carboxylic acid residues. The bifunctional TPE derivative **6.9** can potentially form a ribbon-like network with similar electroactivity as the dual component assemblies previously described.

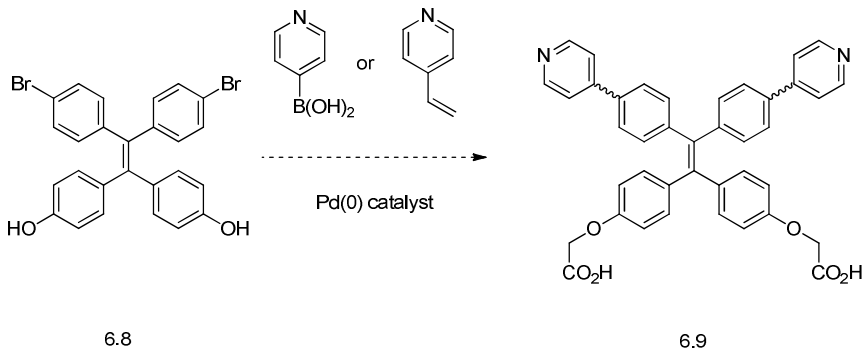

Scheme 6.2 Synthesis of bifunctional TPE derivative **6.9**.

6.2.2 Halogen bond donors based on TPE core

As it was described in previous chapters, halobenzoyl esters of TPE derivatives have a propensity to be involved more in arene interactions than participate in halogen bonding interactions. Electron deficiency of halogen can be enhanced by addition of fluorine substituents on an arene ring. Toward this end, an ester **6.11** can be prepared

from previously reported starting materials[29,110] via one step esterification. This compound will not only participate in halogen bonding interactions with same molecules, but it has potential to be co-crystallized with various electronically active Lewis base moieties that can result in formation of neutral electroactive complexes mediated by halogen bonds.

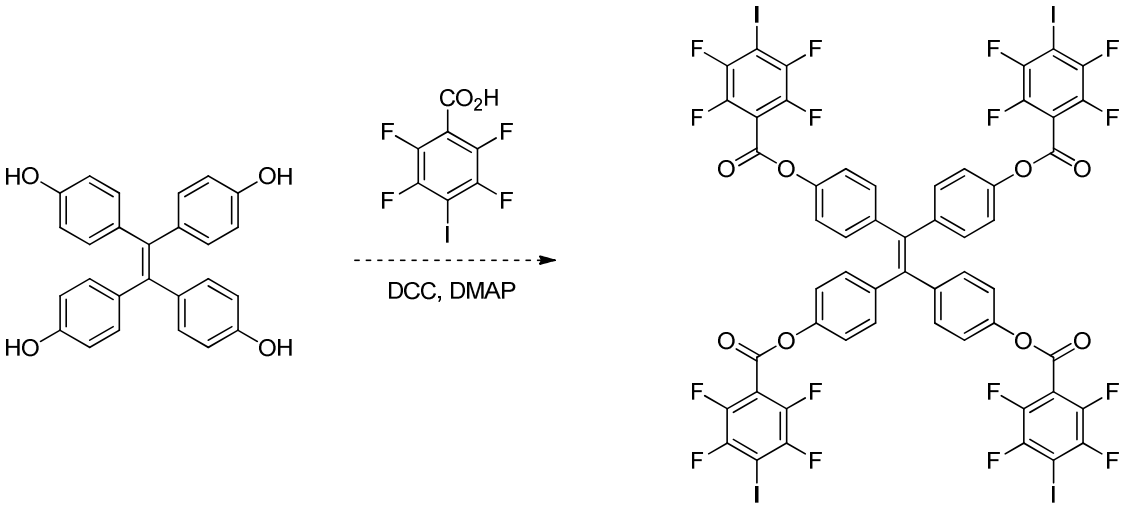

6.10 6.11

Scheme 6.3 Synthesis of iodoperfluorobenzoyl ester of TPE **6.11**.

6.2.3 TPE based linkers for metal organic frameworks

Apart from pyridine groups, carboxylic acid ligands have been widely used as linkers in metal organic frameworks. Two rigid tetra-carboxylic substituted TPE's **6.12** and **6.13** can be prepared and crystallized with various metal salts. Compound **6.12** may be conveniently prepared from previously known tetratolylethylene[111] and compound **6.13** may be prepared from previously known cyano derivative by hydrolysis.[18]

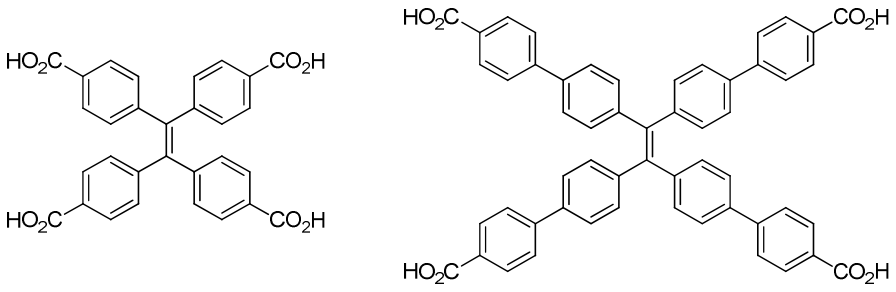

6.12 6.13

Figure 6.2 Other fluorescent linkers for MOFs

Coupled with accessibility of the TPE derivatives with their interesting opto-electronic properties at the molecular level, we hope to utilize TPE derivative in variety of supramolecular functional materials.

CHAPTER VII

EXPERIMENTAL

7.1 General experimental details

All commercially available starting materials were used as received unless otherwise noted. All reactions were performed under argon atmosphere. Solvents were dried and purified by passage through activated alumina columns. Proton nuclear magnetic resonance (^{1}H-NMR) spectra and carbon nuclear magnetic resonance (^{13}C-NMR) spectra were recorded at 300 MHz and 75 MHz, respectively. Chemical shifts are recorded as δ values in parts per million (ppm) relative to tetramethylsilane for ^{1}H-NMR and ^{13}C-NMR in $CDCl_3$ and residual undeuterated solvent for all other spectra. High resolution mass spectra were obtained using electro spray ionization (ESI). Melting points were recorded using a capillary melting point apparatus and are uncorrected. Infra-red spectrum were collected Diffraction data were collected on a Nonius-Kappa CCD diffractometer. Fluorescence spectroscopy was performed on a Horiba Jobin Yvon Fluoromax 4 fluorospectrometer in a 1 cm quartz cell and commercially available spectroscopy grade solvents were used. Slit width for excitation and emission were 1 nm each and integration time was 0.1 s. Thermogravimetric analysis (TGA) was performed on TA Instruments Q500. Approximately 5-10 mg of the sample in an open aluminum pan was heated in the TGA from room temperature to 450°C at 5°C/min under nitrogen purge. Topographic height imaging and I-V measurements were performed using a commercially available atomic force microscope (MFP 3D, Asylum Research, Santa Barbara, CA) with a conducting probe module (ORCA, Asylum Research, Santa Barbara, CA). Samples were first imaged using AC mode to determine crystal morphology. All imaging and measurements were collected using a diamond coated tip (NANOSENSORS, Switzerland) with a tip radius of curvature of 150 ± 50 nm and spring constant of 0.02-0.77 N/m.

SHELXTL was used for processing of X-ray data. Crystallographic data were processed using full matrix least squares refinement of F^2 against all reflections. The weighted R-factor (wR) and goodness of fit S are based on F^2, conventional R-factors (R) are based on F, with F set to zero for negative F^2. The threshold expression of $F^2 > 2\sigma(F^2)$ is used only for calculating R-factors(gt) etc., and is not relevant to the choice of reflections for refinement. R-factors based on F^2 are statistically about twice as large as those based on F, and R-factors based on all data will be even larger.

7.2 Experimental data for Chapter 2

Tetramethoxy TPE **2.7** and tetraphenol **2.8** were synthesized according to the procedure published by Schultz *et al.*[29] Bis(pyridyl)acetylene BPA was synthesized according to the procedure published by Coe at al.[43]

7.2.1 Synthesis and characterization of tetraester **2.9**

Under argon, tetraphenol **2.8** (0.25 g, 0.63 mmol), K_2CO_3 (1.05 g, 7.57 mmol) and ethyl bromoacetate (0.7 mL, 6.31 mmol) were mixed in THF (20 mL) and heated to reflux for 72 h. The reaction was diluted with water and extracted with EtOAc (3 x 25 mL). The organic layers were combined and washed with 10% aq. NaOH solution (50 mL) and brine (50 mL). After drying over anhydrous $MgSO_4$ the solvent was removed under vacuum and the residue was purified by silica gel flash column chromatography (1:1 EtOAc:Hexanes) to yield **2.9** as a yellow semi-solid (0.32 g, 68%).

^{1}H NMR (300 MHz, $CDCl_3$, 298 K): δ 6.90 (d, *J* = 8.76 Hz, 8H), 6.63 (d, *J* = 8.76 Hz, 8H), 4.54 (s, 8H), 4.25 (q, *J* = 7.14 Hz, 8H), 1.28 (t, *J* = 7.14 Hz, 12H).

^{13}C NMR (75 MHz, $CDCl_3$, 298 K) δ 168.8, 156.1, 138.4, 137.4, 132.4, 113.8, 65.3, 61.2, 14.0.

IR (neat) (cm^{-1}) 1756.

HRMS (ESI) calculated for $C_{42}H_{44}O_{12}\cdot Na$ $[M+Na]^+$ 763.2730, found 763.2706.

7.2.2 Synthesis and characterization of **2.2** (**TCA**)

Tetraester **2.9** (0.25 g, 0.23 mmol) and 0.27 g (6.75 mmol) NaOH were combined in a 1:1 solution of THF:water (20 mL) and the mixture was heated to reflux for 4 h. The volume of solvent was then reduced under vacuum and the remaining aqueous residue was diluted with H_2O to a volume of 30 mL. The solution was acidified by addition of 50% aq. HCl to pH ~2 which resulted in precipitation of the desired tetraacid as a pale yellow solid. The solid was collected by vacuum filtration, washed with H_2O (50 mL), and dried in air to give **2.2** (0.17 g, 82%).

^{1}H NMR (300 MHz, DMSO-*d6*, 298K) δ 6.81 (d, *J* = 8.75 Hz, 8H), 6.62 (d, *J* = 8.75 Hz, 8H), 4.45 (s, 8H).

^{13}C NMR (75 MHz, DMSO-*d6*, 298K) δ 171.2, 156.3, 138.7, 132.1, 115.6, 114.7, 65.9.

IR (neat) (cm^{-1}) 1756, 3460.

HRMS (ESI) calculated for $C_{34}H_{27}O_{12}$ $[M–H]^-$ 627.1503, found 627.1500.

Melting Point 208-210°C (dec).

7.2.3 Preparation of **TCA·bis(pyridine)** single crystals

Single crystals were grown in 4 mL sample vials. To a solution of **TCA** in methanol (1 mL) was added a solution of bis(pyridine) (either **BPE**, **BPEt**, **Bpy or BPA**) in acetone (1 mL) at room temperature. The molar ratio of **TCA** to bis(pyridine) was 1:2 in each case. The solutions were thoroughly mixed by gently swirling the reaction vial. The solution was allowed to slowly evaporate at room temperature to yield crystals suitable for X-ray diffraction after 3-4 days.

TCA·BPE: 20 mg **TCA** and 6 mg **BPE**. Yield of single crystals (pink): 4.3 mg (19%).

TCA·BPEt: 20 mg **TCA** and 6 mg **BPEt**. Yield of single crystals (yellow): 6.2 mg (27%).

TCA·Bpy: 20 mg **TCA** and 5 mg **Bpy**. Yield of single crystals (orange): 5.1 mg (23%).

TCA·BPA: 20 mg **TCA** and 5 mg **BPA**. Yield of single crystals (orange): 5.1 mg (23%).

7.2.4 Preparation of **TCA·bis(pyridine)** bulk sample

To a solution of **TCA** in methanol (10 mL) was added a solution of bis(pyridine) in acetone (10 mL) at room temperature. The molar ratio of **TCA** to bis(pyridine) was 1:1 in each case. The solution was thoroughly mixed and then allowed to evaporate to near dryness over 5-6 days. The solid residue which formed during this time was collected by filtration and washed sequentially with methanol and acetone. Solid samples were then dried under vacuum at room temperature for 3 h to yield microcrystalline materials which were characterized by PXRD, TGA, and CP-AFM.

TCA·BPE: 200 mg **1** and 58 mg **BPE**. Yield of pink powder: 124 mg (60%).

TCA·BPEt: 200 mg **1** and 59 mg **BPEt**. Yield of yellow powder: 180 mg (88%).

TCA·Bpy: 200 mg **1** and 50 mg **Bpy**. Yield of orange powder: 164 mg (80%).

We were not able to obtain a bulk sample of **TCA·BPA** using this procedure.

7.2.5 Experimental procedure for DFT calculations

This work was performed by our collaborator Dr. Jonas Baltrusaitis. X-ray structural data obtained for **TCA·BPE**, **TCA·BPEt**, **TCA·Bpy** and **TCA·BPA** was subjected to further quantum chemical refinement. Geometry optimization was performed using a hybrid B3LYP Hamiltonian[112] and all electron 6-31G(d) basis sets for C, N, C and H atoms with H basis set having outer shell exponents of 0.1613 and 1.1 bohr-2, previously successfully used in urea electronic structure calculations. Radial and angular points of the grid were generated through Gauss–Legendre radial quadrature and Lebedev two-dimensional angular point distributions with a pruned grid of 75 radial and 974 angular points. Structure optimizations were performed using analytical energy gradients with respect to atomic coordinates, within a quasi-Newton scheme combined with the Broyden–Fletcher–Goldfarb–Shanno scheme for Hessian updating. Convergence was checked on both gradient components and nuclear displacements and was signaled when RMS gradient was 0.0003 and RMS displacement was 0.0012. Only atom positions were

optimized while the unit cell parameters were kept fixed. Symmetry relationships were fully exploited in these calculations. Truncation criteria for bielectronic integrals were set to 7, 7, 7, 20 and 50 with shrinking factors of 4. For density of states (DOS) projection calculations, shrinking factors of 6 were used to get a denser grid and a more accurate DOS representation. Periodic *ab initio* solid state program suite CRYSTAL'09 was used in all calculations. It uses the functions localized on atoms as the basis for expansion of the crystalline orbitals via linear combination of atomic orbitals (LCAO) technique.

7.3 Experimental data for Chapter 3

TetrabromoTPE **3.4** was synthesized according to the modified procedure published by Schultz *et al.*[18] In this case, after bromination, the reaction mixture was diluted with EtOAc and excess bromine was removed by treatment with 10% aq. $Na_2S_2O_3$ until the organic layer was almost colorless. The organic layer was then washed with water and dried over Na_2SO_4 and concentrated in vacuo to yield **3.4** as yellow solid. It was purified using silica gel flash column chromatography by 5% CH_2Cl_2 in hexanes as the eluent.

7.3.1 Synthesis and characterization of **3.1**

To a 250-mL 3-neck flask was added **3.4** (1.00 g, 1.54 mmol), 3-pyridine boronic acid (1.14 g, 9.26 mmol), dimethoxyethane (DME, 60 mL), and 2 M aq Na_2CO_3 solution (60 mL). The reaction mixture was deoxygenated by bubbling Ar through the solution for 20 min. Tetrakis(triphenylphosphine)-palladium(0) (0.37 g, 0.33 mmol, 20 mol %) was then added and the reaction was heated to reflux for 32 h. After cooling to rt, water (100 mL) was added which resulted in formation of a precipitate. This solid was collected by filtration and the filtrate was extracted with EtOAc (2 × 50 mL) and CH_2Cl_2 (2 × 50 mL). The combined organic extracts were dried over anhydrous Na_2SO_4, filtered, and concentrated in vacuo. The residue remaining was combined with the solid collected from the reaction mixture and purified by silica gel flash column chromatography (10%

MeOH in EtOAc) to afford **3.1** (0.47 g, 47%) as a pale solid.

^{1}H NMR ($CDCl_3$, 300 MHz) d 8.83 (s, 4H), 8.55 (d, J = 4.1 Hz, 4H), 7.85 (dt, J = 7.9 Hz, 1.7 Hz, 4H), 7.34 (dd, J = 7.9 Hz, 4.8 Hz, 4H), 7.42 (d, J = 8.3 Hz, 8H), 7.23 (d, J = 8.3 Hz, 8H).

^{13}C NMR ($CDCl_3$, 75 MHz) d 148.8, 148.4, 143.5, 140.9, 136.4, 136.2, 134.4, 132.5, 126.9, 123.8.

HRMS (ESI) Calcd for $C_{46}H_{33}N_4$ ($[M+H]^+$), 641.2705; found 641.2700.

Mp >230 °C.

Tetrapyridine **3.2** was prepared from **3.4** and 4-pyridine boronic acid in an analogous fashion. Spectroscopic properties of **3.2** matched those reported previously.[30]

7.4 Experimental data for Chapter 4

7.4.1 Synthesis and characterization of tris(4-iodophenoxy) trimesoate **4.2**

1,3,5-Benzenetricarbonyl trichloride **4.1** (2.0 mmol, 0.53 g), Et_3N (10 mmol, 1.4 mL), and DMAP (1.0 mmol, 0.12 g) were combined in dichloromethane (15 mL) and cooled to 10 °C. To this reaction mixture, 4-iodophenol (6.6 mmol, 1.45 g) dissolved in dichloromethane (10 mL) was added dropwise. The reaction was allowed to gradually warm to rt and maintained for 4 h. Water was added to the reaction mixture and the layers were separated. The aqueous phase was extracted with additional CH_2Cl_2 and the combined organic layer was washed with 10% aq. HCl solution, 5% aq. NaOH solution, and brine, followed by drying over anhydrous Na_2SO_4. Filtration and removal of the solvent afforded crude product that was subjected to purification by flash column chromatography (SiO_2, 1:1 hexanes:EtOAc) to afford **4.2** (1.06 g, 65%) as a colorless solid.

^{1}H-NMR (300 MHz, $CDCl_3$) δ 7.05 (d, *J* = 4.5 Hz, 6H), 7.79 (d, *J* = 4.5 Hz, 6H), 9.2 (s, 3H).

^{13}C-NMR (75 MHz, $CDCl_3$) δ 90.8, 123.9, 131.2, 136.4, 138.9, 150.5, 163.1.

IR (neat) cm^{-1} 1744, 1219.

Anal. Calcd. for $C_{27}H_{15}I_3O_6$: C, 39.71; H, 1.84. Found: C, 39.92; H, 1.89.

7.4.2 Synthesis and characterization of haloesters **4.3** to **4.7**

Tetraphenol **4.8**[29] (100 mg, 0.25 mmol) was dissolved in 10 mL THF, and 0.211 mL (1.50 mmol) Et_3N, 3.1 mg (0.025 mmol) DMAP and 4.5 molar equivalents of halobenzoyl chloride were added under argon at room temperature. Reactions were maintained for 12 h, and then concentrated *in vacuo* to afford white solids. The solids were combined with 10 mL 10% aq. NaOH solution and vigorously stirred for 15 min. Stirring was stopped and the solids were allowed to settle at the bottom of the flask and the NaOH solution was decanted. This procedure was repeated twice with 10 mL of H_2O. After the final treatment the remaining solids were collected by vacuum filtration, washed thoroughly with H_2O, and dried in air. Analytical samples were obtained by recrystallization from pyridine. Solubility issues prevented collection of ^{13}C NMR data.

4-Bromo ester **4.3**: Mp > 220 °C. ^{1}H NMR (DMF-d_7, 300 MHz): δ 8.06 (d, J = 8.7 Hz, 8H), 7.93 (d, J = 8.4 Hz, 8H), 7.25 (s, 16H).

4-Iodo ester **4.4**: Mp > 220 °C. ^{1}H NMR (DMF-d_7, 300 MHz): δ 8.06 (d, J = 8.7 Hz, 8H), 7.93 (d, J = 8.4 Hz, 8H), 7.25 (s, 16H). HRMS (ESI^+): Calcd for $C_{54}H_{32}I_4O_8 \cdot Na$ ($[M+Na]^+$), 1338.8174; found 1338.8189.

3-Bromo ester **4.5**: Mp > 220 °C. ^{1}H NMR (DMF-d_7, 300 MHz): δ 8.28 (s, 4H), 8.17 (d, J = 8.1 Hz, 4H), 7.98 (d, J = 8.1 Hz, 4H), 7.62 (t, J = 7.95 Hz, 4H), 7.28 (s, 16H). HRMS (ESI^+) Calcd for $C_{54}H_{32}Br_4O_8 \cdot Na$ ($[M+Na]^+$), 1148.8708; found, 1148.8710.

2-Bromo ester **4.6**: Mp > 220 °C. ^{1}H NMR (DMF-d_7, 300MHz): δ 8.08 (m, 4H), 8.02 (m, 4H) 7.86 (m, 4H), 7.61 (m, 4H), 7.29 (s, 16H). HRMS (ESI^+) Calcd for $C_{54}H_{32}Br_4O_8$ ($[M^+.]$), 1123.8831; found, 1123.8840.

2-Iodo ester **4.7**: Mp > 220 °C. ^{1}H NMR (DMF-d_7, 300 MHz): δ 8.15 (m, 4H), 8.04 (m, 4H), 7.82 (m, 4H), 7.63 (m, 4H), 7.29 (s, 16H). HRMS (ESI^{+}) Calcd for $C_{54}H_{32}I_4O_8 \cdot Na$ ([M+Na]$^{+}$), 1338.8174; found 1338.8182.

7.5 Experimental data for Chapter 5

Syntheses of all three TPE derivatives **5.1**, **5.2** and **5.3** are provided in experimental section for Chapters 2 and 3.[42,66]

7.5.1 Synthesis of Zn complex **5.4**

20 mg of tetraacid **5.1** was mixed with 24 mg of $Zn(ClO_4)_2 \cdot xH_20$ in methanol. Solvent was allowed to evaporate and **5.4** was obtained as colorless crystals after 3-4 days. Crystallographic yield was not determined.

7.5.2 Synthesis of Zn complex **5.5**

20 mg Tetrapyridyl TPE **5.2** was mixed with 9 mg $ZnCl_2$ in a 1:1 mixture of DMF and DMA (2 mL). The mixture was heated in a 10 mL glass sample vial to 135 °C in a programmable oven at 1 °C/min and was maintained at 135 °C for 24 hours, and then cooled to room temperature at 0.1 °C/min. X-ray quality crystals of **5.5** were obtained as colorless bars. The crystallographic yield was not determined.

7.5.3 Synthesis of **5.6** and **5.7**

20 mg Tetrapyridyl TPE **5.3** was mixed with 25 mg 1,4-diiorotetrafluorobenzene in 1:1 mixture of EtOAc and methanol (2 mL). Solvent was allowed to evaporate and **5.6** was obtained as pale yellow needles after 3-4 days. A similar procedure was used to prepare **5.7** with same amount of **5.3** and 25 mg of 1,2-diiodotetrafluorobenzene. The crystallographic yields were not determined.

APPENDIX

CRYSTALLOGRAPHIC DATA TABLES

Table A1 Crystallographic data for Chapter 2.

	TCA·BPE	**TCA·BPEt**	**TCA·Bpy**	**TCA·BPA**
CCDC number	pending	pending	pending	pending
Formula	$C_{48.3}H_{43.3}N_2O_{13}$	$C_{47.40}H_{45.58}N_2O_{13.40}$	$C_{47}H_{48}N_2O_{15}$	$C_{50.36}H_{43.69}N_2O_{14}$
MW	859.75	857.50	880.87	900.91
Cryst. system	monoclinic	monoclinic	triclinic	orthorhombic
Space group	C2/c	C2/c	P-1	
a / Å	35.414(4)	36.557(4)	9.4628(10)	9.4674(19)
b / Å	12.6212(14)	12.5100(14)	14.4930(15)	28.214(6)
c / Å	9.2922(10)	9.2151(10)	16.2100(17)	16.483(3)
α / °	90	90	99.907(5)	90
β / °	95.497(5)	96.781(5)	98.249(5)	90
γ / °	90	90	90.148(5)	90
V / $Å^3$	4134.2(8)	4184.8(8)	2166.5(4)	4402.9(15)
Z	4	4	2	4
D_{calc}	1.381	1.361	1.350	1.359
μ (mm^{-1})	0.101	0.100	0.101	0.100
T / K	150(2)	190(2)	150(2)	190(2)
No. of reflns	24467	22063	30930	40294
No. of unique reflns	3160	2719	6016	2988
No. of reflns I > 2σ(I)	2172	1487	3505	1755
Parameters	291	299	590	605
R_1 [I > 2σ(I)]	0.0574	0.0572	0.1067	0.0759
wR_2 all reflns	0.1587	0.1522	0.3246	0.1755

Table A2 Crystallographic data for Chapter 3.

	3.1·(EtOAc)	**3.1·(DMA)**	**3.2·(NMP)**	**3.5**	**3.6**
CCDC number	CCDC-811775	CCDC-811776	pending	CCDC-823825	CCDC-823824
Formula	$C_{50}H_{40}N_4O_2$	$C_{50}H_{41}N_5O$	$C_{56}H_{50}N_6O_2$	$C_{46}H_{40.35}Cl_4N_4O_{18.17}$	$C_{47}H_{46}Cl_4N_4O_{20}$
MW	728.86	727.88	839.02	1081.77	1128.68
Cryst. system	Monoclinic	Triclinic	monoclinic	Monoclinic	Monoclinic
Space group	$P2_1/c$	P-1	$P2_1$	$P2_1/n$	$P2_1/n$
a / Å	15.3307(16)	10.8926(12)	13.0349(14)	8.8607(10)	19.689(2)
b / Å	39.832(4)	12.9890(14)	9.6770(11)	36.330(4)	9.4722(10)
c / Å	19.455(2)	12.2807(15)	18.719(2)	14.7571(16)	27.058(3)
α / °	90	97.369(5)	90	90	90
β / °	104.832(5)	101.612(5)	102.804(5)	93.049(5)	102.182(5)
γ / °	90	94.508(5)	90	90	90
V / $Å^3$	11485(2)	1951.4(4)	2302.5(4)	4743.7(9)	4932.6(9)
Z	12	2	2	4	4
D_{calc}	1.265	1.239	1.210	1.515	1.520
μ (mm^{-1})	0.078	0.075	0.075	0.332	0.325
T / K	150	190(2)	210(2)	190(2)	210(2)
No. of reflns	203698	22527	29971	42623	53649
No. of unique reflns	20210	5741	2660	7273	5477
No. of reflns I > 2σ(I)	12431	3485	1565	4329	2678
Parameters	1600	561	463	655	567
R_1 [I > 2σ(I)]	0.0476	0.0544	0.1091	0.0578	0.0821
wR_2 all reflns	0.1274	0.1433	0.3354	0.1283	0.2259

Table A3 Crystallographic data for Chapter 4.

	4.3·(py)	**4.3·(dmf)$_2$**	**4.4·(py)**	**4.4·(dmf)$_2$**	**4.4·(py)$_3$**
CCDC number	pending	pending	pending	pending	pending
Formula	$C_{57.88}H_{35.88}Br_4N_{0.77}O_8$	$C_{57.48}H_{40.12}Br_4N_{1.16}O_{9.16}$	$C_{58.53}H_{36.53}I_4N_{0.91}O_8$	$C_{58.719}H_{43.011}I_4N_{1.573}O_8$	$C_{68.74}H_{46.74}I_4N_{2.974}O_8$
MW	1189.80	1213.23	1388.11	1431.45	1549.54
Cryst. system	triclinic	triclinic	triclinic	triclinic	triclinic
Space group	P-1	P-1	P-1	P-1	$P2_1/n$
a / Å	10.543(4)	10.2173(11)	10.6242(12)	10.2230(11)	10.3097(11)
b / Å	16.296(5)	16.4911(17)	16.3746(17)	16.4842(17)	37.511(4)
c / Å	17.040(6)	19.045(2)	16.9432(18)	19.0391(19)	16.7490(18)
α / °	112.180(16)	65.831(5)	111.993(5)	65.799(5)	90
β / °	90.699(15)	85.161(5)	91.015(5)	85.211(5)	107.176(5)
γ / °	106.481(19)	73.224(5)	106.380(5)	73.177(5)	90
V / Å^3	2576.0(16)	2801.0(5)	2596.8(5)	2798.9(5)	6188.4(11)
Z	2	2	2	2	4
D_{calc}	1.534	1.439	1.775	1.698	1.663
μ (mm^{-1})	3.180	2.928	2.456	2.284	2.072
T / K	210(2)	190(2)	200(2)	200(2)	190(2)
No. of reflns	12376	33797	27748	40387	69935
No. of unique reflns	3814	7279	8664	7290	11341
No. of reflns I > 2σ(I)	2715	5250	6397	4182	6764
Parameters	202	650	687	666	714
R_1 [I > 2σ(I)]	0.1273	0.0748	0.0523	0.0589	0.0499
wR_2 all reflns	0.2879	0.2400	0.1189	0.1335	0.1047

Table A4 Crystallographic data for Chapter 4.

	4.5·(DMF)	**4.5·(py)**	**4.6**	**4.7**
CCDC number	pending	pending	pending	pending
Formula	$C_{57}H_{39}Br_4NO_9$	$C_{59}H_{37}Br_1NO_8$	$C_{54}H_{32}Br_4O_8$	$C_{54}H_{32}I_4O_8$
MW	1201.53	1207.54	1128.44	1316.40
Cryst. system	monoclinic	triclinic	monoclinic	triclinic
Space group	$P2_1/n$	P-1	$P2_1/n$	P-1
a / Å	11.3913(12)	11.9174(13)	22.073(3)	10.2588(11)
b / Å	14.9677(16)	15.3574(16)	8.6817(10)	15.3024(16)
c / Å	29.896(3)	16.0001(17)	23.886(3)	30.704(4)
α / °	90	65.224(5)	90	96.614(5)
β / °	93.341(5)	70.717(5)	94.603(5)	90.414(5)
γ / °	90	77.858(5)	90	95.087(5)
V / $Å^3$	5088.7(9)	2500.8(5)	4562.5(10)	4768.4(9)
Z	4	2	4	4
D_{calc}	1.568	1.604	1.643	1.834
μ (mm^{-1})	3.222	3.277	3.586	2.669
T / K	190(2)	190(2)	190(2)	190(2)
No. of reflns	45136	29682	54032	46871
No. of unique reflns	6649	8967	5974	16697
No. of reflns $I > 2\sigma(I)$	4033	5412	3415	8161
Parameters	642	677	595	1189
R_1 [$I > 2\sigma(I)$]	0.0519	0.0478	0.0597	0.0563
wR_2 all reflns	0.1124	0.0886	0.1178	0.0938

Table A5 Crystallographic data for Chapter 5.

	5.4	**5.5**	**5.6**	**5.7**
CCDC number	pending	pending	pending	pending
Formula	C36.55H38.21O17.45Zn	$C_{59.768}H_{53.536}Cl_2N_8O_4Zn$	$C_{58}H_{32}F_8I_4N_4$	$C_{58}H_{32}F_8I_4N_4$
MW	822.05	1093.89	1444.48	1444.48
Cryst. system	$P2_1$	I222	P1	$P2_1/c$
Space group	monoclinic	orthorhombic	triclinic	monoclinic
a / Å	9.3642(10)	11.8883(13)	14.1443(15)	14.4076(15)
b / Å	11.1788(12)	14.3578(15)	14.3491(15)	16.0078(17)
c / Å	18.1526(19)	17.3070(18)	15.0776(16)	22.228(3)
α / °	90	90	109.334(5)	90
β / °	101.359(5)	90	105.904(5)	93.266(5)
γ / °	90	90	99.933(5)	90
V / $Å^3$	1830.0(3)	2954.1(5)	2657.6(5)	5118.2(10)
Z	2	2	2	4
D_{calc}	1.465	1.230	1.805	1.875
μ (mm^{-1})	0.738	0.557	2.415	2.508
T / K	150(2)	210(2)	210(2)	210(2)
No. of reflns	51730	17558	27749	89655
No. of unique reflns	6540	2706	16688	12179
No. of reflns I > 2σ(I)	5917	2239	9093	9637
Parameters	530	208	1334	753
R_1 [I > 2σ(I)]	0.0502	0.0479	0.0831	0.0341
wR_2 all reflns	0.1356	0.1303	0.1912	0.0779

BIBLIOGRAPHY

(1) Lehn, J. *Science (Washington DC, U. S.)* **1993**, *260*, 1762.

(2) Latimer, W. M.; Rodebush, W. H. *J. Am. Chem. Soc.* **1920**, *42*, 1419.

(3) Watson, J. D.; Crick, F. H. C. *Nature (London, U. K.)* **1953**, *171*, 737.

(4) Pedersen, C. J. *J. Am. Chem. Soc.* **1967**, *89*, 7017.

(5) Cram, D. J.; Cram, J. M. *Science (Washington DC, U. S.)* **1974**, 183, 803.

(6) Goodman, C. *Nat. Chem. Biol.* **2007**, 3, 685.

(7) *The Nobel prize in chemistry 1987*. http://www.nobelprize.org/nobel_prizes/chemistry/laureates/1987/ (accessed 11/11/2011)

(8) Steed, J. W.; Atwood, J. L. *Supramolecular Chemistry*; 2nd Ed.; Wiley: Chichester, UK, 2009.

(9) Rathore, R.; Lindeman, S. V.; Kumar, A. S.; Kochi, J. K. J. Am. Chem. Soc. **1998**, 120, 6931.

(10) *J. Chem. Soc., Abstracts* **1888**, *54*, 928.

(11) Wang, W.; Lin, T.; Wang, M.; Liu, T.-X.; Ren, L.; Chen, D.; Huang, S. *J. Phys. Chem. B* **2010**, *114*, 5983.

(12) Schreivogel, A.; Maurer, J.; Winter, R.; Baro, A.; Laschat, S. *Eur. J. Org. Chem.* **2006**, 3395.

(13) Okuma, K.; Kojima, K.; Oyama, K.; Kubo, K.; Shioji, K. *Eur. J. Org. Chem.* **2004**, 820.

(14) Tezuka, Y.; Hashimoto, A.; Ushizaka, K.; Imai, K. *J. Org. Chem.* **1990**, *55*, 329.

(15) Barhdadi, R.; Courtinard, C.; Nedelec, J. Y.; Troupel, M. *Chem. Commun. (Cambridge, U. K.)* **2003**, 1434.

(16) Sajna, K. V.; Srinivas, V.; Kumara Swamy, K. C. *Adv. Synth. Catal.* **2010**, *352*, 3069.

(17) Nadri, S.; Joshaghani, M.; Rafiee, E. *Organometallics* **2009**, *28*, 6281.

(18) Schultz, A.; Laschat, S.; Diele, S.; Nimtz, M. *Eur. J. Org. Chem.* **2003**, 2829.

(19) Sengupta, S. *Synlett* **2004**, 2004, 1191.

(20) Verkerk, U.; Fujita, M.; Dzwiniel, T. L.; McDonald, R.; Stryker, J. M. *J. Am. Chem. Soc.* **2002**, 124, 9988.

(21) Fry, A. J.; Allukian, M.; Williams, A. D. *Tetrahedron* **2002**, 58, 4411.

(22) Navale, T. S.; Thakur, K.; Rathore, R. *Org. Lett.* **2011**, 13, 1634.

(23) Hong, Y.; Lam, J. W. Y.; Tang, B. Z. *Chem. Commun. (Cambridge, U. K.)* **2009**, 4332.

(24) Cheng, K. H.; Zhong, Y.; Xie, B. Y.; Dong, Y. Q.; Hong, Y.; Sun, J. Z.; Tang, B. Z.; Wong, K. S. *J. Phys. Chem. C* **2008**, *112*, 17507.

(25) Liu, L.; Zhang, G.; Xiang, J.; Zhang, D.; Zhu, D. *Org. Lett.* **2008**, *10*, 4581.

(26) Bian, N.; Chen, Q.; Qiu, X.-L.; Qi, A.-D.; Han, B.-H. *New J. Chem.* **2011**, *35*, 1667.

(27) Hu, X.-M.; Chen, Q.; Zhou, D.; Cao, J.; He, Y.-J.; Han, B.-H. *Polym. Chem.* **2011**, *2*, 1124.

(28) Kato, T.; Kawaguchi, A.; Nagata, K.; Hatanaka, K. *Biochem. Biophys. Res. Commun.* **2010**, *394*, 200.

(29) Schultz, A.; Diele, S.; Laschat, S.; Nimtz, M. *Adv. Funct. Mater.* **2001**, *11*, 441.

(30) Wang, M.; Zheng, Y.-R.; Ghosh, K.; Stang, P. J. *J. Am. Chem. Soc.* **2010**, *132*, 6282.

(31) Minyaev, M. E.; Lyssenko, K. A.; Belyakov, P. A.; Antipin, M. Y.; Roitershtein, D. M. *Mendeleev Commun.***2007**, *17*, 102.

(32) Roitershtein, D. M.; Minyaev, M. E.; Lyssenko, K. A.; Belyakov, P. A.; Antipin, M. Y. *Russ. Chem. Bull.* **2004**, *53*, 2152.

(33) Naarmann, H. In *Ullmann's Encyclopedia of Industrial Chemistry*; Wiley-VCH Verlag GmbH & Co. KGaA: 2000.

(34) Anthony, J. E. *Chem. Rev.* **2006**, 106, 5028.

(35) Moon, H.; Zeis, R.; Borkent, E. J.; Besnard, C.; Lovinger, A. J.; Siegrist, T.; Kloc, C.; Bao, Z. *J. Am. Chem. Soc.* **2004**, *126*, 15322.

(36) Burroughes, J. H.; Bradley, D. D. C.; Brown, A. R.; Marks, R. N.; Mackay, K.; Friend, R. H.; Burns, P. L.; Holmes, A. B. *Nature (London, U. K.)* **1990**, *347*, 539.

(37) McCullough, R. D.; Tristram-Nagle, S.; Williams, S. P.; Lowe, R. D.; Jayaraman, M. *J. Am. Chem. Soc.* **1993**, *115*, 4910.

(38) Wudl, F.; Wobschall, D.; Hufnagel, E. J. *J. Am. Chem. Soc.* **1972**, *94*, 670.

(39) Frere, P.; Skabara, P. J. *Chem. Soc. Rev.* **2005**, *34*, 69.

(40) Bryce, M. R. *Chem. Soc. Rev.* **1991**, *20*, 355.

(41) Segura, J. L.; Martín, N. *Angew. Chem., Int. Ed.* **2001**, *40*, 1372.

(42) Kapadia, P. P.; Ditzler, L. R.; Baltrusaitis, J.; Swenson, D. C.; Tivanski, A. V.; Pigge, F. C. *J. Am. Chem. Soc.* **2011**, *133*, 8490.

(43) Coe, B. J.; Harries, J. L.; Harris, J. A.; Brunschwig, B. S.; Coles, S. J.; Light, M. E.; Hursthouse, M. B. *Dalton Trans.* **2004**, 2935.

(44) Kapadia, P. P.; Magnus, M. A.; Swenson, D. C.; Pigge, F. C. *J. Mol. Struct.* **2011**, *1003*, 82.

(45) Pisani, C.; Dovesi, R.; Roetti, C. *Hartree-Fock ab initio treatment of crystalline systems*; Springer-Verlag: Berlin ; New York, 1988.

(46) Ditzler, L. R.; Karunatilaka, C.; Donuru, V. R.; Liu, H. Y.; Tivanski, A. V. *J. Phys. Chem. C* **2010**, *114*, 4429.

(47) Spear, K. E.; Dismukes, J. P.; Electrochemical Society. *Synthetic diamond : emerging CVD science and technology*; Wiley: New York, 1994.

(48) Guo, S.; Akhremitchev, B. B. *Langmuir* **2007**, *24*, 880.

(49) Kao, K. C.; Hwang, W. *Electrical Transport in Solids*, 1981.

(50) Coropceanu, V.; Cornil, J.; da Silva Filho, D. A.; Olivier, Y.; Silbey, R.; Brédas, J. L. *Chem. Rev.* **2007**, *107*, 926.

(51) Brown, A. R.; de Leeuw, D. M.; Havinga, E. E.; Pomp, A. *Synth. Met.* **1994**, *68*, 65.

(52) Paasch, G.; Lindner, T.; Scheinert, S. *Synth. Met.* **2002**, *132*, 97.

(53) Molinari, A. S.; Alves, H.; Chen, Z.; Facchetti, A.; Morpurgo, A. F. *J. Am. Chem. Soc.* **2009**, 131, 2462.

(54) Wolf, M. O.; Fox, H. H.; Fox, M. A. *J. Org. Chem.* **1996**, *61*, 287.

(55) Sokolov, A. N.; Friščić, T.; MacGillivray, L. N. *J. Am. Chem. Soc.* **2006**, *128*, 2806.

(56) Skoog, D. A. *Analytical chemistry : an introduction*; 7th ed.; Saunders College Pub.: Fort Worth, 2000.

(57) Förster, T.; Kasper, K. Z. *Phys. Chem. (Muenchen, Ger.)* **1954**, *1*, 275.

(58) Borisov, S. M.; Wolfbeis, O. S. *Chem. Rev. (Washington, DC, U. S.)* **2008**, *108*, 423.

(59) Tan, W.; Wang, K.; Drake, T. J. *Curr. Opin. Chem. Biol.* **2004**, *8*, 547.

(60) Thomas, S. W.; Joly, G. D.; Swager, T. M. *Chem. Rev. (Washington, DC, U. S.)* **2007**, *107*, 1339.

(61) Tang, B. Z.; Zhan, X.; Yu, G.; Sze Lee, P. P.; Liu, Y.; Zhu, D. J. *Mater. Chem.* **2001**, *11*, 2974.

(62) Luo, J.; Xie, Z.; Lam, J. W. Y.; Cheng, L.; Chen, H.; Qiu, C.; Kwok, H. S.; Zhan, X.; Liu, Y.; Zhu, D.; Tang, B. Z. *Chem. Commun. (Cambridge, U. K.)* **2001**, 1740.

(63) Zeng, Q.; Li, Z.; Dong, Y.; Di, C. a.; Qin, A.; Hong, Y.; Ji, L.; Zhu, Z.; Jim, C. K. W.; Yu, G.; Li, Q.; Li, Z.; Liu, Y.; Qin, J.; Tang, B. Z. *Chem. Commun. (Cambridge, U. K.)* **2007**, 70.

(64) Qin, A.; Tang, L.; Lam, J. W. Y.; Jim, C. K. W.; Yu, Y.; Zhao, H.; Sun, J.; Tang, B. Z. *Adv. Funct. Mater.* **2009**, *19*, 1891.

(65) Kokado, K.; Chujo, Y. *Macromolecules* **2009**, *42*, 1418.

(66) Kapadia, P. P.; Widen, J. C.; Magnus, M. A.; Swenson, D. C.; Pigge, F. C. *Tetrahedron Lett.* **2011**, *52*, 2519.

(67) Metrangolo, P.; Meyer, F.; Pilati, T.; Resnati, G.; Terraneo, G. *Angew. Chem., Int. Ed.* **2008**, *47*, 6114.

(68) Metrangolo, P.; Resnati, G. *Science (Washington DC, U. S.)* **2008**, *321*, 918.

(69) Clark, T.; Hennemann, M.; Murray, J.; Politzer, P. *J. Mol. Model.* **2007**, *13*, 291.

(70) Valerio, G.; Raos, G.; Meille, S. V.; Metrangolo, P.; Resnati, G. *J. Phys. Chem. A* **2000**, *104*, 1617.

(71) Metrangolo, P.; Pilati, T.; Resnati, G. *CrystEngComm* **2006**, *8*, 946.

(72) Lommerse, J. P. M.; Stone, A. J.; Taylor, R.; Allen, F. H. *J. Am. Chem. Soc.* **1996**, *118*, 3108.

(73) Sun, A.; Lauher, J. W.; Goroff, N. S. *Science (Washington DC, U. S.)* **2006**, *312*, 1030.

(74) Bruce, D. *Halogen Bonding*; Metrangolo, P., Resnati, G., Eds.; Springer Berlin / Heidelberg: 2008; Vol. 126, p 161.

(75) Imakubo, T.; Sawa, H.; Kato, R. *Synth. Met.* **1995**, *73*, 117.

(76) Iwasaki, F.; Yoshikawa, J. H.; Yamamoto, H.; Kan-nari, E.; Takada, K.; Yasui, M.; Ishida, T.; Nogami, T. *Acta Crystallogr. Sect. B* **1999**, *55*, 231.

(77) George, S.; Nangia, A.; Lam, C.-K.; Mak, T. C. W.; Nicoud, J.-F. *Chem. Commun. (Cambridge, U. K.)* **2004**, 1202.

(78) Caronna, T.; Liantonio, R.; Logothetis, T. A.; Metrangolo, P.; Pilati, T.; Resnati, G. *J. Am. Chem. Soc.* **2004**, *126*, 4500.

(79) Mele, A.; Metrangolo, P.; Neukirch, H.; Pilati, T.; Resnati, G. *J. Am. Chem. Soc.* **2005**, *127*, 14972.

(80) Voth, A. R.; Hays, F. A.; Ho, P. S. *Proc. Natl. Acad. Sci., U. S. A.* **2007**, *104*, 6188.

(81) Pigge, F. C.; Vangala, V. R.; Swenson, D. C. *Chem. Commun. (Cambridge, U. K.)* **2006**, 2123.

(82) Pigge, F. C.; Vangala, V. R.; Swenson, D. C.; Rath, N. P. *Cryst. Growth Des.* **2009**, *10*, 224.

(83) Pigge, F. C.; Vangala, V. R.; Kapadia, P. P.; Swenson, D. C.; Rath, N. P. *Chem. Commun. (Cambridge, U. K.)* **2008**, 4726.

(84) Spek, A. L. *PLATON – A Multipurpose Crystallographic Tool*, University of Utrecht, The Netherlands, 1999

(85) Schollmeyer, D.; Shishkin, O. V.; Ruhl, T.; Vysotsky, M. O. *CrystEngComm* **2008**, *10*, 715.

(86) Swierczynski, D.; Luboradzki, R.; Dolgonos, G.; Lipkowski, J.; Schneider, H.-J. *Eur. J. Org. Chem.* **2005**, 1172.

(87) Kumar, V. S. S.; Pigge, F. C.; Rath, N. P. *CrystEngComm* **2004**, 6, 102.

(88) Lehmann, G. *Angew. Chem. Int. Ed.* **1976**, 15, 787.

(89) Atwood, J. L.; Steed, J. W. *Encyclopedia of supramolecular chemistry*; M. Dekker: New York, 2004.

(90) J. Kepert, C.; J. Rosseinsky, M. *Chem. Commun. (Cambridge, U. K.)* **1999**, 375.

(91) Eddaoudi, M.; Moler, D. B.; Li, H.; Chen, B.; Reineke, T. M.; O'Keeffe, M.; Yaghi, O. M. *Acc. Chem. Res.* **2001**, *34*, 319.

(92) Murray, L. J.; Dinca, M.; Long, J. R. *Chem. Soc. Rev.* **2009**, *38*, 1294.

(93) Han, S. S.; Furukawa, H.; Yaghi, O. M.; Goddard, W. A. *J. Am. Chem. Soc.* **2008**, *130*, 11580.

(94) Rowsell, J. L. C.; Millward, A. R.; Park, K. S.; Yaghi, O. M. *J. Am. Chem. Soc.* **2004**, *126*, 5666.

(95) Rosi, N. L.; Eckert, J.; Eddaoudi, M.; Vodak, D. T.; Kim, J.; O'Keeffe, M.; Yaghi, O. M. *Science (Washington DC, U. S.)* **2003**, *300*, 1127.

(96) Czaja, A. U.; Trukhan, N.; Muller, U. *Chem. Soc. Rev.* **2009**, *38*, 1284.

(97) Millward, A. R.; Yaghi, O. M. *J. Am. Chem. Soc.* **2005**, *127*, 17998.

(98) Cho, S.-H.; Ma, B.; Nguyen, S. T.; Hupp, J. T.; Albrecht-Schmitt, T. E. *Chem. Commun. (Cambridge, U. K.)* **2006**, 2563.

(99) Lee, J.; Farha, O. K.; Roberts, J.; Scheidt, K. A.; Nguyen, S. T.; Hupp, J. T. *Chem. Soc. Rev.* **2009**, *38*, 1450.

(100) Lu, G.; Hupp, J. T. *J. Am. Chem. Soc.* **2010**, *132*, 7832.

(101) Lan, A.; Li, K.; Wu, H.; Olson, D. H.; Emge, T. J.; Ki, W.; Hong, M.; Li, J. *Angew. Chem., Int. Ed.* **2009**, *48*, 2334.

(102) Pigge, F. C. *Encyclopedia of Supramolecular Chemistry*; Taylor & Francis: **2007**, p 1.

(103) Moore, M. H.; Nassimbeni, L. R.; Niven, M. L. *J. Chem. Soc., Dalton Trans.* **1987**, 2125.

(104) Roper, L. C.; Präsang, C.; Kozhevnikov, V. N.; Whitwood, A. C.; Karadakov, P. B.; Bruce, D. W. *Cryst. Growth Des.* **2010**, *10*, 3710.

(105) Banerjee, M.; Emond, S. J.; Lindeman, S. V.; Rathore, R. *J. Org. Chem.* **2007**, *72*, 8054.

(106) Čarsky, P.; Hünig, S.; Stemmler, I.; Scheutzow, D. *Liebigs Ann. Chem.* **1980**, 291.

(107) Han, Y.-F.; Lin, Y.-J.; Jia, W.-G.; Jin, G.-X. *Organometallics* **2008**, *27*, 4088.

(108) Neels, A.; Mantero, D. b. G. l.; Stoeckli-Evans, H. *Cryst. Growth Des.* **2008**, *8*, 1147.

(109) Guha, S.; Saha, S. *J. Am. Chem. Soc.* **2010**, *132*, 17674.

(110) Aakeroy, C. B.; Chopade, P. D.; Ganser, C.; Desper, J. *Chem. Commun. (Cambridge, U. K.)* **2011**, *47*, 4688.

(111) Duan, X.-F.; Zeng, J.; Lü, J.-W.; Zhang, Z.-B. *J. Org. Chem.* **2006**, *71*, 9873.

(112) Lee, C.; Yang, W.; Parr, R. G. *Phys. Rev. B* **1988**, *37*, 785.